Republic of Iraq
Ministry of Higher Education
and Scientific Research
University of Babylon
College of Engineering
Civil Engineering Department

STRUCTURAL BEHAVIOR OF NON-PRISMATIC REINFORCED CONCRETE FRAMES USING HYBRID CONCRETE UNDER MONOTONIC AND REPEATED LOADS

A Thesis
Submitted to The College of Engineering/ University of Babylon In Partial Fulfillment of The Requirements For The Degree of Doctor of Philosophy In Engineering / Civil Engineering/ Structural

By

Dhurgham Hussein Ali Hussein

Supervised by

Prof. Dr. Mustafa B. Dawood **Prof. Dr. Ghalib M. Habeeb**

2023 A.D 1445 A.H

بسْمِ اللَّهِ الرحمن الرَّحِيمِ

مَنْ عَمِلَ صَالِحًا مِنْ ذَكَرٍ أَوْ أنثى
وَهُوَ مُؤْمِنٌ فَلَنُحْيِيَنَّهُ حَيَاةً طَيِّبَةً ۖ
وَلَنَجْزِيَنَّهُمْ أَجْرَهُمْ بِأَحْسَنِ مَا كَانُوا
يَعْمَلُونَ

صدق الله العلي العظيم

سورة النحل آية 97

DEDICATION

To my father

who left me with his body but his soul is still fluttering in the sky of my life and supports me at all times to be a better person

CERTIFICATION

We certify that this thesis which is entitled " **STRUCTURAL BEHAVIOR OF NON-PRISMATIC REINFORCED CONCRETE FRAMES USING HYBRID CONCRETE UNDER MONOTONIC AND REPEATED LOADS**", and submitted by the student" ***Dhurgham Hussein Al-Saffar***", was prepared under our supervision at the Department of Civil Engineering/ College of Engineering, Babylon University, as a partial fulfillment of the requirements for the degree of doctor of philosophy in structural / civil engineering.

Signature: M.B. Dawood
supervisor: **Prof. Dr. Mustafa B. Dawood**
Date: / / 2023

Signature:
supervisor: **Prof. Dr. Ghalib M. Habeeb**
Date: / / 2023

We certify that this thesis mentioned above has been completed in Civil Engineering in the College of Engineering/ University of Babylon.

Signature: 21/01

Head of Department: **Asst. Prof. Dr. Zaid H. Majeed Al-Hasoon**

Date: 21 / 01 / 2023

EXAMINING COMMITTEE CERTIFICATE

We certify that we have read this thesis entitled **"STRUCTURAL BEHAVIOR OF NON-PRISMATIC REINFORCED CONCRETE FRAMES USING HYBRID CONCRETE UNDER MONOTONIC AND REPEATED LOADS"**, and as an examining in cee examined the student **"Dhurgham Hussein Al-Saffar"** in its content and that in our opinion, it meets a standard of thesis for the degree of doctor of philosophy in Civil Engineering /Structural Engineering.

Signature:
Name: Prof.
Dr. Nameer A. Alwash
(Chairman)
Date: / /٢٠٢٣

Signature:
Name: Prof.
Dr. Wissam D. Salman
(Member)
Date: / /٢٠٢٣

Signature:
Name: Prof.
Dr. Abbas Al-Ameeri
(Member)
Date: / /٢٠٢٣

Signature:
Name: Ass. Prof.
Dr. Najla'a H. Al-Shareef
(Member)
Date: / /٢٠٢٣

Signature:
Name: Ass. Prof.
Dr. Khalid K. Shadhan
(Member)
Date: / /٢٠٢٣

Signature:
Name: Prof.
Dr. Mustafa B. Dawood
(Supervisor and Member)
Date: / /٢٠٢٣

Signature:
Name: Prof.
Dr. Ghalib M. Habeeb
(Supervisor and Member)
Date: / /٢٠٢٣

Approved of Head of Department

Signature:
Name: ***Ass.Prof. Zaid H. Majeed Al-Hasoon***
Date: ٢١ / ٠١ /٢٠٢٣

Approved of The Dean of College

Signature:
Name: ***Prof. Laith Ali Abdul-Rahaim***
Date: / /٢٠٢٣

ACKNOWLEDGMENT

In the name of Allah, the most gracious, the most merciful

First, great thanks are to **ALLAH, HIS MAJESTY,** for enabling me to complete this work

My sincere appreciation and deepest gratitude are to my supervisors **Prof. Dr. Mustafa B. Dawood** and **Prof. Dr. Ghalib M. Habeeb**. I had the honor of being under their guidance, and supervision. Their constructive suggestions, patience, and constant encouragement have been greatly appreciated throughout this research and their help in finding some of the materials involved in the research that are not available in my country.

I extend my sincere and special thanks to my wife **(Ranin Abd Sharif)** for standing beside me in the most difficult situations in the research, providing support and love, and enduring my suffering throughout my studies.

I do not know how I can express my profound respect and thanks to my family **(my mother, my brothers "Ali and Karrar", and my sisters)** for their encouragement, help, support, and love.

I also extend my sincere thanks to my friends, **Dr. Haider Ali and Dr. Haider Al-Kateb, and Haider Mardan** for their assistance during the testing of the specimens.

Finally, I would like to express my deepest thanks to the staff of the Civil Engineering Department / College of Engineering / University of Babylon for their facilities and assistance throughout this study, as well as thanks to the staff of the Structural Laboratory of the College of Engineering/ University of Kufa, especially "**Eng. Afrah Ali**" for their assistance in the specimens testing stage.

Dhurgham H. Al-Saffar

ABSTRACT

This study includes experimental and theoretical investigations of planar concrete frames with prismatic and non-prismatic sections through casting eighteen specimens with different types of concrete and hybrid concrete. The specimens were tested under monotonic and repeated loads.

The aim of this research is to optimize the use of concrete in the concrete frame by redistributing the concrete along the structural members using non-prismatic sections in the columns and beam. The research also aims to know the behavior of the concrete frame when using glass fiber reactive powder concrete (GRPC), as well as when hybridizing conventional concrete with GRPC under monotonic and repeated loads.

The main variables in the experimental program include the use of non-prismatic sections in the columns and the beam, where the ratio of the large dimension to the small dimension is 1.3. A frame concrete using steel fiber reactive powder concrete (SRPC) and GRPC was also studied in addition to conventional concrete. In addition to using frame concrete with conventional concrete hybridized with GRPC at a different percentage, ranging from 25%-100%, in different locations. In addition to studying all of the above cases under the influence of a repeated load of ten cycles for each cycle, a maximum load of 65% of the ultimate load for the specimen with a monotonic load.

The results showed an increase in the ultimate load of (16%-25%) when using a concrete frame with non-prismatic sections compared to a prismatic frame. The ultimate load also increases by 41% and 46% when

using a concrete frame with GRPC and SRPC, respectively, compared to a frame with conventional concrete. When hybridizing conventional concrete frame with GRPC, it is observed that there is good agreement between the two types of concrete and that no separation occurs between them upon testing, as well as a clear improvement in the behavior of the concrete frame, as the ultimate load increases by (4-22) % depending on the ratio and location of the hybridization.

In addition, when testing the frames under repeated load, the ultimate load is greatly reduced in the conventional concrete frame, where the decrease is 27% compared to the monotonic load frame. When a frame is used with SRPC or GRPC or even conventional concrete hybridized with GRPC, the resistance of the frame to repeated loads improves, as the percentage of decrease in the ultimate load of the frame with SRPC and GRPC is only 2%. As for the frame with hybrid concrete, the percentage of decrease will be (4%-16%) according to the location and proportion of GRPC.

The improvement in the behavior of the concrete frame by using GRPC and SRPC is not only in the ultimate load but also improves the shear strength of the concrete frame and changes the type of failure from shear failure in the concrete frame with conventional concrete to flexural failure, as well as an increase in the stiffness of the concrete frame. The use of hybridization with GRPC in some regions also strengthens the shear strength of the concrete frame, changes the type of failure to flexural failure, and also increases the stiffness of the concrete frame.

On the other hand, three-dimensional finite element analysis (ABAQUS/CAE2017) was used to simulate a prismatic and non-prismatic concrete frame with one or more types of concrete. The results showed a good

convergence between the results of the theoretical analysis and the experimental tests of the specimens, as the difference in the ultimate load does not exceed 7%, while the corresponding deflection does not exceed 23%. So, the program was used to investigate a new parametric study.

Using the Abaqus program, it was found that the use of a non-prismatic frame in the whole beam with the ratio of the large depth of the beam to the small depth (1.1-2.0) increases the ultimate load by (13%-20%) and the best ratio is (1.5-2.0). While if a non-prismatic frame is used in the two-thirds of the two edges of the beam only by (1.1-2.0), the ultimate load increases by (16%-42%).

Also, when the frame is hybridized with GRPC in two-thirds of the end beam (shear stress zone) with a percentage hybridization of 18%-70%, the increase in ultimate load is almost constant at about 6%. And when the clear span of the beam only (without joints) is hybridized with a hybridization percentage of (13%-62%), the ultimate load increases by (0%-17%).

List of Contents

List of Tables

List of Figures

List of Plates

NOTATIONS

Most commonly used symbols are listed below, these and others are defined where they appear in the research:

Symbol	Definition	Unite
d_c	Compression damage parameters.	
d_t	Tension damage parameters.	
E	Modulus of elasticity of concrete.	MPa
E_{RPC}	Modulus of elasticity of reactive powder concrete.	MPa
E_s	Modulus of elasticity of steel.	MPa
f_c'	Compressive strength of concrete (cylinder test).	MPa
f_{cu}	compressive strength of cubic.	MPa
f_r	Modulus of rupture.	MPa
H	beam depth.	mm
h_{RPC}	thickness of the RPC layer.	mm
T	Splitting tensile strength of concrete.	MPa
P	ratio of the longitudinal reinforcing steel.	
ε_o	corresponding strain to peak compression load.	
ν	Poisson's ratio.	
ε	Strain.	
σ_{co}	yield stress.	MPa
σ_{cu}	ultimate compressive stress value.	MPa

ABBREVIATION

Symbol	Definition
ACI	American Concrete Institute
CDP	concrete damage plasticity
CF	carbon fibers
CFRP	Carbon-fiber-reinforced polymers
GF	glass fibers
GRPC	Reactive Powder Concrete with glass fibers
HSC	High-Strength Concrete
NSC	normal-strength concrete
PPF	polypropylene fibers
RPC	Reactive Powder Concrete
SF	steel fibers
SRPC	Reactive Powder Concrete with steel fibers
UHPC	Ultra-High-Performance Concrete

CHAPTER ONE

Chapter One

Introduction

1.1: Overview:

Over the years, the functional and architectural requirements of construction are becoming increasingly complex, so many engineers and consultants have explored to achieve these requirements. One of the biggest challenges for designers is the use of small-sized sections with high strength capacity. The need for high-strength concrete is imperative in the construction industry today. The cost of constructing high-strength concrete is very expensive compared to normal-strength concrete, and the cost of the structure is considered one of the most important factors for the success of the designer, so some researchers resorted to using high-strength concrete in specific zones only. While some researchers tended to identify zones that contain high stresses in which failure is expected, and then increase those sections only.

1.2: Non-Prismatic Section:

Since the first decades of the last century, non-prismatic sections began to appear in the beams. In recent decades their use has increased due to the development of structural engineering techniques in design and implementation **(Nabbat, 2015).** The existence of non-prismatic sections gave architects the freedom to creatively create new architectural designs with different styles, which required the structural engineers to search for non-prismatic section designs to meet those requirements and to obtain low-weight and high-strength sections through the redistribution of materials along the

structural members **(Jung et al, 2005)**. **Plate (1-1)** shows a non-prismatic beam during implementation. This was not the only purpose of using the non-prismatic beams, as the researchers found that non-prismatic beams can provide other benefits such as optimal use of concrete and reinforcing steel, reducing the weight of the structure for the purpose of lateral stiffness, reducing gases emitted from concrete and reinforcing steel, inelastic behavior, increasing ductility especially at shear failure. **(Tena-Colunga et al, 2008), (Kaveh et al, 2022)**

Plate (1-1) Typical non-prismatic beam in Tongzihe bridge in China

In many cases, the work requires passing ducts and pipes under beams and over false ceilings such as (electricity, sewage, air condition pipes, etc.). The presence of non-prismatic sections enables us to pass those ducts under the small sections of the beams, thus reducing the dead space between the edge of the lower beams and the false ceiling, and this reduces the overall

height of the structure, so the construction cost will decrease absolutely, as shown in **Figure (1-1).**

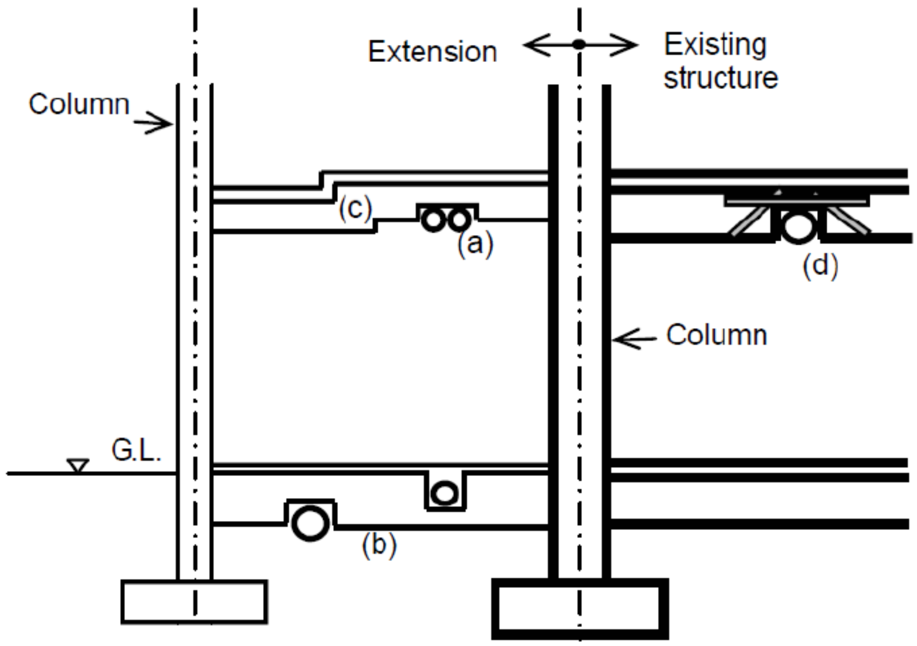

Figure (1-1) Example of non-prismatic beams. (a)Floor beams, (b) Ground beam, (c) Stepped beam, (d) Retrofitted beam. (Jung et al, 2005)

1.3: Reactive Powder Concrete:

Reactive Powder Concrete (RPC) is an evolution of cement-based products and is one of the high-strength concrete technologies. It was invented for the first time by two scientists, Richard and Cheyrezy, in the early 1990s in France at Bouygues Laboratories. RPC can be called Ultra-High-Performance Concrete (UHPC) and can be used interchangeably.

In 1994 Forster defined UHPC as "concrete made of certain materials according to a selected mix design with specific mixing ratios, mixed, transported, placed, consolidated and cured well, so the concrete results give excellent performance in the structure that it is exposed to throughout its design life". The American Concrete Institute (ACI) defines UHPC as

"concrete that meets specific performance needs and system requirements that cannot be consistently achieved using conventional concrete and standard mixing, placement, and curing practices". These improvements include mechanical properties, casting without segregation, and volume stability. (**Forster, 1994), (ACI Committee 318, 2006)**

RPC is a special concrete in which the microstructure of the concrete is improved by fine grading of the mixture to obtain the greatest possible density. It consists of Portland cement, which acts as a binder to hold the materials together, and silica fume, whose granules fill the voids between the large granules of the mixture due to their small size, thus increasing the density of the mixture and improving its workability due to the greasy texture of its granules. Also, RPC contains a fine aggregate with sizes (0.15-0.6) mm, which are the largest granules in the mixture. One of the unique properties of RPC is the low water content of the mixture, so Super Plasticizer is used to improve workability. To give the concrete the ductile property, steel fibers or other types of fibers such as (glass fiber, polypropylene fibers, etc.) are added to the mix. The absence of coarse aggregates, science was considered the key to the development of the microstructure of the mixture, by reducing the heterogeneity between the matrix of the cement paste and the aggregates. **(Lubbers, 2003)**

RPC has many advantageous mechanical properties in addition to its high resistance. Therefore, an RPC (or named UHPC) can be considered an HSC, but the opposite is not true. **Table (1-1)** shows a comparison between RPC and HSC.

Table (1-1) Compared between RPC and HSC (Lubbers, 2003)

Material Characteristic	UHPC Compared with HSC
Compressive Strength	2–3 times greater
Tensile Strength	2–6 times greater
Elastic Modulus	1.5 times greater
Total Porosity	4 – 6 times lower
Micro-porosity	10 – 50 times lower
Permeability	50 times lower
Water Absorption	7 times lower
Chlorine Ion Diffusion	25 times lower
Abrasive Wear	2.5 times lower
Corrosion Velocity	8 times lower

1.4: Advantage and Disadvantage of RPC:

1.4.1: Advantages of RPC

There are many advantages to RPC over conventional concrete. which can be summarized as follows: **(Kaveh et al, 2022)**, **(Christophe, 1997), (O'Neil and Dowd, 1995)**, **(Yen Lei Voo et al, 2010)**

1. It has a very high strength, especially shear strength, compared to conventional concrete. Thus, eliminating supplementary shear reinforcement compared to conventional concrete. It also provides the possibility of reducing structural sections and, as a result, reducing dead load and providing more interior spaces. Thus, eliminating supplementary shear reinforcement compared to conventional concrete. It has high shear strength, thus eliminating complementary shear reinforcement compared with conventional concrete.

2. It has a minimal shrinkage and creep properties compared to conventional concrete and is perfect for pre-stressed members.
3. Due to low permeability, it is highly resistant to corrosion, thus increasing the life of the structure and reducing maintenance throughout its service life.
4. It has a very little porosity and is non-interfering and thus prevents the transmission and penetration of liquids and gases. Therefore, it is suitable for nuclear reactors and aggressive chemical factories.
5. Improving seismic performance, as a result of the small size of the sections, and thus provides a high elastic deformation, and as a result of the light weight of the sections, it provides a low moment of inertia and has a high energy absorption capacity. So, it is also good in facilities subject to explosions, such as shelters and military installations.
6. RPC provides high fluidity and ease of casting in small sections and complex reinforcements.
7. Despite the high cost per cubic meter of RPC compared to conventional concrete, the small size of the sections, the dispensing of reinforcing steel in some cases, and the low cost of maintenance lead to a reduction in the final cost of the project. **Figure (1-2)** shows the difference in depth between RPC sections, reinforced concrete sections, steel wide flange, and pre-stressed concrete with equal moment capacity (675 kN.m).

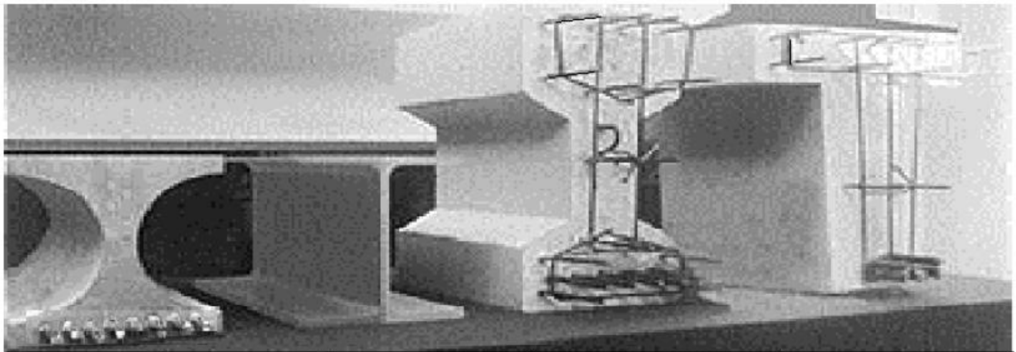

Section Parameteric	RPC X-shaped	Steel wide-flange	Prestressed concrete	Reinforced concrete
Section Depth	360 mm	360 mm	700 mm	700 mm
Weight	130 Kg/m	110 Kg/m	470 Kg/m	530 Kg/m

Figure (1-2) Comparisons in the depth of beam with equal moment capacity (675kN.m). (Christophe, 1997)

1.4.2: Disadvantages of RPC

Every construction material has some disadvantages that must be noticed and evaluated before using it. The main disadvantages of RPC are summarized as follows:

1. The high cost of forming one cubic meter compared to conventional concrete.
2. It needs skilled workers in mixing, as it needs a necessary sequence in place the materials in the mixer, and it also needs specific timings when mixing each material to obtain good mechanical properties.
3. It needs clean and well-lined molds, as the presence of small holes in the mold may not affect the casting of the conventional concrete, but it affects the RPC and causes the mixture to leak.

1.5: Concept of Hybrid Section:

The biggest challenge for engineers is to design the structure with high strength and durability at the lowest cost of construction or maintenance.

Many researchers have exerted abundant effort in studying the possibility of using more than one material in one structural member to obtain the best properties of each material and overcome its disadvantages. For example, in beams subjected to bending stresses, concrete with high compressive strength can be used in the part subjected to compressive stresses and lightweight concrete in the parts subjected to tensile stresses, thus obtaining a structural member with high strength, lightweight and low-cost. Where the structural member consisting of more than one material is called a hybrid member.

The hybrid system for concrete combines all the advantages of precast (quality, accuracy, speed, finishes, shape, and pre-stressing) and all the advantages of in situ casting (economics, flexibility, formation, continuity, permanence, and durability). The hybrid concrete system achieves what the customer desires in terms of low cost and high strength structure by providing simple and buildable structures and providing competitiveness that combines performance and quality. **(Goodchild and Glass, 2004)**

1.6: Cyclic Loading:

Cyclic loading is the process of applying loads in different directions, and its definition differs according to the intensity of the loads, whether variable or constant, as well as its different directions. It is divided into two types according to the direction of the cyclic loading: **(Ihssan, 1993)**

1. Unidirectional cyclic loading:

It is the applying and lifting of loads in one direction (positive or negative) and with specific periods and intensity. It is also called the repeated load. Examples of this type are the loads resulting from the movement of

vehicles and the collision of water. **Figure (1-3-a)** shows an illustration of this type of loading.

2. Reverse cyclic loading:

This type of loading is when the loads are applied in two opposite directions, where each load cycle contains a positive load and a negative load. An example of this type of load is loads resulting from wind movement and earthquakes. Earthquakes (seismic loads) are the most dangerous type of cyclic load, as they happen suddenly without warning and are severe. **Figure (1-3-b)** shows an illustration of this type of loading.

The application of load cycles causes the material or member to fail even though the load level is not high enough for the failure to occur and the reason for the failure by the fatigue of concrete. Where due to cyclic loads, cracks are initiated and propagate inside the specimen until the final failure. Also, it caused a modification in the mechanical parameters of the concrete, which causes a change in the structural responses of the members. **(Mínguez et al, 2019)**

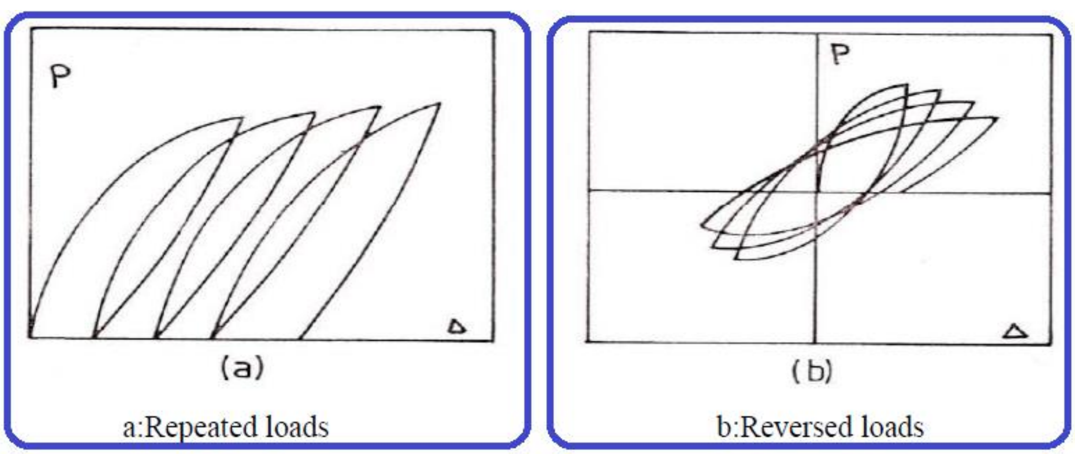

Figure (1-3) Type of cyclic loading (Ihssan, 1993)

1.7: Aims and Objects:

The distribution of stresses in structural members is variable according to the dimensions of the member and the method of applying loads. The member is designed according to the high concentrated stress, which causes a lot of loss of resources (concrete) in regions at low stresses. In this research, concrete is redistributed in regions with low stresses and transferred to regions with high stresses. Thus, it is expected to reduce the project's cost and make shear failure less brittle.

The research also aims to study the effect of using GRPC in the frame and the extent of its difference from SRPC under monotonic and repeated loads. The hybridization of the frame with GRPC is also studied, and the best location for hybridization is determined, as well as the minimum quantity of hybridization that gives good results to obtain a frame with high characteristics and at a lower cost.

Therefore, in this study, two aspects will include an experimental program and a numerical analysis. The experimental program includes studying a frame with prismatic and non-prismatic cross sections in the beam and columns, in addition to studying a concrete frame using GRPC and SRPC. The study also includes the use of a concrete frame with conventional concrete hybridized with GRPC in the shear zones and flexural zones. The specimens were also tested under repeated load to determine the frame behavior using GRPC and hybrid concrete.

The numerical study will create a model using the Abaqus program. New models with non-prismatic sections will also be studied differently than

those in the experimental specimens. The study will also deal with the effect of hybridization in different quantities and locations on the concrete frame.

1.8: Layout of Thesis:

This research includes six chapters, where the **first chapter** presents an overview to describe non-prismatic sections and RPC and also describes the hybrid concrete system as well as cyclic loads. **The second chapter** deals with previous studies conducted on the concrete frame, members with non-prismatic sections, hybrid concrete members, and some members of the research study under repeated loads. **The third chapter** presents a description of the specimens used in this thesis, the initial testing of all materials used, and the method of testing frame.

Chapter Four presents the results, discussions, and interpretations of the tested specimens. **The fifth chapter** deals with the use of nonlinear analysis to study selected frames using the Abaqus program. The results of the program are compared with experimental work to ensure compatibility between theoretical and experimental, and new parametric studies are taken into account for the study. Finally, **Chapter Six** deals with the conclusions obtained from the results of the experimental program. Conclusions from the results of numerical analysis using FEM (ABAQUS) are also presented. Finally, some recommendations for future work related to the research topic were suggested.

CHAPTER TWO

Chapter Two

Literature Review

2.1: Introduction:

The objective of this chapter is to give a brief review of the previous studies dealing with concrete frame, non-prismatic beam section, the reactive powder concrete structure, hybrid concrete structure and experimental analysis for structure under repeated load

2.2: Research studies of the concrete frame:

Kadhim (2007), investigated theoretically the reinforced concrete frames with prismatic and non-prismatic (tapered) members and subjected to cyclic loading as shown in **Figure (2-1)**. The effect of the tapered beam with different measurements in the depth and width of the beam under cyclic loads was studied. The results indicated that the best beam-tapered in depth (h_2/h_1) and width (b_2/b_1) was equal to (1.2-1.625) and (1.2-1.375), respectively. Where the number of load cycles until failure is equal to 2, 1, 4, 3, 3 and 2 for (h2/h1) equals 1, 0.75, 1.2, 1.375, 1.625 and 2, respectively.

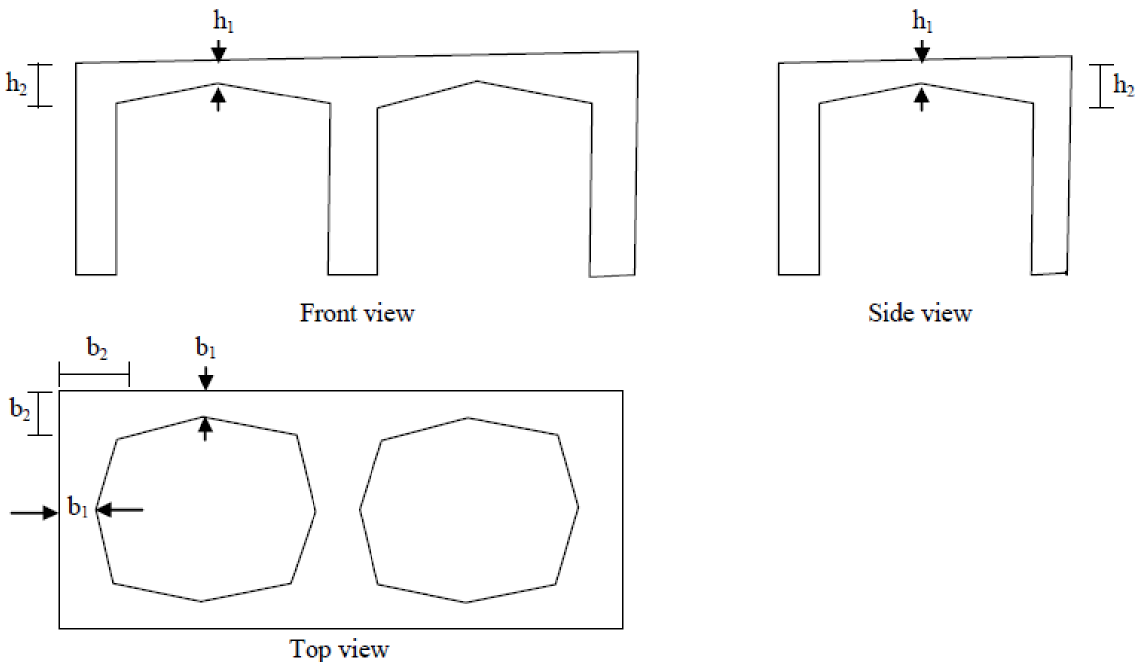

Figure (2-1) Tapering shape for frame used by Kadhim (2007)

Al-Nasrawi (2008), presented a theoretical and experimental study of a space-reinforced concrete frame under cyclic loading. The research dealt with the investigation of the behavior of confined concrete by CFRP fabric jacket by the nonlinear finite element approach (Region Approach), where the parameter study includes the effect of coupling between bending moment, axial and shear forces, geometric non-linearity, and material nonlinearity. To represent the wrapping of CFRP fabrics in the theoretical study, five experimental specimens were made that were strengthened with CFRP in different technic. The experimental results showed that strengthening concrete with CFRP can increase the ultimate flexure strength of the space frame by up to 75%. **Figure (2-2)** shows the details of the experimental specimen dimensions.

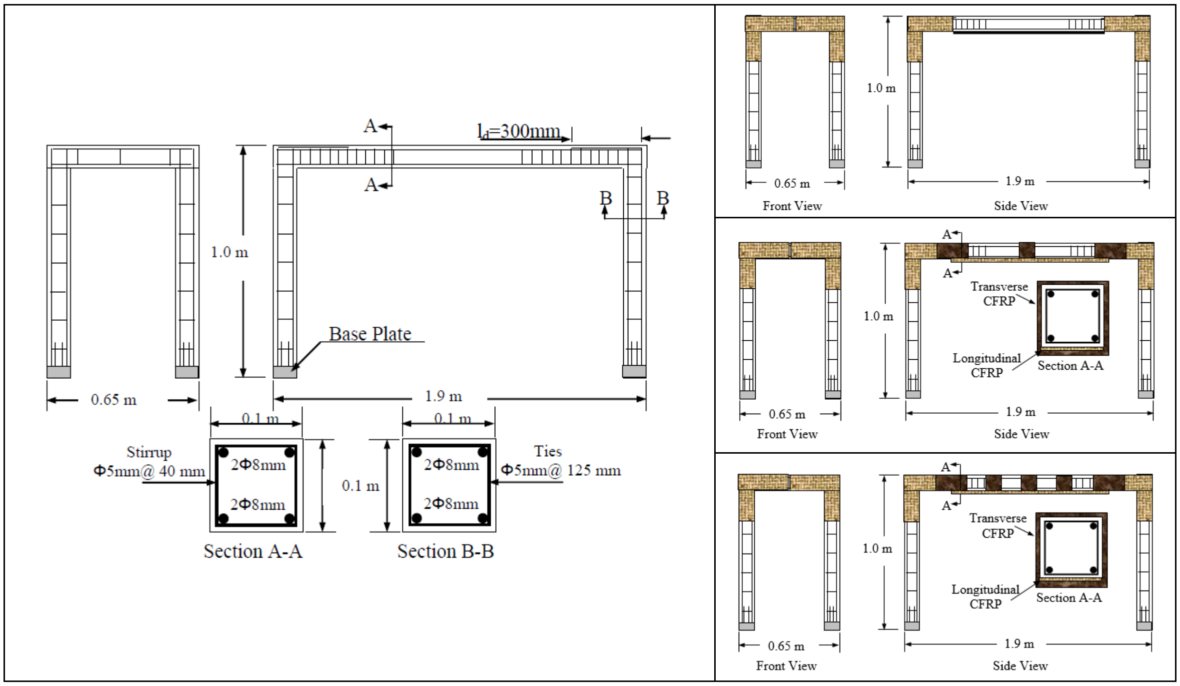

Figure (2-2) Details of the experimental specimens' dimensions used by Al-Nasrawi (2008)

Al-hussainy (2015), investigated the behavior of self-compacting reinforced concrete portal frames strengthened with different types of CFRP composite products. The support of columns was considered fixed by using a support cup, the proof for that is the rotation in the deflected shape of the columns near the cups is approximately zero or minimal values at the large loads. The experimental work consists of the fabrication and testing of fourteen reinforced concrete portal frames with beam cross-section (150 x 200 mm) and length (1500 mm) and column cross-section (150 x 150 mm) and length (1000 mm) as shown in **Figure (2-3)**. The effect of monotonic and repeated load, uniform and two-point load has been studied, in addition to studying the effect of strengthening with various lengths and locations of CFRP sheet. The experimental results showed an increase in the ultimate load capacity of CFRP frames (5.68%- 25%). Also, when the specimens were tested under a distributed load, the specimens gave a higher ultimate load than

the specimens tested under two concentrated loads (66%-72%). The decrease in ultimate load due to repeated load applying was 3%. When casting the frame in two different stages, the decrease in the ultimate load was 11.26%.

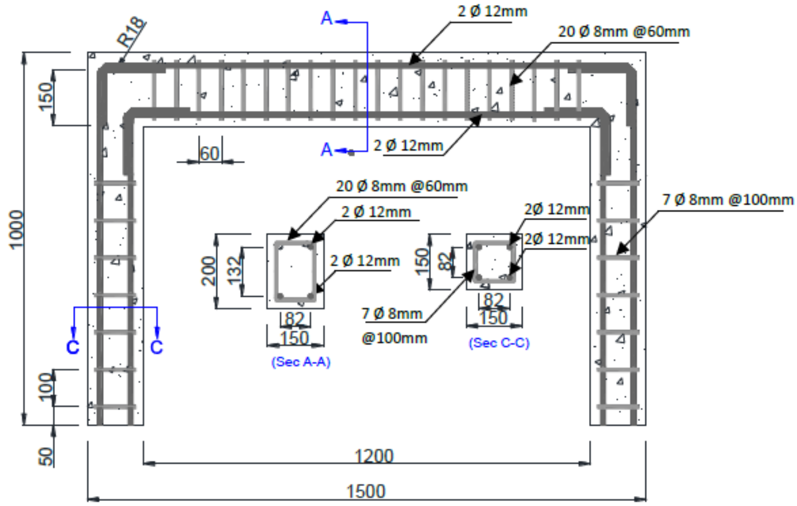

Figure (2-3) Dimension of the specimens of Al-hussainy (2015)

Hemmati et al (2017), studied the rehabilitation of the reinforced concrete frame to resist the effects of earthquakes. **Figure (2-4)** shows the details of the experimental specimens used. Three experimental specimens were used in this research, the first was a reinforced concrete frame, the second was a reinforced concrete frame with concentric bracing, and the third was a reinforced concrete frame with eccentric bracing, and the effect of the cyclic behavior of them was studied and comparisons between the results. The results indicated that the concrete frames with concentric bracing and eccentric bracing were better in the ultimate load, where the results were 2.11 and 1.9 times more than that of the concrete frame without bracing.

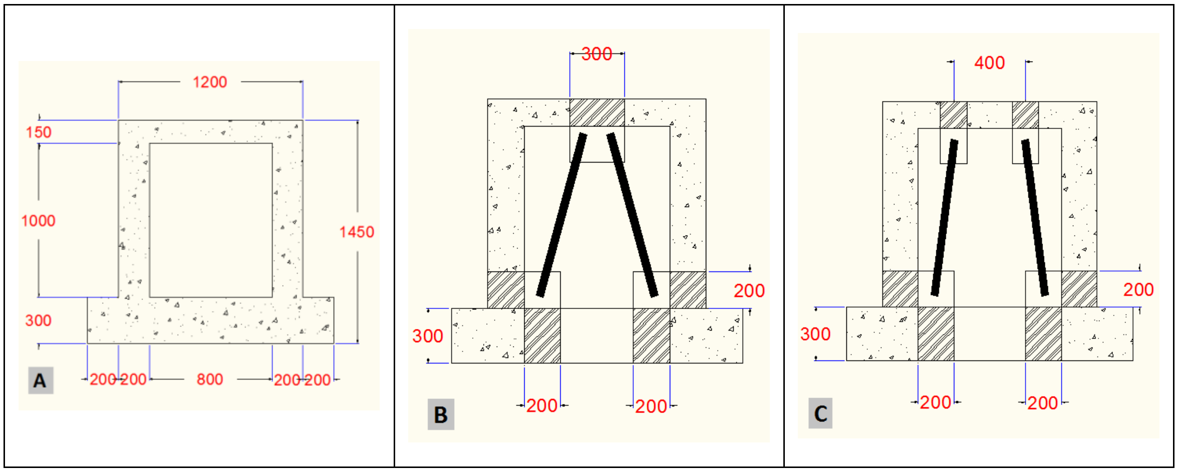

Figure (2-4) Details of concrete frame used by Hemmati et al (2017) A: control frame. B: concentric bracing. C: eccentric bracing

Basim et al (2019), studied the effect of the embedded carbon fiber-reinforced polymer rods in reinforced concrete frames with ultra-high-performance concrete subjected to dynamic load. The embedded carbon fiber-reinforced polymer rods were used at joints of columns and beam as shown in **Figure (2-5)**. The support of the columns in this study was fixed support. The exposure of the reinforced concrete frame to dynamic loads causes cracks in the beam-column joints, thus it was easy to corrode the steel reinforcement and thus the failure of the frame. The performance of the frames reinforced was improved under lateral load resistance capacity, failure mechanism, overall stiffness, and ductility behavior.

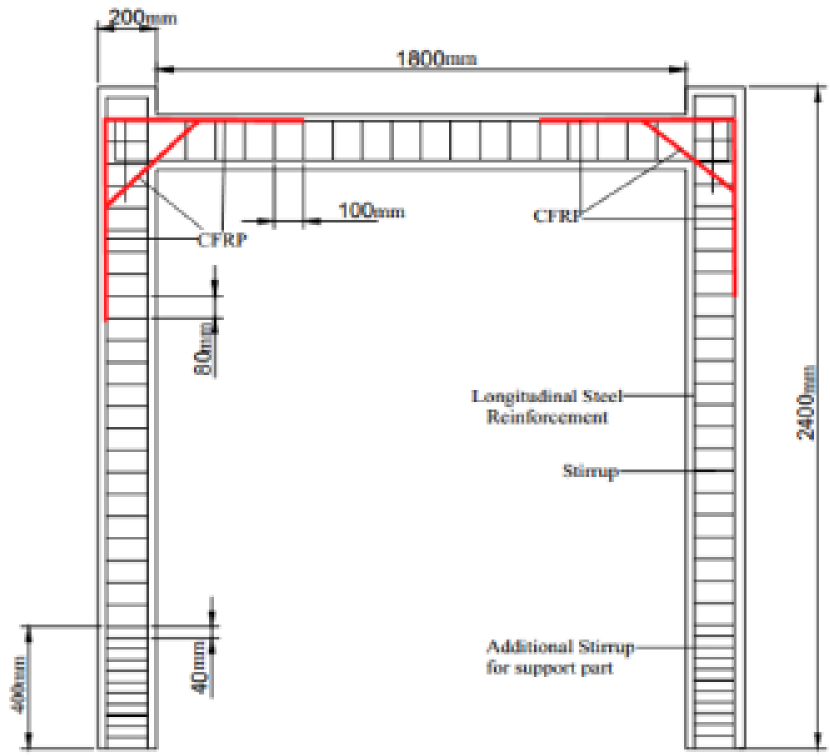

Figure (2-5) Details of tested frame by Basim et al (2019)

2.3: Research studies of the Non-Prismatic Sections:

Tena-Colunga et al (2008), presented ten prototypes of simply-supported reinforced concrete beams under monotonic load with prismatic and non-prismatic sections (eight non-prismatic and two prismatic) to estimate the development of shear failure. The experimental work included two groups, where the first group consisted of five beams (one prismatic and four non-prismatic) that were tested without stirrups, while the second group consisted of five beams/ also (one prismatic and four non-prismatic) were tested with minimum stirrups, as the stirrups were designed according to the requirements of the prismatic beam. The percentage of the non-prismatic section (h_2/h_1) was

changed (1-1.8) to study its effect on the shear strength, as shown in **Figure (2-6).** The results showed and confirmed that the non-prismatic beams have a different behavior than the prismatic beams, where it was found that the non-prismatic beams prefer the arching action in the haunched length as a major mechanical failure resistance. The study discussed the deformation capacity and shear strength. It was found that the non-prismatic beams increase the deformation capacity before failure, thus making the specimen less fragile in shear failure with respect to the prismatic beam and that the non-prismatic beams increase slightly in the ultimate load. The effect of the presence of stirrups in the non-prismatic beam is less than in the prismatic beam, as the presence of stirrups increases the ultimate load of the prismatic beam by 240%, while in the non-prismatic beam, the increase is (75%-160%).

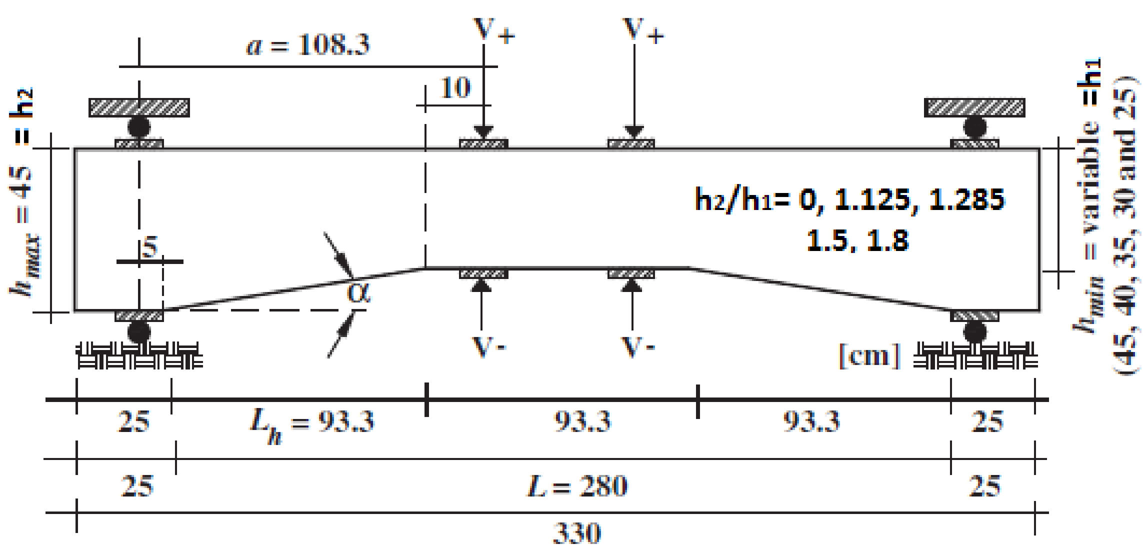

Figure (2-6) Geometry for the test specimens of the research of Tena-Colunga et al (2008)

Ghadhban (2013), presented an experimental study of five solid and hollow non-prismatic concrete beams (one solid and four hollows) with simple support under two concentric loads. The parametric study of this research used

for different shear reinforcement in beams (three specimens with stirrups Ø4@150mm and two specimens Ø4@100mm), as well as studying the effect of circular and square openings in the beams and retrofit with carbon fiber reinforced polymer (CFRP). **Figure (2-7)** shows the external dimensions of the beam. The test results show that increasing the shear reinforcement increases the ultimate load by 30% and that the presence of circular and square openings for the same shear reinforcement reduces the ultimate load by 53% and 17%, respectively.

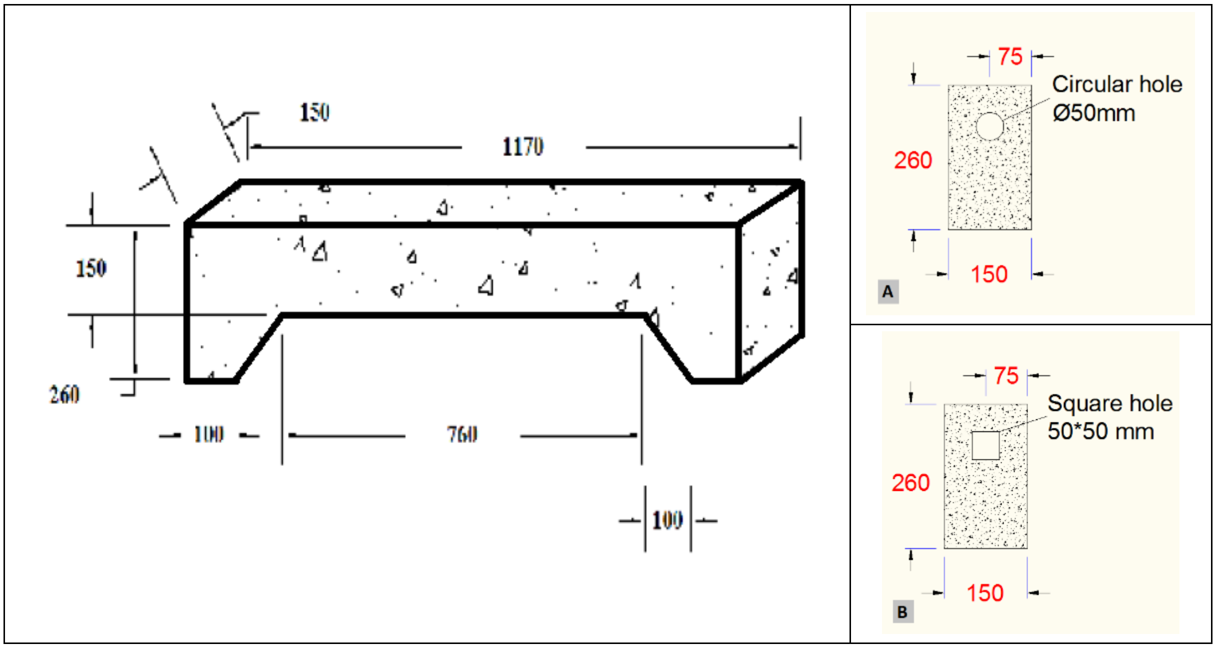

Figure (2-7) Geometry of the beams of Ghadhban (2013) A: cross section of specimens with circular hole. B: cross section of specimens with square hole

Qissab and Dhaiban (2015), presented a practical and theoretical study of the behavior and performance of reinforced concrete beams with prismatic and non-prismatic sections in shear. The practical program includes testing thirteen beams with different parametric studies, which include changing the geometric shapes of the cross sections (using three different

cross sections as in **Figure (2-8)**), changing the compressive strength of concrete, and changing the ratio of the shear span to the length of the beam (a/d). The results showed a change in the behavior of the beams with a change in the parametric study, where the ultimate load when using non-prismatic beams decreased by (4-11) % compared to prismatic beams. On the other hand, deformations and energy absorption capacity increase (noting that the amount of concrete is not equal). The ultimate beam load increased by 19% and 39% when the compressive strength was increased from 36 MPa to 54 MPa and 69 MPa respectively. While the ultimate load decreases by 9% when changing the a/d from 1.5 to 2.5.

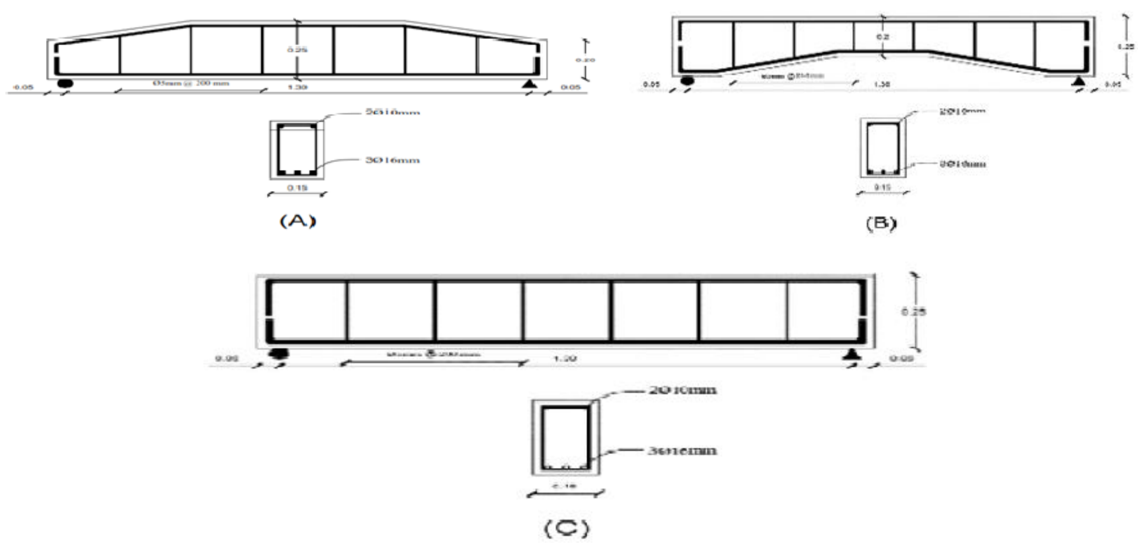

Figure (2-8) Geometry for the test specimens of the research of Qissab and Dhaiban, (2015)

Balduzzi (2016), presented a theoretical study to discuss the equilibrium, compatibility, and constitutive equations for a non-prismatic planar beam especially the model proposed based on the standard Timoshenko kinematics. A simple beam model was derived describing the effect of non-prismatic shape on the beam behavior and motivating the terms of the

equations with mathematical and physical arguments. He presented several numerical and analytical solutions and compared them with previous studies, and summarized the conclusions as follows. (i) The simple model has proven its efficiency and accuracy in predicting the actual behavior of non-prismatic beams. (ii) The stress distribution is not insignificant as in prismatic beams, especially the shear stresses, where the horizontal stresses and bending moment depend in addition to their dependence on the vertical stresses. (iii) The non-prismatic shape makes deformations dependent on all the stresses, which is the opposite of prismatic beams. (iv) The behavior of non-prismatic beams is completely different from that of prismatic beams, even if the cross-sectional change is minimal. (v) Shear and bending problems are closely related.

AlAli et al (2022), experimentally studied prismatic and non-prismatic reinforced beams under a monotonic load. The parametric study includes a variety of the inclination angle of the beam depth at edges, where four beams with different h_2/h_1 (1, 1.33, 1.98, and 4.24) were studied, as shown in **Figure (2-9)**. Note that the volume of concrete for the specimens was unequal. The results showed that changing the h_2/h_1 from 1 to 1.33, 1.98, and 4.24 reduced the ultimate load by 4%, 14%, and 41%, respectively, due to the decrease in the volume of the concrete.

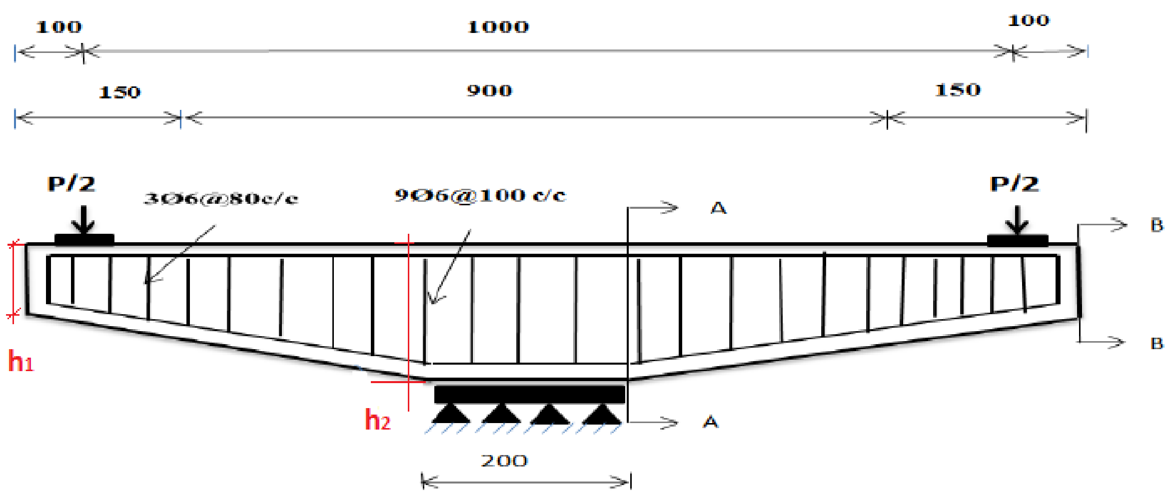

Figure (2-9) Geometry for the tested beams of the research of AlAli et al (2022)

2.4: Research studies of the Reactive Powder Concrete:

Rahmani et al (2011), presented an experimental study of adding polypropylene fibers (PPF), glass fibers (GF), and steel fibers (SF) to concrete to find out their effect on the durability properties of concrete. The properties included compressive strength (f_c'), flexural strength (f_r), gas permeability, water penetration, and electrical resistivity. Fiber volume ratios of 0.125%, 0.125%, and 0.5% were added for PPF, GF, and SF, respectively. The results showed that adding PPF and GF increases f_r, gas permeability, water penetration, and electrical resistivity and reduce in f_c' compared to plain concrete. In comparison, the presence of SF in concrete increases f_c', f_r, gas permeability, and water penetration while reducing electrical conductivity resistance. **Figure (2-10)** shows the results of the tests for all types of concrete used.

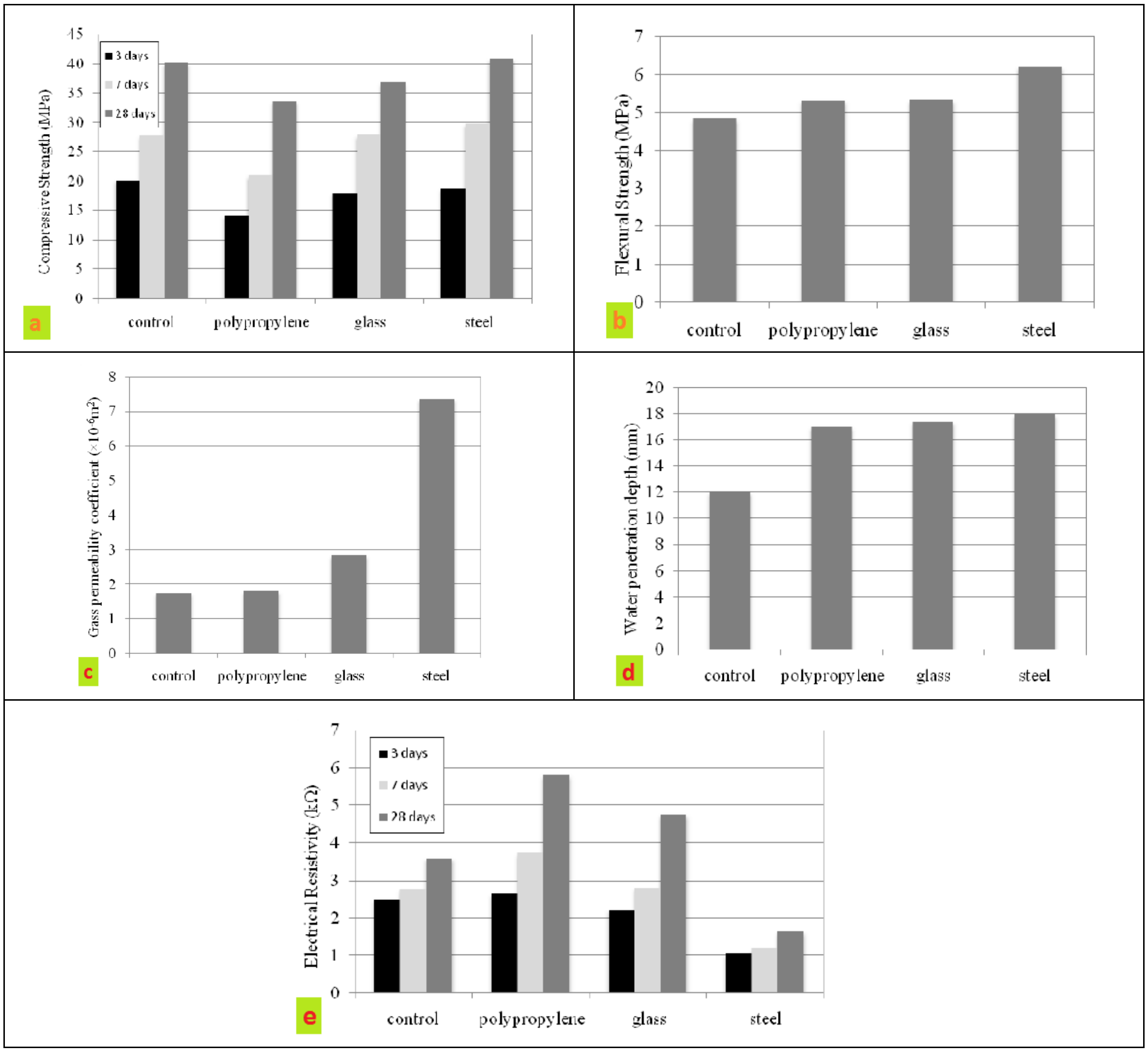

Figure (2-10) a. compressive strength b. flexural strength c. gas permeability d. water penetration e. electrical resistivity for the research of Rahmani et al (2011)

Kushartomo and Ivan (2017), presented experimental research to find out the effect of the addition the glass fibers (GF) and steel fibers (SF) to reactive powder concrete. In this study, different percentages of GF and SF (1%, 1.5%, 2%) by volume were added and their effect on compressive strength, flexural strength, splitting strength, and concrete density was investigated. The samples were steam cured for 12 hours. The results showed that the best percent for GF was 2%, which gives the best results for the

mechanical properties of concrete, while the best percent for steel fibers was 1.5%. **Figure (2-11)** shows the results of the mechanical tests of the samples tested.

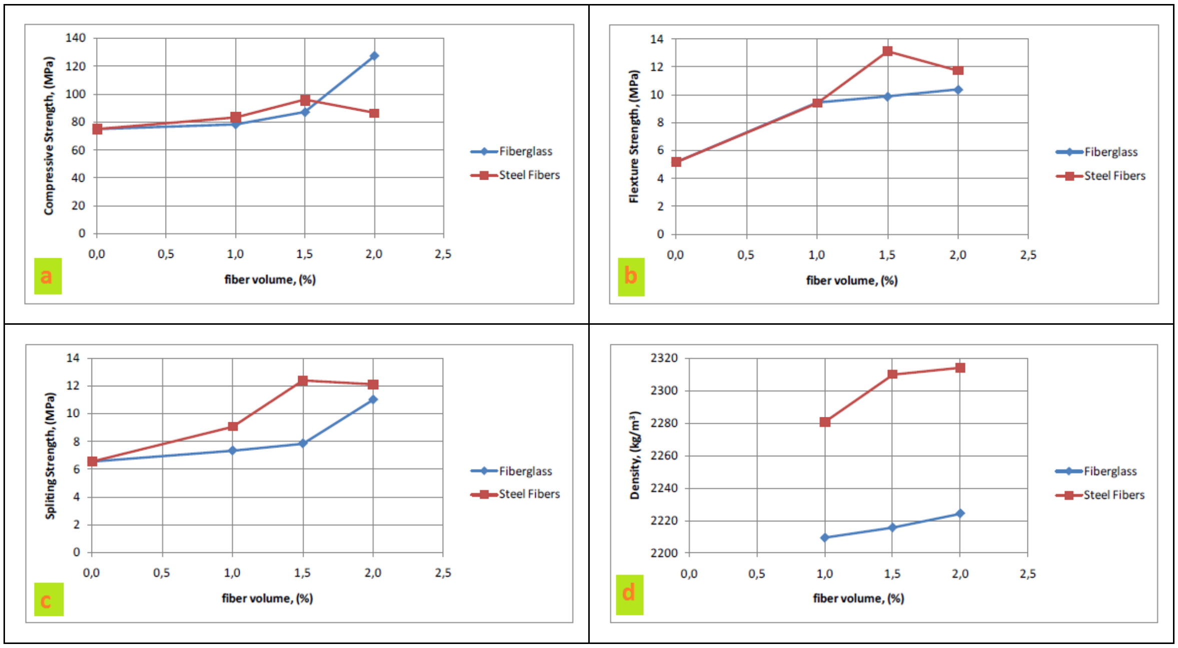

Figure (2-11) a. compressive strength b. flexural strength c. splitting strength d. concrete density for the research of Kushartomo and Ivan (2017)

Algburi et al (2018), presented experimental research to study the effect of the presence of different types of fibers in the RPC mixture. In this study, four types of the concrete mixture were used, including RPC without fibers, RPC with steel fibers (SF) with a volume percentage of 1.5%, RPC with glass fibers (GF) by 1.5%, and RPC with hybrid steel and glass fibers(SF-GF) by 1.5%.The study included the effect of fiber change on compressive strength (f_c'), modulus of elasticity (E_{RPC}), splitting strength (T), and direct shear strength(τ). The results showed an improvement in all RPC properties when adding SF, while the properties deteriorated when adding GF, or SF-GF except for the direct shear strength, which improved. By adding SF,

the increase in RPC properties was 6.6%, 3%, 30%, and 150% for f_c', E_{RPC}, T, and τ, respectively. While when adding the GF, the decrease in the RPC properties was 10%, 5%, and 25% for f_c', E_{RPC}, and T respectively, while τ increased by 60%.

Raza et al (2020), presented experimental research to study the behavior of Reactive Powder Concrete (RPC) using different fibers. The experimental program included the addition of steel fibers (SF), carbon fibers (CF), and glass fibers (GF), as well as the addition of a hybrid of fibers, which included a hybrid of SF&CF, SF&GF, and CF&GF. The study focused on compressive strength, splitting strength, flexural strength, modulus of elasticity, and total energy absorbed. The results showed a clear improvement in the mechanical properties of RPC when adding fibers. The compressive strength increases by (7.26-13.6) %, while the splitting strength increases by (9.1-32.1) %, and the bending strength increases by (17.2-38.9) %.The modulus of elasticity of RPC increases slightly with the addition of fibers, and it depends on the compressive strength and is not affected by the type of fiber. As for the total absorbed energy, it also improves, as the increase was (37-200) %. A summary of what has been mentioned, the addition of fibers improves all mechanical properties of RPC, and the effect of fibers varies according to the type of fibers, and the best types of fibers were SF, then SF & CF, and then SF & GF.

2.5: Research Studies of the Hybrid Concrete:

Mohammad (2013), presented an experimental study of the bending behavior of 24 beams of reinforced concrete with simple support and conventional concrete hybrid with reactive powder concrete (RPC) in the

tensile and compression zone. The variables of the study include a change in the ratio of the longitudinal reinforcing steel (ρ), the percentage of the steel fiber volumetric in the RPC mixture (0%, 1%, 2%), and the ratio of the thickness of the RPC layer to the beam depth (h_{RPC}/h) (0, 0.25, 0.5, 1) as shown in **Figure (2-12)**. The results showed that the effect of having RPC in the compression zone is better than its presence in the tension zone, especially when it is an over-reinforced beam. The effect of (ρ) is very high, as when the reinforcement was increased (0.0121-0.0336), the ultimate load increased by 79%, 101%, and 147% for hybrid beams in the tension region with an h_{RPC}/h of 0.25, 0.5, and 1, respectively. While the increase for a hybrid beam in the compressive region of h_{RPC}/h by 0.25 was 111%.

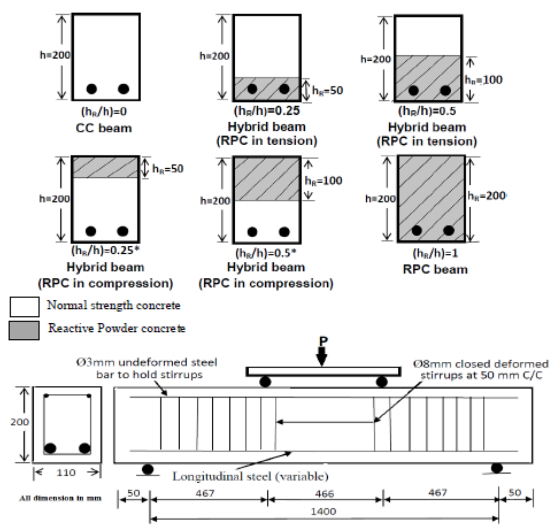

Figure (2-12) Some of the Cases of the research of Mohammad (2013)

Al-Amry (2013), presented an experimental study of deep beams with simple support using normal-strength concrete (NSC) and hybridized with high-strength concrete (HSC), where the HSC was in the compression zone while the NSC was in the tension zone. The study included a change in the

thickness of the hybridization layer of the HSC (25% and 50% of the total depth of the beam), as shown in **Figure (2-13)**. The parametric study also included a change in the method of casting specimens (monolithically and casting in different two times) and also studied the effect of the presence and absence of minimum reinforcing steel web. Use NSC with a compressive strength of 25MPa and HSC with a compressive strength of 45MPa. The results showed that using hybridization with HSC with a layer thickness of (25% - 50%), the increase in the ultimate shear was (11.2% - 19.5%) and (16.75% - 22.25%) for beams without and with web reinforcement, respectively. When casting specimens at different times and placing 1 mm epoxy between the two layers, the ultimate shear decreases by 5% and 4.3% for specimens without and with web reinforcement, respectively.

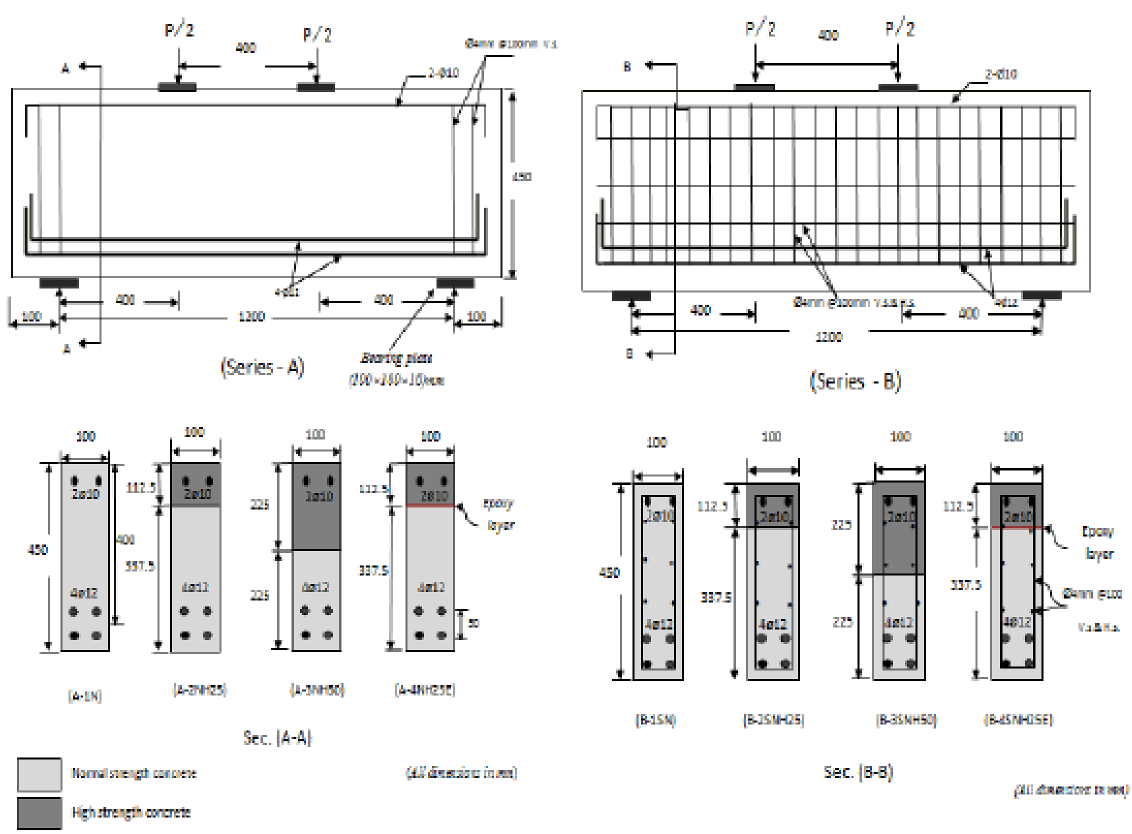

Figure (2-13) Cases details study of the research of Al-Amry (2013)

Al-Hassani et al (2015), studied the flexural behavior of a hybrid T-section beam containing normal-strength concrete (NSC) and reactive powder concrete (RPC) to investigate the possibility of using the two materials in the same section for the purpose of benefiting from the good properties of the RPC and the low cost of the NSC. **Figure (2-14)** shows the cross-sections of the tested beam. The researchers used beams that have NSC, RPC, and three beams with the hybrid of NSC and RPC. The results showed that when using hybrid concrete, enhanced the characteristics of the section for ultimate load, first crack load, and deflection, and the use of RPC in the web area and NSC in the flange area had better results than if the opposite was used.

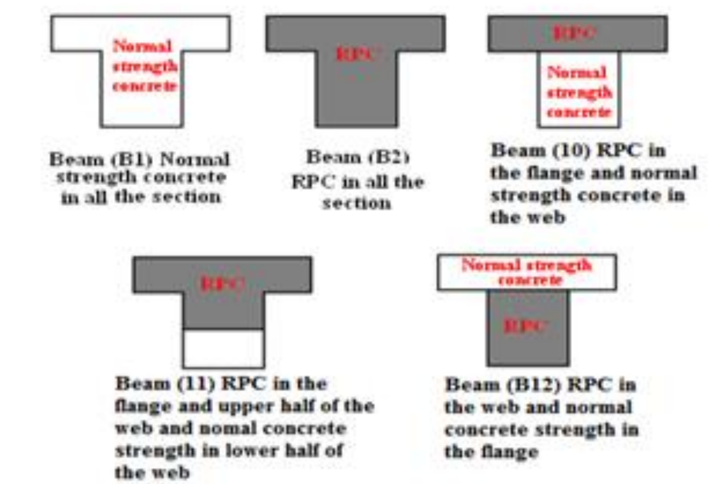

Figure (2-14) Cross section of the tested beam by Al-Hassani et al (2015)

Abd AlRadha (2015), presented experimental and theoretical studies of composite beams by taking twelve specimens that dealt with the presence of hybrid concrete, which consists of normal strength concrete in the slab with dimensions (400*50) mm and girder steel fiber reactive powder concrete with dimensions (100*150) mm and 1600 mm length of the beam. **Figure (2-15)** shows the cases dealt with in this study. The effect of hybridization of

concrete with different amounts of RPC has been studied as well as the effect of steel fiber type was studied (2% by volume ratio straight ultra-fine, or 2% hook, mixing between the straight and hook by 1%+1%, and 0% steel fiber). The experimental results showed that using RPC in all depths of the beam increases the ultimate load by 79%, while the ultimate load increases by 64% when using RPC only in the lower half of the depth of the beam. The results also showed that the best steel fibers were 2% straight, followed by (1% straight + 1% hook), then 2% hook and the weakest was 0% steel fibers. The percentage of decrease in the ultimate load of the specimens compared to the 2% straight specimen was 3%, 8%, and 14% to (1% straight + 1% hook), then 2% hook and the weakest 0% steel fiber, respectively.

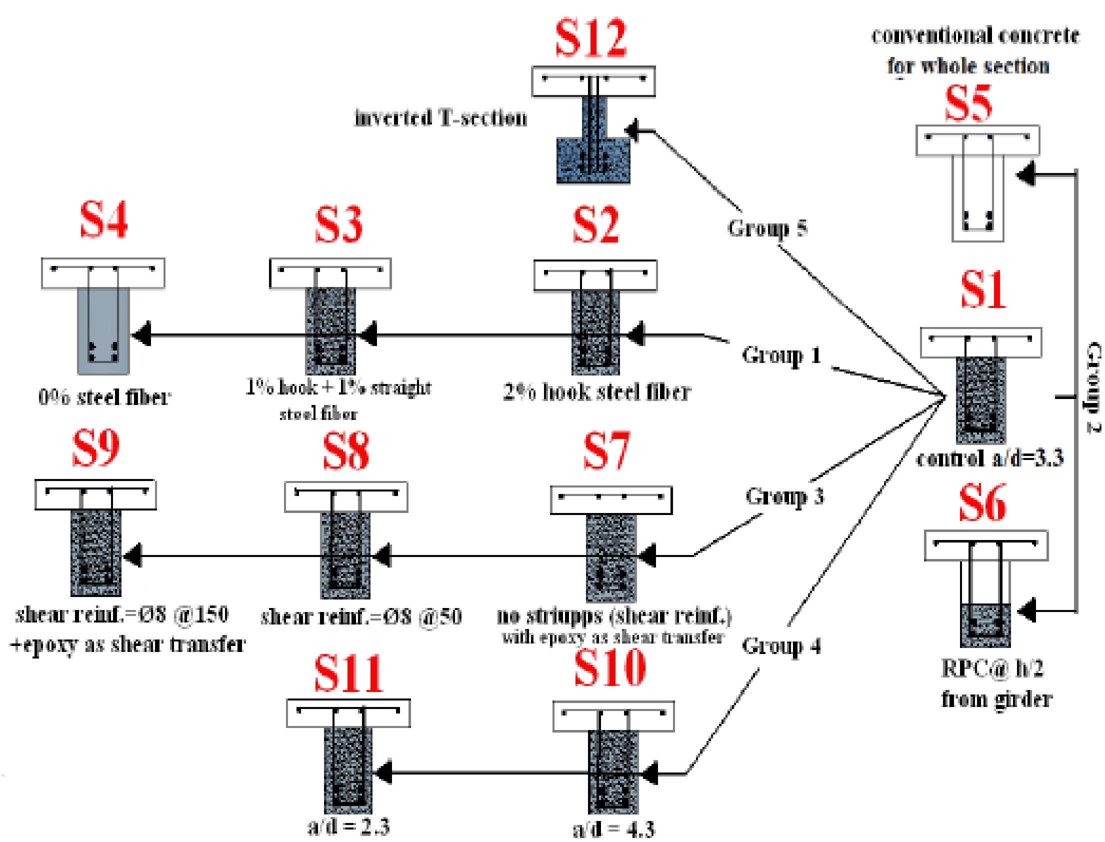

Figure (2-15) The case study of the research of Abd AlRadha (2015)

Resif (2020), presented a study on the use of reactive powder concrete with various types of fibers (steel fiber, polypropylene, and glass fiber) as a cementation repair material for the damages found in concrete structures. The study included two stages to choose the best type of fiber. The first stage included choice of the best bond between RPC and normal strength concrete (NSC) or high strength concrete (HSC) by using a slant shear test. The second stage was making a prism with dimensions (100*100*400) mm from NSC or HSC with a void at the bottom with dimensions (10*100*200) mm filled with RPC and tested by flexural strength test. The results showed that the best type of fiber was glass fiber, as it is a flexible, bendable material that does not lose its strength when bent, and thus the possibility of overlapping it with the substrate concrete within the cavities in it. Unlike steel fibers, which are a hard material with little bendability, so they overlap within the cavities of substrate concrete is minimal. Also, when bent, it leaves cavities in the contact area, which reduces the adhesion strength. After determining the best type of fiber for RPC that can be used as a repairing material, beams with dimensions (125*200*1280) mm were taken with voids that dimensions and locations as shown in **Figure (2-16)** for the purpose of studying the effect of the presence of RPC. The results showed that the beam with damaged concrete and repaired by RPC has better properties than the undamaged concrete beam and that the best location for hybridization is the compression zone of the beam, where the increase is 30%, while the increase is 9.5% and 6.8% when the hybridization is in the tensile zone and shear zone, respectively.

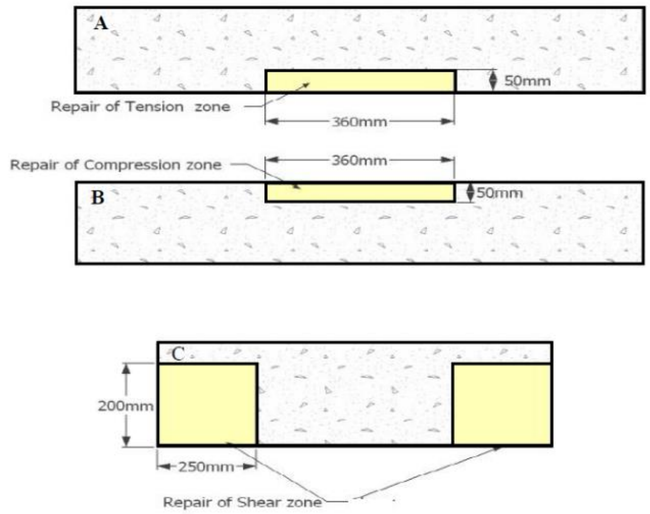

Figure (2-16) Repairing zones in the research of (Resif, 2020)

2.6: Research Studies of the Repeated Load Members:

Archundia-Arandaa et al (2013), presented ten prototypes of simply-supported reinforced concrete beams with prismatic and non-prismatic sections (two prismatic and eight non-prismatic) under cyclic load to study the development of shear failure. Five beams (one prismatic and four non-prismatic) were tested without stirrups, while five beams (one prismatic and four non-prismatic) were tested with minimum stirrups, as the stirrups were designed according to the requirements of the prismatic beam. The percentage of the non-prismatic section (h_2/h_1) was changed (1-1.8) to study its effect on the shear strength, as shown in **Figure (2-17).** It was shown that the results of non-prismatic beams have cyclic shear behavior different with respect to prismatic beams, having a higher deformation and energy dissipation capacity because the non-prismatic beams favor the arching action in the non-prismatic length as the main mechanical resistance, and it is also shown that the non-

prismatic beams develop a smooth crack pattern and make the model less brittle in shear failure.

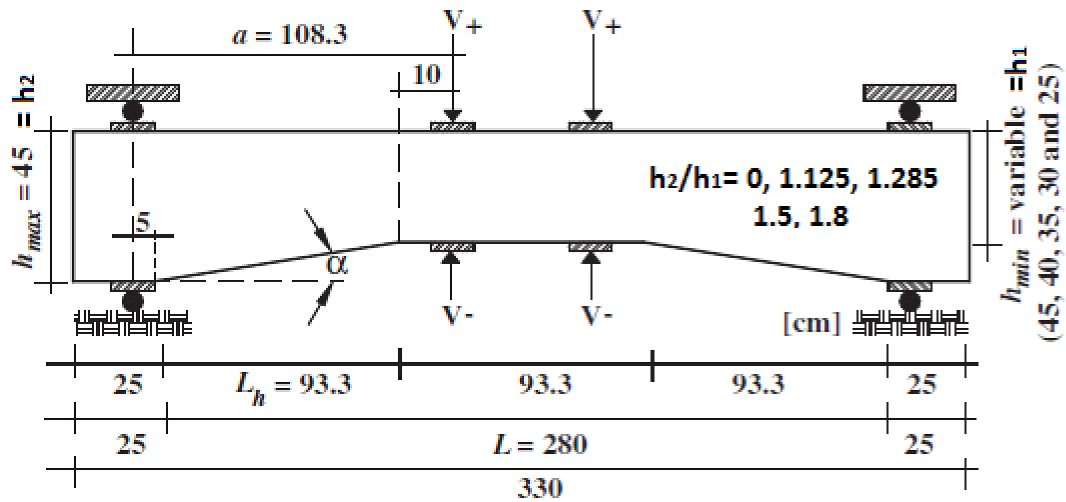

Figure (2-17) Geometry for the test specimens of the research of Archundia-Arandaa et al (2013)

Hassan and Faroun (2016), studied the effect of repeated loads on deep beams with simple support under two points loads. Where the study dealt with the effect of repeated loads on deep beams with different concretes (conventional concrete and normal strength concrete with hooked ends steel fibers), hybrid beams between the two types of concrete, the change in the ratio of steel fibers in concrete (1% and 2%), and the percentage of reinforcing steel web (0, 0.003, and 0.004). **Figure (2-18)** shows the dimensions and details of the web-reinforcing steel in the tested specimens. In the repeated load, five cycle loads were applied, and each cycle with a maximum load equal to 70% of the ultimate load for a monotonic load specimen. The results showed that the percentage of decrease in the ultimate load as a result of the effect of the repeated load ranged from (2%-27%) depending on the variables of this study.

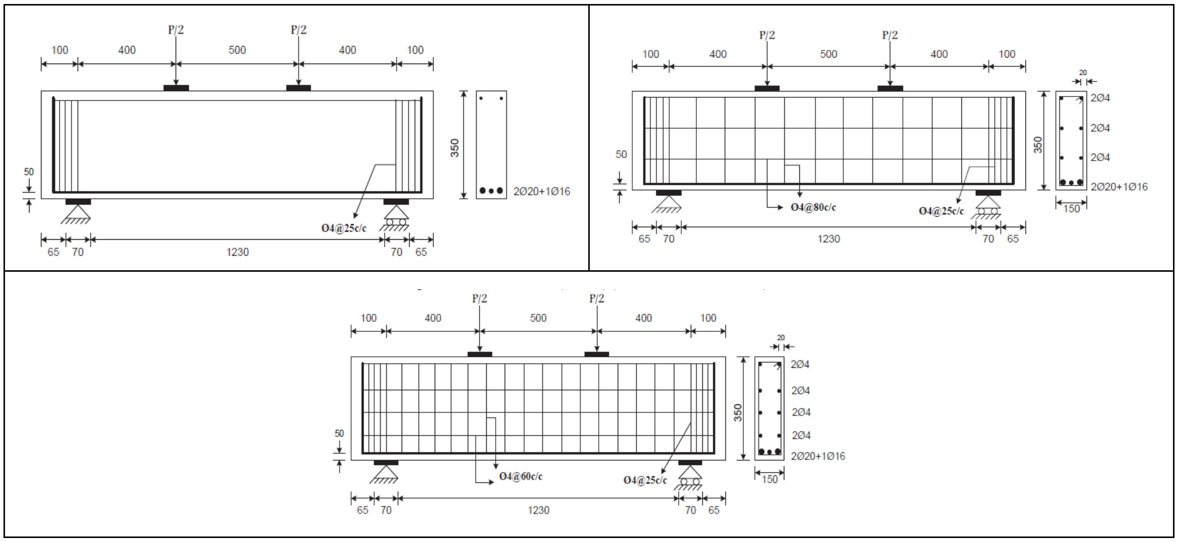

Figure (2-18) Beams dimension and reinforcement details for the research of Hassan and Faroun (2016)

Dawood and Abdulkhaleq (2017), Presented an experimental study of the behavior of continuous beams with prismatic and non-prismatic sections under monotonic and repeated loading. The continuous beam behavior with reactive powder concrete was studied under the effect of repeated load in two cases (the first case was applying 15 cycles from 0-0.75 of ultimate monotonic load (Pu) and then applying load until the failure of the specimen, while the second case of applying five cycles from 0-0.25 of Pu and five cycles of 0-0.5 of Pu and five cycles of 0-0.75 of Pu and then applying the load until the failure of the specimen) as well as the study included increasing the beam section at the middle support only in the form of a tipper (non-prismatic section) as shown in **Figure (2-19)**. The results showed that the effect of applying repeated loads was to increase the deflection for both prismatic and non-prismatic models, where the increase was (29.24%-33%) and (15.38%-29.94%) for fifteen repeated loads (0-0.75 Pu) and the incremental increase case, respectively. While the ultimate load did not decrease significantly, as

the decrease ranged for all cases of the specimens (0%-0.8%). The effect of the tapering ratio was to increase the ultimate load up to 14.39%.

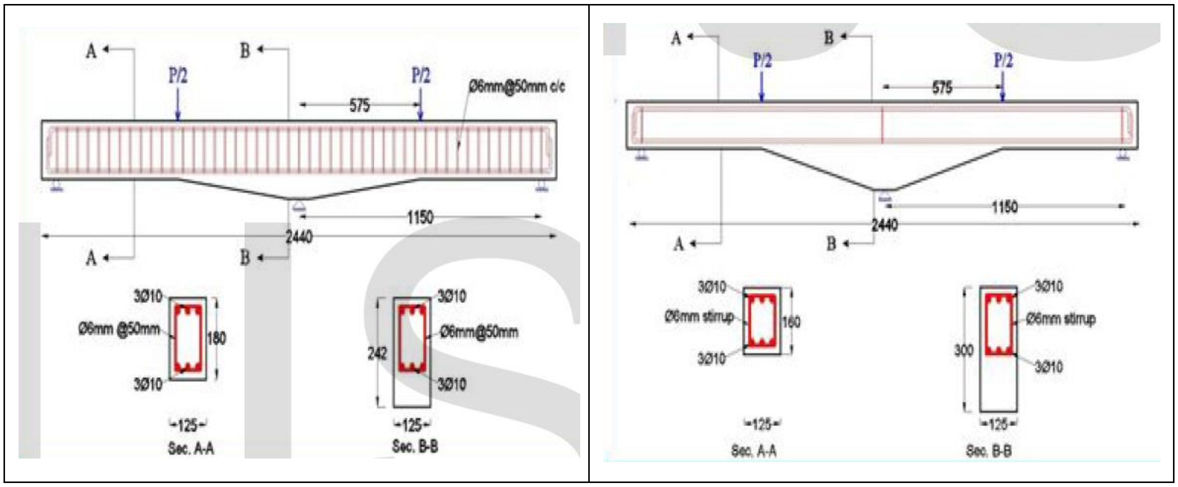

Figure (2-19) Beam dimensions of the research of Dawood and Abdulkhaleq (2017)

Al-Saffar et al (2020), presented an experimental study of six ultra-high strength concrete flexural beams under monotonic and repeated load. The parametric study for this research was the change in the ratio of main steel reinforcement (ρ) to tensile stresses. Where three values of ρ (0.0129, 0.0204, and 0.0323) were used, and for each ratio two specimens were made, one of which was tested under monotonic load and the other under repeated load. **Figure (2-20)** shows the dimensions and details of the reinforcing steel for the tested specimens. In the repeated load test, the specimen was loaded and unloaded with gradual increments for each cycle. For example, in the first specimen, the load was applied in the first cycle up to 35% of the ultimate load for the same specimen under a monotonic load, then the specimen was unloaded and applied again with an increase in the amount of the maximum load, where the maximum load was for the second, third, and fourth cycles, 52%, 69%, and 87%, respectively, and in the fifth cycle, the loaded was

applied until failure. The results showed an increase in the carrying capacity of the specimens when applying repeated loads in this way by (2 %- 6 %).

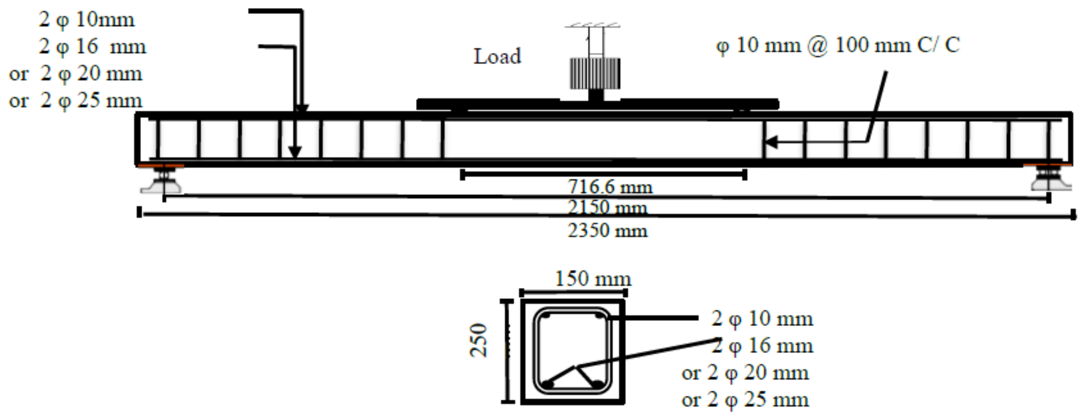

Figure (2-20) Beam cross section and reinforcement details for Al-Saffar et al (2020) research

2.7: Summary:

The most important points drawn from previous studies can be summarized as follows:

1. Some previous research aimed to strengthen the reinforced concrete frames in different ways (changing the geometry of the sections, strengthening by CFRP laminate, strengthening with carbon fiber reinforced rod, using bracing between the members of the frame) to get the best results under the influence of monotonic and repeated load and earthquakes.
2. In the research that dealt with the use of non-prismatic sections in structural members, the shape of the section was determined based on previous studies or the experience of designers, as there are no international standards that adopt determining the shape of a non-

prismatic member. The use of a non-prismatic section increases the deflection of the member and thus makes the member less fragile, especially with members that fail in shear.

3. The use of RPC in structural members is very beneficial as it increases the structural member's load capacity and reduces cross-sections, and the presence of fibers in RPC mixtures improves all mechanical and durable properties of concrete. With the development of science, many fibers appeared, each with its own positive characteristics that distinguish it from the other fibers. These fibers are SF, GF, CF, and PPF.
4. Hybrid members are members that contain more than one type of concrete, and it was resorted to strengthen weaknesses in conventional concrete in the most dangerous regions of the structural member at the lowest cost, through the use of concrete with better specifications. Previous studies showed good compatibility between conventional concrete and RPC, especially RPC with glass fibers, and the absence of any isolation between the two types of concrete.
5. Testing of specimens under a repeated load usually reduces the ultimate load of the structural members by different percentages according to the method of applying the repeated load, the type of concrete used, and the reinforcing steel of the structural member.
6. In this study, a concrete frame will be made of prismatic and non-prismatic sections, with a large to small depth of **1.3**. The reason for choosing non-prismatic sections is to obtain high-benefit structural members through the redistribution of concrete according to the location of critical stresses, since most of the research that dealt with non-prismatic sections did not study the redistribution of concrete, but

worked to reduce or increase concrete when studying this subject. A ratio of **1.3** was chosen because it is located within a range that gives the best behavior for the concrete frame, according to a previous theoretical study. Also, the use of GRPC due to its lack of use in the structural members and its high permanent specifications, and its good compatibility with conventional concrete when hybridized in the structural members. The specimens will be tested under a repeated load, as it is the most dangerous to the frame load, and the results will be discussed with the monotonic load frames.

CHAPTER THREE

Chapter Three

Experimental Work

3.1: Introduction:

The experimental program in this chapter includes a presentation of material properties (cement, fine and coarse aggregates, silica fume, super plasticizers, steel reinforcing bars, and steel and glass fibers for reactive powder concrete). It also presents mixing procedures and trial mixtures, a description of specimen details for the plane concrete frame (dimensions and reinforcement), specimen preparation (casting and curing procedures), and test procedure.

3.2: Material Properties:

3.2.1: Cement:

An ordinary Portland cement manufactured, was used throughout the experimental work for both reactive powder concrete (RPC) and conventional concrete. The compressive strength of the cement paste is shown in **Table (3-1)**. The physical and chemical properties of the cement used are presented in **Appendix A**. Test results indicated that the adopted cement conformed to Iraqi specification **(IQS No.5, 2019)**.

Table (3-1) Compressive strength of the of cement paste *

Age of sample	Test Results	IQS No. 5/2019
3 days (MPa)	30.42	Minimum 15
7 days (MPa)	36.23	Minimum 23

* The tests were carried out in the laboratories of the College of Engineering / University of Kufa.

3.2.2: Fine Aggregate (Sand):

Al-Najaf natural sand was used as fine aggregate for both reactive powder concrete and conventional concrete mixes. The results of sulfate content, specific gravity, and absorption of the fine aggregate were shown in **Table (3-2)**. The results showed that the fine aggregate, according to the Iraqi specification **(IQS No. 45/1984)**.

Table (3-2) Physical properties of fine aggregate*

Physical properties	Test results	IQS No. 45/1984
Specific gravity	2.7	_
Sulfate content	0.33 %	Maximum 0.5 %
Absorption	0.76 %	_

* The tests were carried out in the laboratories of engineering consulting bureau of the university of Kufa- faculty of Engineering.

For conventional concrete, the grading of the fine aggregate was shown in **Table (3-3)** and **Figure (3-1)** while the RPC used fine aggregate with a maximum size of 600 μm. **Table (3-4)** and **Figure (3-2)** show the grading of fine aggregate used in RPC. The results indicated that the fine aggregate grading for both types of concrete was according to the Iraqi specification **(IQS No.45/1984)**.

Table (3-3) Grading of the fine aggregate used for conventional concrete*

Sieve Size (mm)	Cumulative Passing %	IQS No. 45/1984, zone 3
4.75	98.9	90-100
3.36	94.7	85-100
1.18	87.9	75-90
0.6	74.1	60-79
0.3	29.2	12-40
0.15	2	0-10

* The tests were carried out in the laboratories of engineering consulting bureau of the university of Kufa- faculty of Engineering.

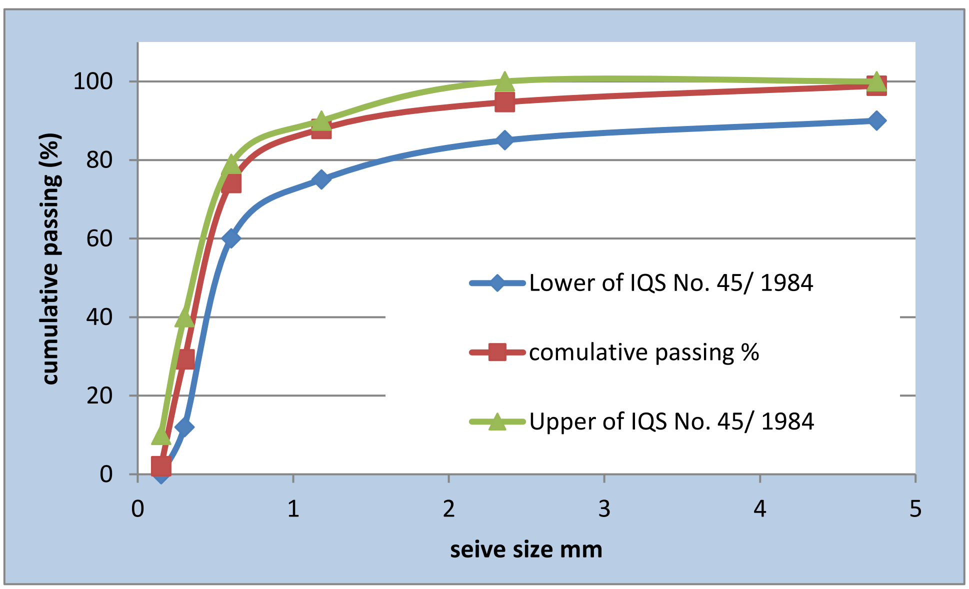

Figure (3-1) Grading sketches of fine aggregate of conventional concrete

Table (3-4) Grading of the fine aggregate used for RPC *

Sieve Size (mm)	**Cumulative Passing %**	**IQS No. 45/1984, zone 4**
4.75	100	95-100
3.36	100	95-100
1.18	100	90-100
0.6	98.5	80-100
0.3	37.3	15-50
0.15	3	0-15

* The tests were carried out in the laboratories of engineering consulting bureau of the university of Kufa- faculty of Engineering.

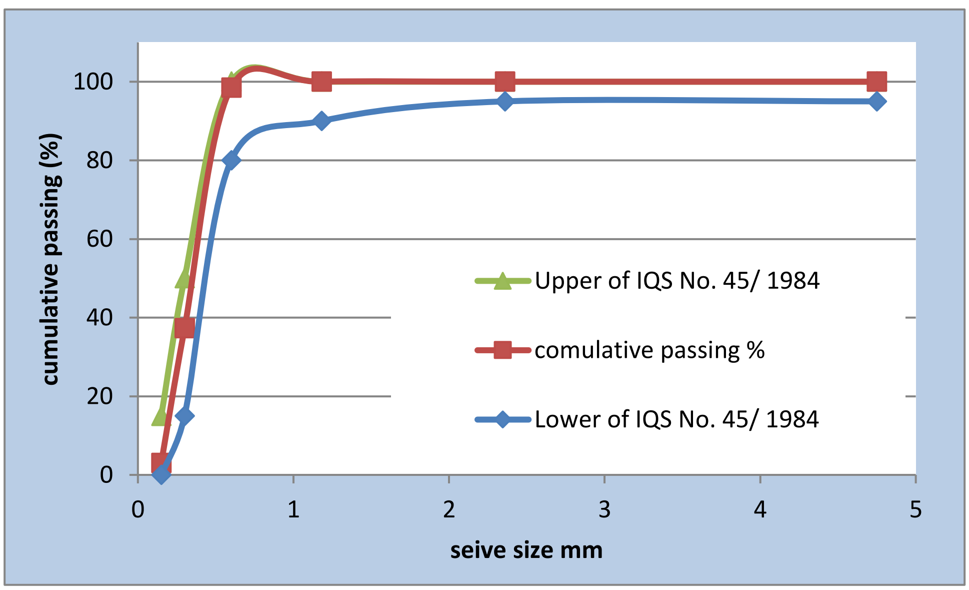

Figure (3-2) Grading sketches of fine aggregate of RPC

3.2.3: Coarse Aggregate (Gravel):

Coarse aggregate with a maximum size of 19mm was used in the conventional concrete mixes. It was washed, then stored in the air to dry the surface, and then used after stored in a saturated dry surface condition. **Tables**

(3-5), (3-6), and **Figure (3-3)** describe the grading and physical characteristics according to **(IQS No.45/1984)**.

Table (3-5) Grading of the coarse Aggregate *

Sieve size (mm)	Cumulative passing (%)	IQS No. 45 /1984
19	100	95-100
10	58.8	30-60
5	2.1	0-10

* The tests were carried out in the laboratories of engineering consulting bureau of the university of Kufa- faculty of Engineering.

Table (3-6) Physical properties of coarse aggregate*

Physical Properties	Test Results	IQS No. 45 /1984
Specific gravity	2.67	
Sulfate content	0.07%	≤ 0.1 %
percentage loss in Loss Anglos test	17.3%	≤ 35%

* The tests were carried out in the laboratories of engineering consulting bureau of the university of Kufa- faculty of Engineering.

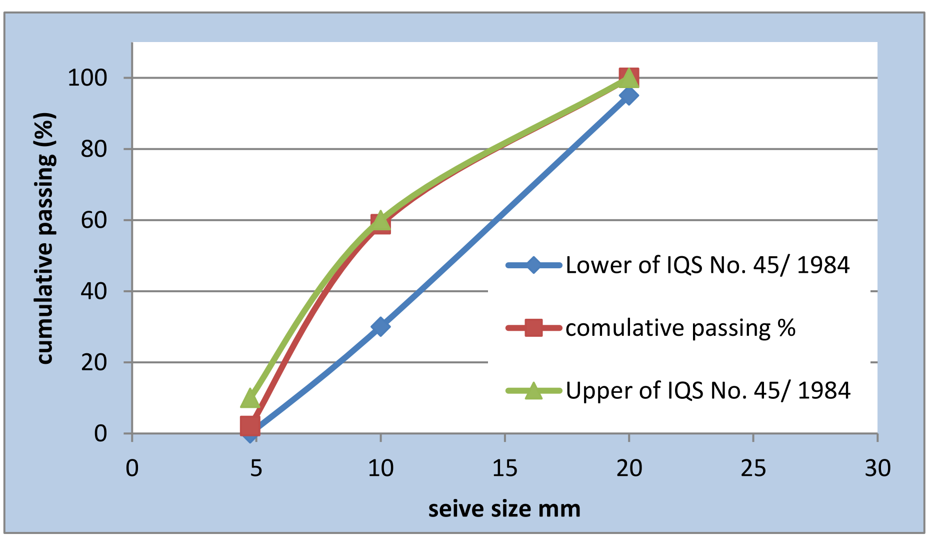

Figure (3-3) Grading sketches of coarse aggregate

3.2.4: Water:

Drinking water was used for mixing and curing all the concrete specimens.

3.2.5: Silica Fume:

Silica fume, as defined in **(ACI 116R-00)**, is "very fine noncrystalline silica produced in electric arc furnaces as a by-product of the production of elemental silicon or alloys containing silicon". The silica fume, which condenses from the gases escaping from the furnaces, has a very high content of amorphous silicon dioxide and consists of very fine spherical particles **(Plate 3-1). (ACI 234R-06)**

It has been found that Slica Fume improves compressive strength, especially at an early age (before 90 days), reduces bleeding, increase bond strength, and protects reinforcing steel from corrosion **(ACI 234R-06)**. In this research, silica fume was used Formerly which is known as Mastertop Aggregate SRA as shown in **Plate (3-2).**

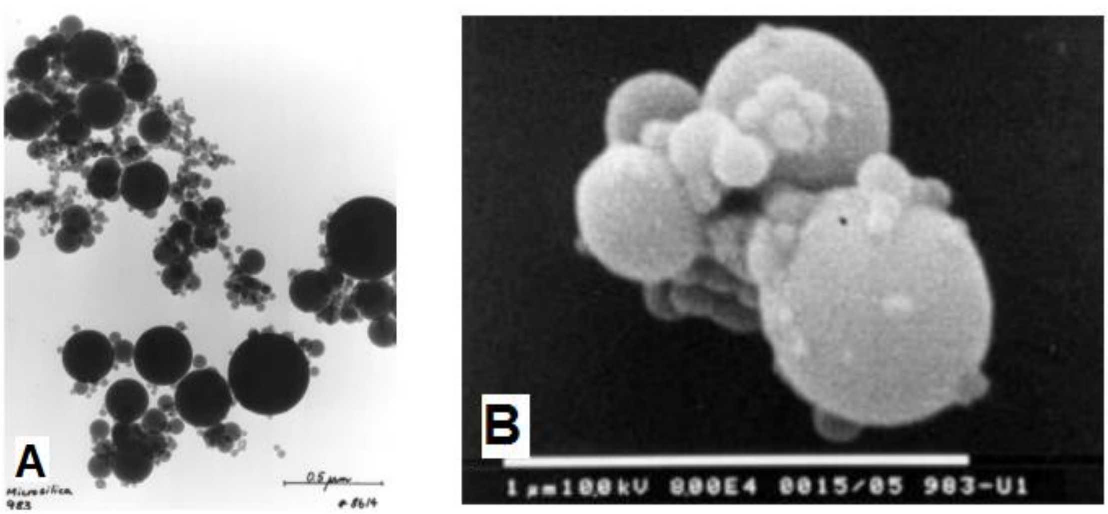

Plate (3-1) A: Transmission electron microscope micrograph of silica fume. B: Scanning electron microscope micrograph of silica fume. (Image courtesy of Elkem ASA materials.) (ACI 234R-06)

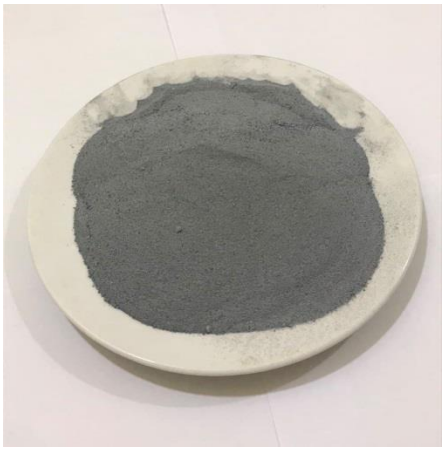

Plate (3-2) Silica fume used in research

3.2.6: Super Plasticizer:

Construction chemicals, UAE. MasterGlenium 54 has not only been developed for applications primarily in precast, but also ready-mix concrete industries where the highest durability and performance are required. It increased early and ultimate compressive strengths, increased flexural strength, reduced shrinkage and creep, increased durability, high workability without segregation or bleeding, less vibration required, and improved surface finish **(MasterGlenium® 54)**. It complied with ASTM C494 Types A and F. The properties of the MasterGlenium 54 are presented in **Table (3-7).**

Table (3-7) Typical properties of MasterGlenium 54 *

Main action	MasterGlenium 54
Form	Whitish to straw-colored liquid
Relative density	1.07
pH	5-8

* The data was supplied by the manufacturer.

3.2.7: Fiber for Reactive Powder Concrete:

Two types of fibers were used in reactive powder concrete mixes in this study; steel fibers and glass fibers:

3.2.7.1: Steel Fiber:

Micro straight steel fibers were used throughout this work with an aspect ratio (L/D = 60). This type of fiber was manufactured by HONGTU STEEL FIBER, China as shown in **Plate (3-3)**. The properties of the used steel fibers are presented in **Table (3-8).**

Figure (3-3): Measurement of the straight steel fiber.

Table (3-8) Physical properties of the straight steel fiber *

Property	Specifications
Surface	Copper coated
Relative Density	7860 Kg/m3
Tensile Strength	Minimum 2850MPa
Form	Straight
Melting Point	1500°C
Length	12mm – 14mm
Diameter	0.2mm - 0.25mm
Aspect ratio (L/D)	60

* The data was supplied by the manufacturer

3.2.7.2: Glass Fiber:

Alkali–resistant glass fibers were used in this research. It was manufactured by OSCRETE 12mm HP in the United Kingdom as shown in **Plate (3-4)**. OSCRETE 12mm HP fiber complies with the requirements of ASTM C1116/C. The physical and mechanical properties of this fiber was listed in **Table (3-9).**

Plate (3-4): Measurement of the straight glass fiber.

Table (3-9) Physical and chemical Properties of the Glass Fiber *

Property	Value
Tensile strength	1,700MPa
Modulus of elasticity	72,000MPa
Fiber length	12mm
Fiber diameter	0.014mm
Aspect ratio	857
Specific gravity	2680 kg/m^3
Softening temperature	860°C

* The data was supplied by the manufacturer.

3.2.8: Steel Reinforcement Bar:

In this study, a deformed steel reinforcement bar was used for all diameters. A reinforced bar with a diameter (Ø10mm) was used for the longitudinal reinforcement of the beams and columns, while a reinforced bar with a diameter (Ø6mm) was used for the stirrups and ties for all specimens. Three tensile specimens for each size were tested under direct tension as shown in **Plate (3-5)**. The results of the testing are represented in **Table (3-10)**.

Plate (3-5) Steel reinforcement under direct tension test

Table (3-10) Results of steel reinforcement bar tests

Specimen diameters	Yield strength (MPa)	Ultimate strength (MPa)	Elongation (%)	ASTM A615 Requirements (Grade 60)		
				Min. Yield Strength (MPa)	Min. Tensile Strength (MPa)	Elongation (%)
Ø 10	512	664	18	420	620	9
Ø 6	422	605	19			9

* Modulus of elasticity of steel bars (Es) is assume equal to 200,000 MPa.

* The tests were carried out in the laboratories of engineering consulting bureau of the university of Kufa- faculty of Engineering.

3.3: Concrete Mixes:

3.3.1: Reactive Powder Concrete (RPC):

The major parameters of the RPC mixture were cement content (**C**), the silica fume–cement ratio (**S/C**), the sand–cement ratio (**Sand**), the water–cementitious material ratio (cement and silica fume) (**W/Cm**), the super plasticizer-cementations ratio (**SP**), and the fiber content by volume (steel fiber (**SF%**) or glass fiber (**GF%**)). The optimum proportions of the major parameters of the mixture were selected by using several trial mixes and were tested with a compressive strength device, where three cubes were tested for each mixture at the age of 7 days and the age of 28 days. **Table (3-11)** and **Figure (3-4)** show the mixes used in this research, while all trial mixes tested are in **Table (B-1)** and **Table (B-2)** in **Appendix B**.

Table (3-11) Results of mixes for SRPC and GRPC used in this research *

Mix no.	Cement type	Cement content (kg/m^3)	S/C (%)	Sand (%)	SP (%)	W/ Cm (%)	SF% (volume ratio)	GF% (volume ratio)	Compressive strength (MPa)	
									7 days	28 days
1	ALJISER	950	25	105	3	22	1.5	-	67.9	89.2
2	ALJISER	950	25	105	3	22	-	1.5	54.4	76.2

* The tests were carried out in the laboratories of the College of Engineering / University of Kufa.

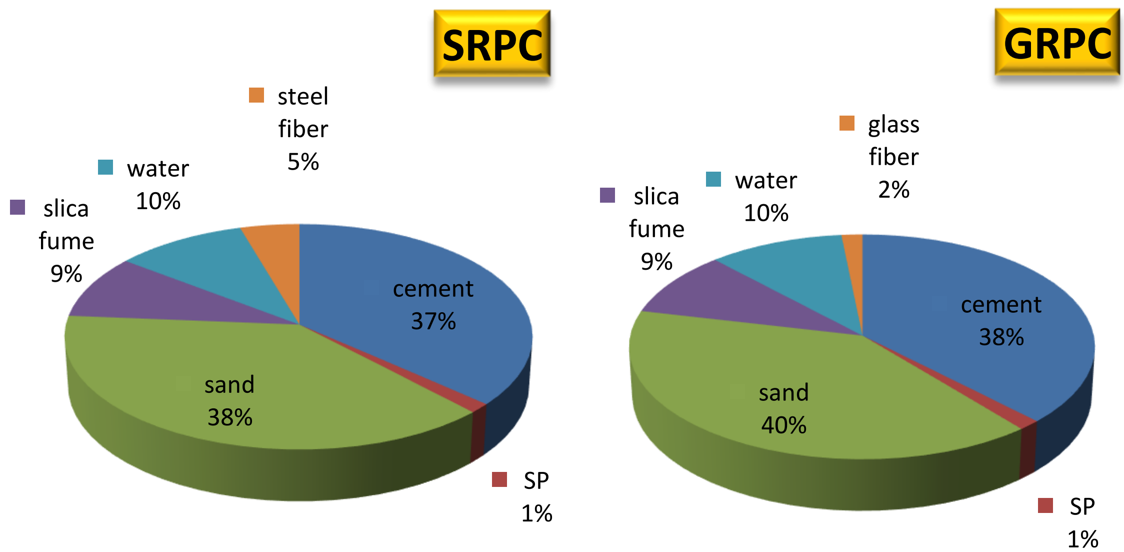

Figure (3-4) Materials proportion in SRPC and SRPC (% of total mix weight)

The mixing sequence of the RPC contents and the time needed to mix each material is necessary to obtain high compressive strength and other physical and mechanical properties. **Figure (3-5)** shows the sequence mixing for RPC where firstly, cement, sand, and silica fume are mixed for about 10 minutes. Then the super plasticizer and water are added in two steps and mixed for 10 minutes. When the mixture is able to flow, the glass fiber or steel fiber is added and mixed for an additional 5 minutes. **(Yanga et al, 2010)**

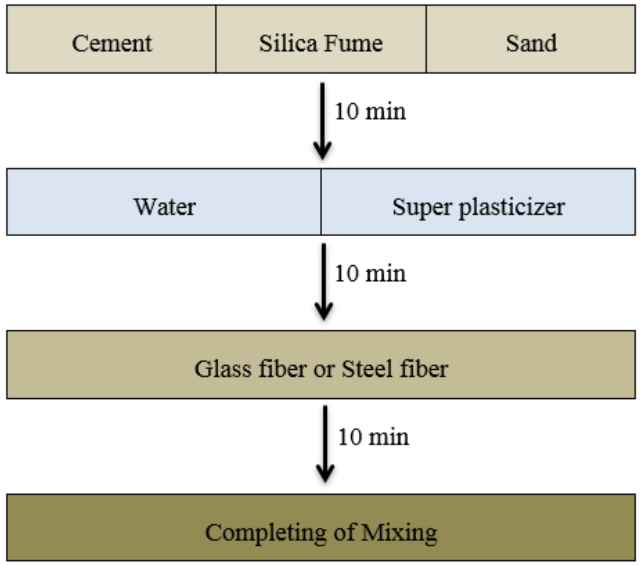

Figure (3-5) Mixing sequence of RPC adopted (Yanga et al, 2010)

3.3.2: Conventional Concrete:

The design of the conventional concrete mix used in this study was according to the **(ACI 211.1-2004)**. The results of the two design mixtures of three cubes (150*150*150) mm are shown in **Table (3-12).**

In this study, a concrete mix with a strength of (37.73 MPa) was used. **Figure (3-6)** shows the materials' proportion of the conventional concrete mix used.

Table (3-12) Compressive strength results for conventional concrete *

Mix no.	Cement content (kg)	Fine agg. Content (kg)	Coarse agg. Content (kg)	Water content (kg)	Compressive strength (MPa)	
					7 days	28 days
1	380	736	1024	205	25.8	37.73
2	365	848	1024	205	20.82	29.89

* The tests were carried out in the laboratories of the College of Engineering / University of Kufa.

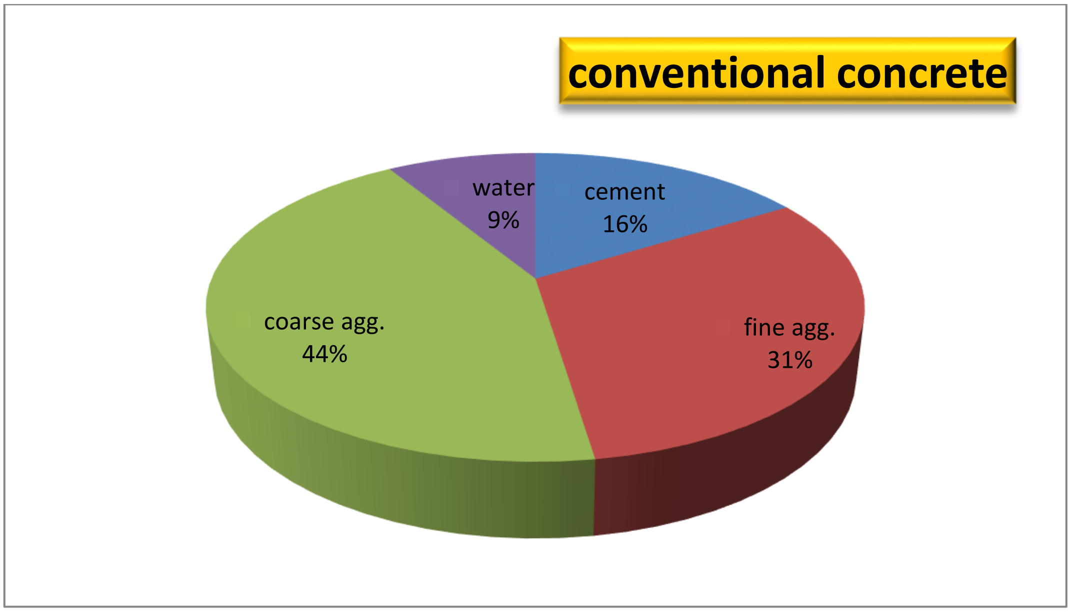

Figure (3-6) Materials proportion in conventional concrete (% of total mix weight)

3.4: Specimens Description:

3.4.1: Fabrication of Molds:

Eighteen prismatic and non-prismatic plane frame sets of plywood formwork with a thickness of (18 mm) were fabricated. The columns have (850 mm) length and cross section (150*150 mm) for the prismatic column and variable from (130*150 mm) at support to (170*150mm) at beam joint for the non-prismatic column. While the beam contains a length of (1000 mm) and a cross-section either constant (150*150 mm) or variable in the form of a taper from (130*150 mm in the middle to 170*150mm at the edges) as shown in **Plate (3-6)**. The dimensions of the specimens used represent miniature dimensions of a real specimen reduced to one-third, and these are the limits allowed in ACI T1.1-01. The ACI stipulates that “Modules shall have a scale large enough to fully represent the complexities and behavior of the real materials and of the load transfer mechanisms in the prototype frame. Modules shall have a scale not less than one-third full size”

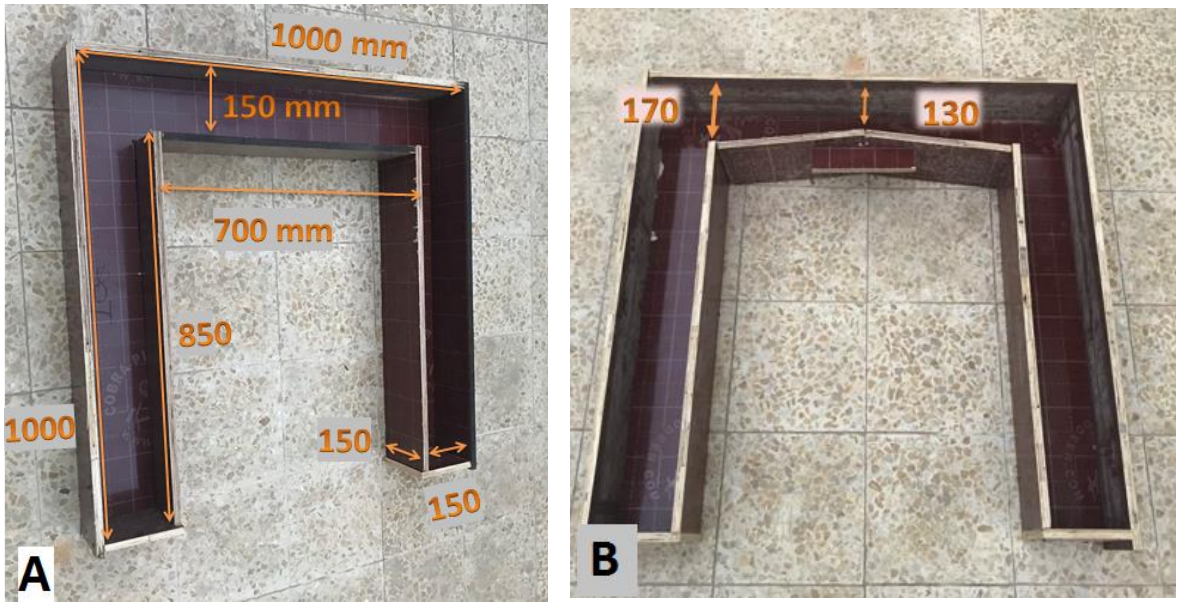

Plate (3-6) Molds fabrication of specimen A: prismatic. B: non prismatic of beam

3.4.2: Specimens reinforcements:

The concrete frame was designed according to the requirements of the American Concrete Institute **(ACI 318-2019)** as shown in **Appendix C**. **Figure (3-7)** shows the details of the reinforcing steel for the concrete frames. Where all specimens have the same reinforcement.

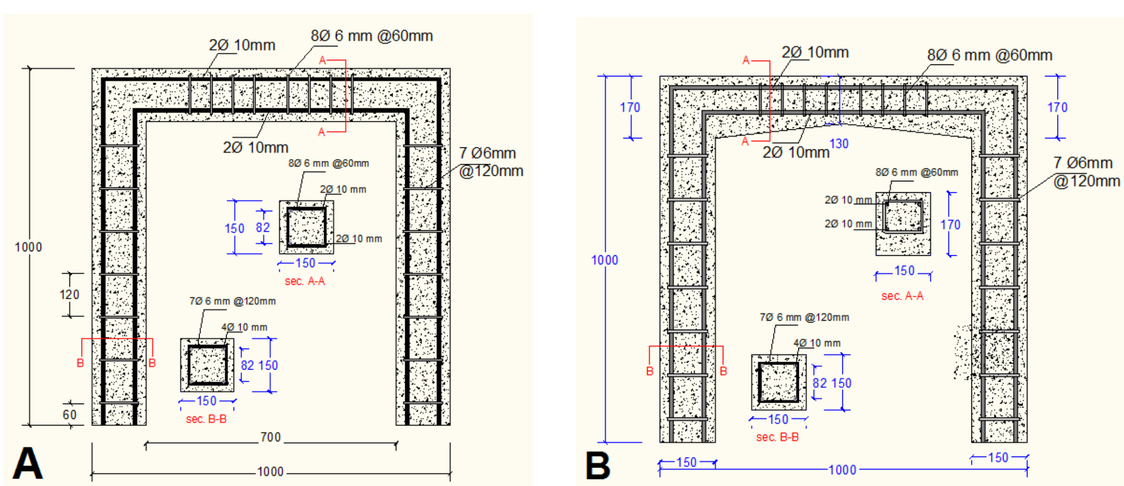

Figure (3-7) Details of reinforcement for frame used A: prismatic. B: non-prismatic.

3.4.3: Specimens Symbols:

The symbols of the specimens used in this study were chosen in three parts, as they represent the geometric shape of the cross-section of the beam and columns, the type of material used in the specimen, and the type of loading. **Table (3-13)** shows the specimen symbols and the definition of each specimen as well as the definition of each symbol.

Table (3-13) Symbols of specimens*

No	Specimens symbols	Details
(group A) prismatic and non-prismatic section		
1	P-C-1	A Conventional reinforced concrete frame with Prismatic cross-sections under monotonic load.
2	NO-C-1	A Conventional concrete frame with Non-prismatic cross-sections in the columns under monotonic load.
3	NB-C-1	A Conventional concrete frame with Non-prismatic cross-sections in the Beam under monotonic load.
(group B) Type of concrete		
4	NB-S-1	Reactive powder concrete frame with Steel fibers with Non-prismatic cross-sections in the Beam under monotonic load.
5	NB-G-1	Reactive powder concrete frame with Glass fibers with Non-prismatic cross-sections in the Beam under monotonic load.
(group C) A hybrid of concrete for shear		
6	NB-25GLE-1	A conventional concrete frame hybrid with reactive powder concrete with Glass fibers by 25% (of the beam's volume) in the Lower half of the beam Edges with a Non-prismatic Beam under monotonic load.
7	NB-50GE-1	A conventional concrete frame hybrid with reactive powder concrete with Glass fibers by 50% (of the beam's volume) at the Edges of the beam with a Non-prismatic Beam under monotonic load.
(group D) A hybrid of concrete for flexural		
8	NB-50GU-1	A conventional concrete frame hybrid with reactive powder concrete with Glass fibers by 50% (of the beam's volume) at the Upper half of the beam with a Non-prismatic Beam under monotonic load.
9	NB-50GL-1	A conventional concrete frame hybrid with reactive powder concrete with Glass fibers by 50% (of the beam's volume) at the Lower half of the beam with a Non-prismatic Beam under monotonic load.

Table (3-13) Continued

10	NB-100G-1	A conventional concrete frame hybrid with reactive powder concrete with **G**lass fibers by **100%** (of the beam's volume) at all the beam with a **N**on-prismatic **B**eam under monotonic load.
(group E) type of loading		
11	NB-C-2	A **C**onventional concrete frame with **N**on-prismatic cross-sections in the **B**eam under repeated load.
12	NB-S-2	Reactive powder concrete frame with **S**teel fibers with **N**on-prismatic cross-sections in the **B**eam under repeated load.
13	NB-G-2	Reactive powder concrete frame with **G**lass fibers with a **N**on-prismatic cross-section in the **B**eam under repeated load.
14	NB-25GLE-2	A conventional concrete frame hybrid with reactive powder concrete with **G**lass fibers by **25%** (of the beam’s volume) in the **L**ower half of the beam **E**dges with a **N**on-prismatic **B**eam under repeated load.
15	NB-50GE-2	A conventional concrete frame hybrid with reactive powder concrete with **G**lass fibers by **50%** (of the beam’s volume) at the **E**dges of the **B**eam with a **N**on-prismatic **B**eam under repeated load.
16	NB-50GU-2	A conventional concrete frame hybrid with reactive powder concrete with **G**lass fibers by **50%** (of the beam's volume) at the **U**pper half of the beam with a **N**on-prismatic **B**eam under repeated load.
17	NB-50GL-2	A conventional concrete frame hybrid with reactive powder concrete with **G**lass fibers by **50%** (of the beam's volume) at the **L**ower half of the beam with a **N**on-prismatic **B**eam under repeated load.
18	NB-100G-2	A conventional concrete frame hybrid with reactive powder concrete with **G**lass fibers by **100%** (of the beam's volume) at all the beam with a **N**on-prismatic **B**eam under repeated load.

Where:

P: **P**rismatic frame.

C: **C**onventional Concrete.

NB: Frame with **N**on prismatic **B**eam

NO: Frame with **N**on prismatic c**o**lumn.

S: Reactive powder concrete with **S**teel fiber.

G: Reactive powder concrete with **G**lass fiber.

1: Frame tested under monotonic load.

2: Frame tested under repeated load.

U: Hybrid frame at the **U**pper half of the beam.
L: Hybrid frame at the **L**ower half of the beam.
E: Hybrid frame at the **E**dges of the beam.
25: Hybrid frame with **25** % of beam's volume with reactive powder concrete.
50: Hybrid frame with **50** % of beam's volume with reactive powder concrete.
100: Hybrid frame with **100** % of beam's volume with reactive powder concrete.

3.4.4: Details of specimens:

The main objectives of this work are to study a set of variables and to know their effect on the behavior of the concrete frame. The study deals with the effect of change of cross-sections of the reinforced concrete frame, the effect of using glass fiber reactive powder concrete (GRPC) in the concrete frame and compared with steel fiber reactive powder concrete (SRPC), use of conventional concrete with hybridization with GRPC, as well as studying all previously mentioned variables under monotonic and repeated loads. For more information about the main variables studied in this work, the work was divided into five groups, which are as follows:

Group A: Changing the cross-section of the beam and columns.

Group B: Changing type of concrete frame.

Group C: Hybridization of conventional concrete with GRPC at shear region.

Group D: Hybridization of conventional concrete with GRPC at bending region.

Group E: Type of loading (monotonic load and repeated load).

The details of each group are listed in the following paragraphs:

1. **Group A: Changing the cross-section of the beam and columns:**

This group includes three conventional concrete frames with prismatic and non-prismatic cross-sections. Where the first frame (A) is prismatic for all cross-sections of the members **"P-C-1"**, while the second frame (B) is prismatic with the beam and non-prismatic with the columns in a tapering style, as it starts with a small section at the base of the column and ends with a large section at its top **"NO-C-1"**. The third frame (C) is prismatic with the columns and non-prismatic with the beam. It starts with a deep section at the ends and then gradually gets smaller until it reaches the center of the beam **"NB-C-1"**, as shown in **Figure (3-8)**. All specimens were tested under monotonic load. The use of non-prismatic sections is to optimally redistribute the concrete to obtain the many benefits mentioned in chapter one. All specimens in this group have an equal as concrete quantity.

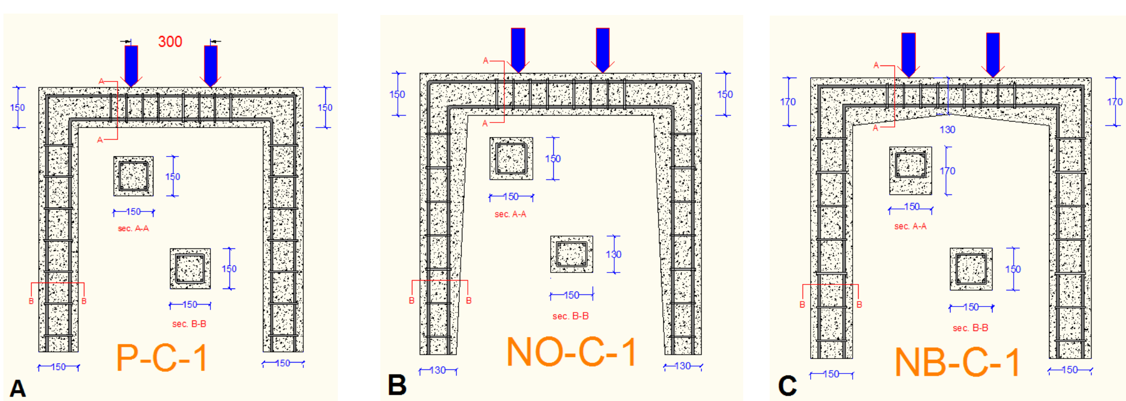

Figure (3-8) Details of the group "A" specimens A: P-C-1. B: NO-C-1. C: NB-C-1.

2. **Group B: Changing type of concrete frame:**

This group includes two specimens of the reactive powder concrete frame with different fibers **"NB-S-1"** and **"NB-G-1"**. Where the first frame

(A) includes steel fiber reactive powder concrete (SRPC), while the second frame (B) consists of glass fiber reactive powder concrete (GRPC). The dimensions, details of reinforcement, and method of loading are similar, as in **Figure (3-9)**. All specimens have a non-prismatic cross-section in the beam and were tested under monotonic load.

The purpose of the study of this group is to find out the behavior of the GRPC frame and compare it with the behavior of the commonly used SRPC frame and conventional concrete frame.

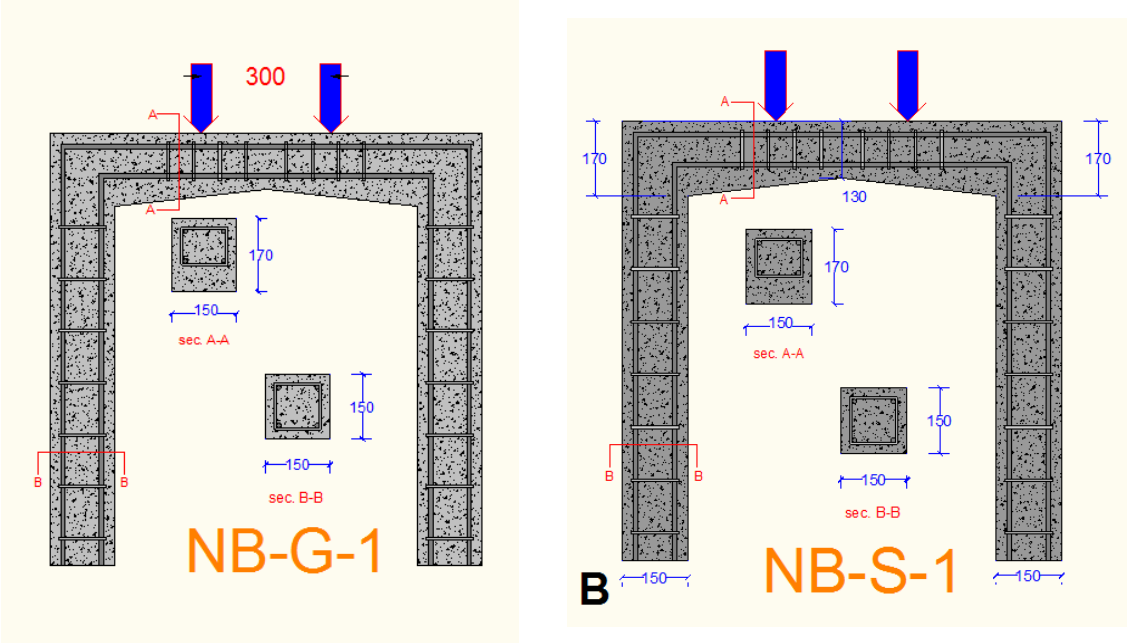

Figure (3-9) Dimensions of A: NB-S-1. B: NB-G-1.

3. Group C: Hybridization of conventional concrete with GRPC at shear region:

This group includes two specimens of the conventional concrete frame hybridized with GRPC in the shear zone only. Where the first frame was made of conventional concrete and hybridized at the edges of the beam and for the lower half only, at a percentage of 25% of the volume of the beam concrete

"NB-25GLE-1". While in the second frame, the hybridization was at the edges of the beam, at a percentage of 50% **"NB-50GE-1"**, as illustrated in **Figure (3-10)**. All specimens have a non-prismatic cross-section in the beam and were tested under monotonic load.

The purpose of studying this group is to find out the effect of hybridization in the specific zones and percentages of this group on the behavior of the concrete frame.

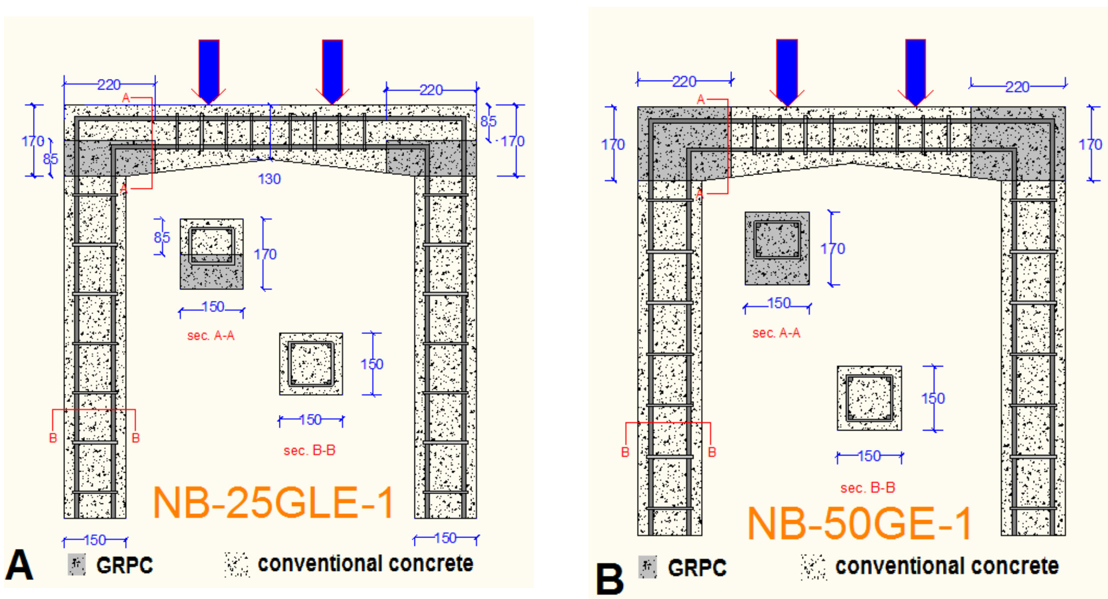

Figure (3-10) Dimensions of A: NB-25GLE-1. B: NB-50GE-1.

4. **Group D: Hybridization of conventional concrete with GRPC at flexural region:**

This group includes three specimens of conventional concrete frames and a hybrid with GRPC in specific zones to resist tensile or compressive stresses resulting from bending moment. The first frame (A) is the hybridization with GRPC in the upper half of the beam (end of shear failure path and compression stress for the positive moment and tension stress for the

negative moment) by 50% of the beam's volume "**NB-50GU-1"**. In the second frame (B), the hybridization is opposite to the first frame, where the GRPC is in the lower half of the beam "**NB-50GL-1"**. While the third frame (C) was hybridized with GRPC at all beam concrete with a percentage of 100% "**NB-100G-1"**. All specimens have a non-prismatic cross-section in the beam and were tested under monotonic load, as shown in **Figure (3-11)**.

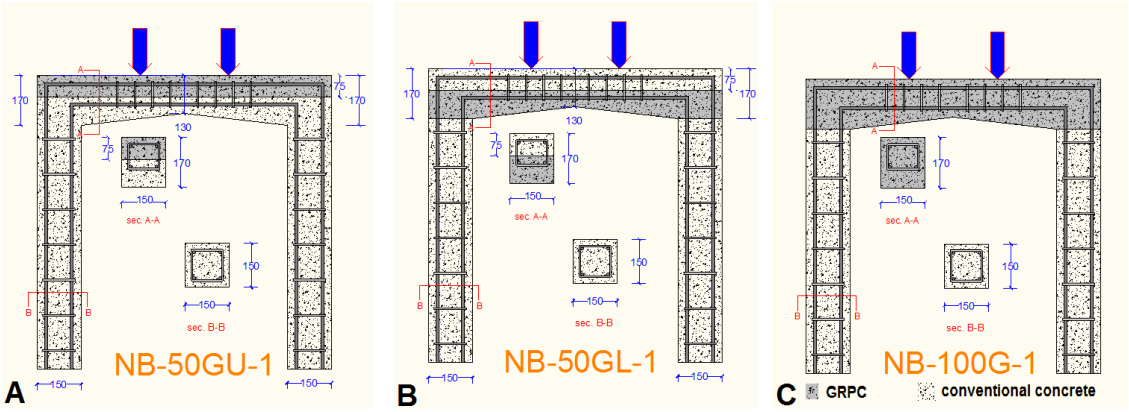

Figure (3-11) Details the dimensions of the group "D" A: NB-50GU-1. B: NB-50GL-1. C: NB-100G-1.

5. Group E: Type of Loading:

This group consists of eight specimens, and it is similar to all specimens of the previous four groups, but it was tested under repeated load and as shown in **Figure (3-12)**.

The aim of the study of this group is to find out the effect of the behavior of the concrete frames with conventional concrete, hybrid concrete, SRPC, and GRPC to resist repeated loads.

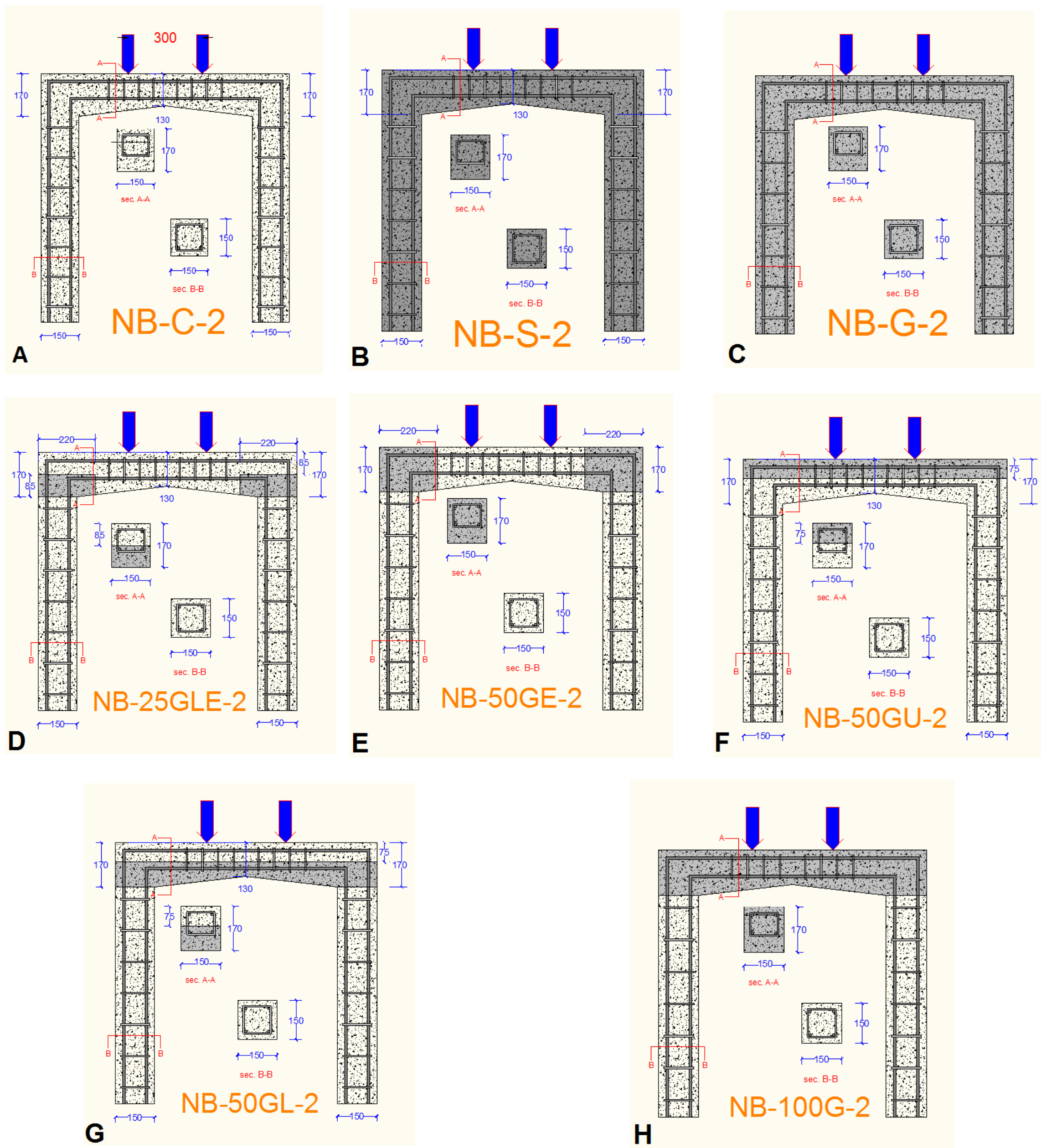

Figure (3-12) Details the dimensions of the group "E" A: NB-C-2. B: NB-S-2. C: NB-G-2. D: NB-25GLE-2. E: NB-50GE-2. F: NB-50GU-2. G: NB-50GL-2. H: NB-100G-2.

3.5: Concrete Casting and Curing:

The first step in forming the plane frame in this study is to prepare the plywood mold with the required dimensions according to the variables of each specimen as mentioned previously. Then the reinforcing steel is placed in the

mold and fixed in a certain position so that there is a space that separates it from the wooden mold by 20 mm, and this is done by a plastic spacer. **Plate (3-7)** shows the presence of reinforcing steel inside the wooden mold.

Plate (3-7) Specimens molds with reinforcement

In the case of specimens containing one type of concrete (conventional concrete or SRPC or GRPC), all the molds are filled with concrete in layers and external vibrators were used to reduce air voids and obtain a compact concrete. Whereas, in the case of the hybrid concrete specimens, steel barriers with a thickness of 2 mm were used to separate the different concretes with varying dimensions and locations according to each specimen. The mold is filled with conventional concrete and GRPC together in place in layers, then the barriers are lifted with great care and attention, and then vibrators are used in the area of the barrier line to increase the bonding between the different parts of the concrete. This method was chosen based on **(Zabala, 2020)**. The upper surface of the concrete was leveled with a steel trowel and after 24

hours the molds were opened and the curing stage began. **Plate (3-8)** shows various pictures of the casting specimen's stages.

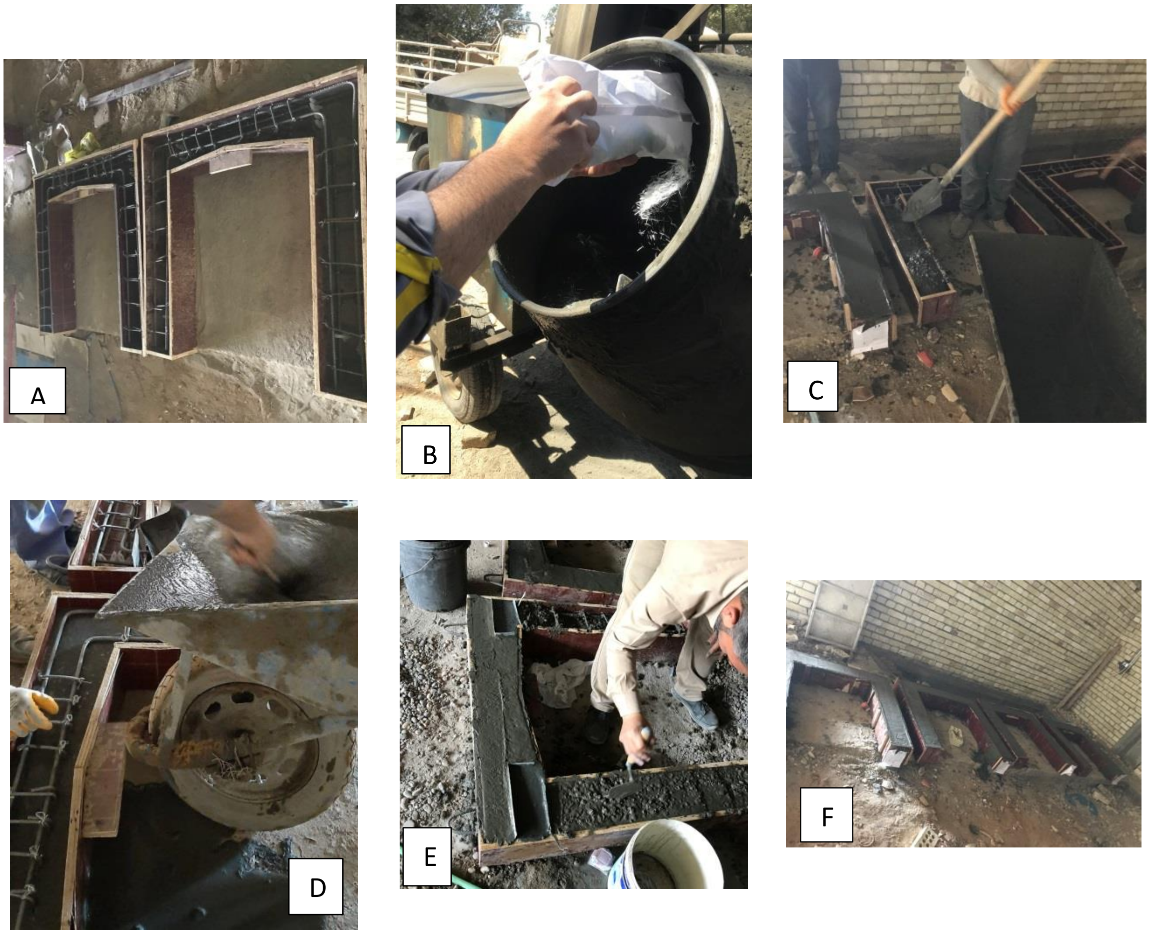

Figure (3-8) Casting of specimens A: specimens ready to casting. B: adding glass fibers. C: adding concrete. D: continue adding concrete. E: leveled casting. F: finish casting.

The following samples were cast for the purpose of determining the properties of hardening concrete:

1. 50mm x 50mm x 50mm cubs for RPC compressive strength.

2. 150mm x 150mm x 150mm cubs for conventional concrete compressive strength.

3. 100mm x 100mm x 400mm prisms for modulus of rupture.

After opening the molds, all the specimens were covered by canvases and sprayed with water for 28 days as shown in **Plate (3-9)**, while the samples of cubes and prisms were placed in the tank and immersed in water as shown in **Plate (3-10)**.

Figure (3-9) Curing of specimens

Figure (3-10) Curing of cubs and prisms

3.6: Mechanical Properties of Hardened Concrete:

3.6.1: Compressive Strength:

The compression test was used according to **(ASTM C39/C39M-15a)** and **(BS-4-2000, EN 12390)** using a hydraulic testing machine with a loading rate of 0.25 MPa/sec on cubes (50*50*50) mm for RPC mixes and (150*150*150) mm for conventional concrete mixes, as shown in **Plate (3-11).** The compressive strength was taken as an average of three cubes for each mix.

Plate (3-11) The hydraulic compressive strength Test

3.6.2: Modulus of Rupture:

This test determines the flexural strength of concrete (Modulus of Rupture) by using a simple beam with two third -point loading. A Modulus of

Rupture test machine was used on a prism model with dimensions (100*100*400) mm according to the device in the laboratory and the **(ASTM C78/C78M − 15a)**, as shown in **Plate (3-12)**.

Plate (3-12) Modulus of the Rupture test machine

3.6.3: Hardened Unit Weight:

To determine the density of the concrete used for each type, the mass of the compression test cubes was measured and divided by the volume to find the density.

3.7: Instrumentation:

3.7.1: Deformation Measurement:

Two dial gages were used below the beam (one dial gage under concentrated load while the another under the center line of the beam) to measure the deflections at the beam. Also, two dial gages were used at the side of the column to measure the lateral displacement of the column. **Figure (3-13)** is an illustration of the presence of the dial gages in the specimen. The dial gages have an accuracy of (0.01) mm. **Plate (3-13)** shows the presence of the dial gages in the frame.

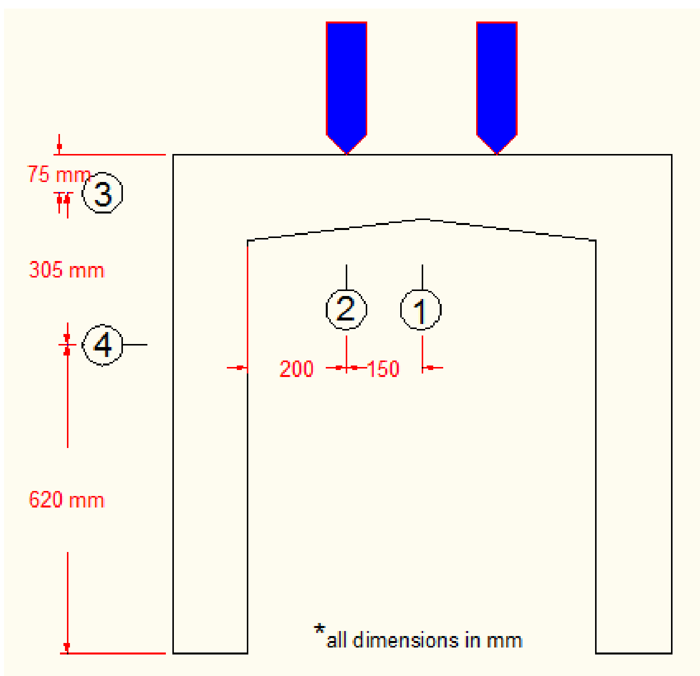

Figure (3-13): The distributions of dial gages on specimen.

Plate (3-13): Dial gages of deformation on the frame.

3.7.2: Crack Width Measurement:

To measure the crack width of the specimens, a crack meter with an accuracy of (0.01) mm was used, as shown in **Plate (3-14).**

Plate (3-14): Crack meter

3.8: Test Procedure:

The specimens were cast and cured by water as previously mentioned, and after 28 days the curing of the specimens was stopped and left for some time to dry. The specimens were painted with light paint so that the cracks of the concrete appear clearly (as the specimens were painted in two different colors according to the type of concrete, as the white color was used for conventional concrete and the yellow color for RPC). The specimen was placed in the universal testing machine and the dial gages installed in the specific positions (two for the beam and two for the column) were installed.

Two-point load was subjected to the beam, and the distance between them is 300 mm. The rubber plates were placed under the load concentration to avoid the occurrence of stress concentration in that area, thus preventing the occurrence of local crushing, while to avoid the event of local crushing of the supports, support cups were placed under each column. “The supporting of the cups was approximately fixed. The proof for that is the rotation in the deflected shape of the columns near the cups is approximately zero or minimal values at the large loads” **(Al-hussainy, 2015)**. The Cup Support is welded to the base of the device test to ensure that there is no horizontal movement in the supports. **Plate (3-15)** shows the dimensions of the support cups.

Plate (3-15) Support cups A: dimension of cups. B: cups on test machine

The specimen was tested by applying a load on the frame gradually by many sub-steps (every 20 kN), and the deflection of the beam, deformation at the column, and crack width of the beam when appeared were measured at each sub-step. Test of specimens are divided into two types, depending on the method of loading:

I. Specimens with monotonic loading: These specimens have gradually applied the load by many sub-steps until failure, and the ultimate load of the specimen was determined (In order to take readings and draw a load-deflection curve in a non-linear and be more accurate).

II. Specimens with repeated loading: These specimens were applied load as the monotonic load specimens but in the form of many cycles. Where each cycle applied load gradually up to approximately 65% of the ultimate load of monotonic load specimens, after which the unloading frame rests for some time (about three minutes), after which the second cycle is performed, and so on up to 10 cycles, Then after that the frame

was loaded up for failure. The deformations are read in two sub-steps when the load is applied, and the same is true when the load is raised so that the curve of the change in deformation with the change in load is drawn accurately and the curve is non-linear. The method of shedding the load is similar to what was adopted in the research of **Al-husseini (2015)**. **Plate (3-16)** shows the frame ready for testing.

Plate (3-16) Frame ready to testing

CHAPTER FOUR

Chapter Four

Experimental Results and Discussion

4.1: Introduction:

In this chapter, the results and discussions of the specimens will be dealt which based on the experimental work through:

1. The mechanical properties of the concrete for conventional concrete, GRPC, and SRPC then comparing the results.
2. Study the structural behavior through studying the strength of the section (crack pattern), ultimate load capacity, load-deflection at mid-span beam, visible first crack load, crack width, and deflected shape of all plane frames with loading.

4.2: Results of Hardened Concrete:

For each type of concrete mix (Conv.C., GRPC, and SRPC), several specimens were cast, cured, and tested to work on the mechanical properties of the concrete. The tests represent compressive strength, modulus of rupture, and density. Each result represented the average of three specimens for all mechanical properties tests.

4.2.1: Compressive Strength:

The compressive strength of concrete is an important property of concrete and is the most useful. Also, it is a good indicator for concrete evaluation. Other properties of concrete such as durability, Young's modulus,

resistance to shrinkage, imperviousness, etc. are related to the compressive strength of concrete **(Maroliya and Modhera, 2010)**. The purpose of the compression test is to determine the crushing resistance of hardened concrete and is conducted on cube specimens of 150x150x150mm for the conventional concrete and 50x50x50mm size for the GRPC and SRPC. **Tables (4-1)** and **(4-2)** and **Figure (4-1)** show the results of concrete compressive strength of conventional concrete and RPC, respectively.

Table (4-1) Results of compressive strength tests of conventional concrete

Concrete type	Compressive strength at 28 days (MPa)
Conventional concrete	37.66

Table (4-2) Results of compressive strength tests of GRPC and SRPC

concrete type	compressive strength at 28 days (f'_c) (MPa)
GRPC	76.22
SRPC	89.20

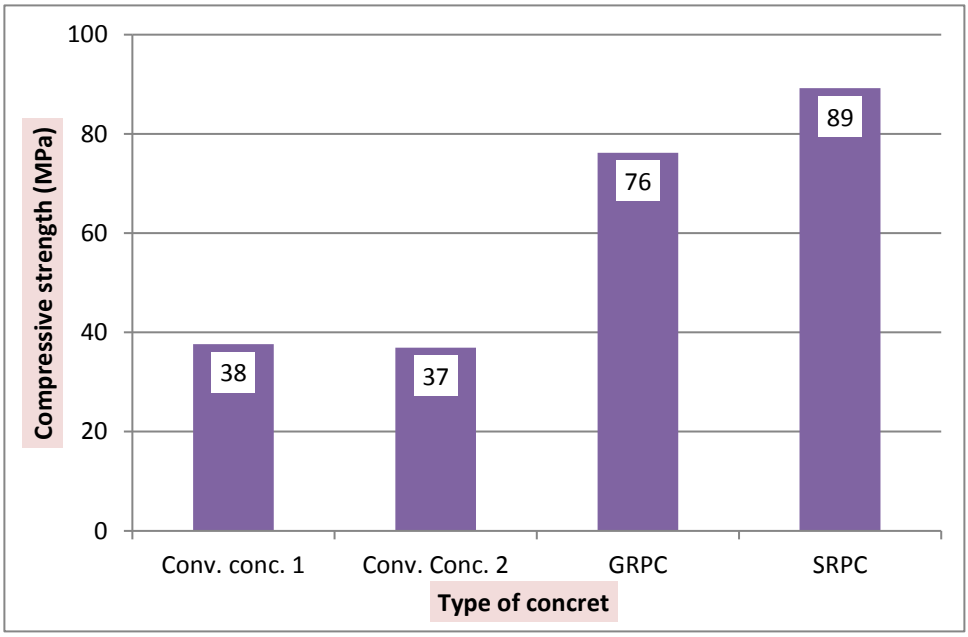

Figure (4-1) Compressive Strength for different types of concrete

(Graybeal and Davis, 2008) and **(Aziz and Ahmed, 2012)** concluded that the compressive strength of the cube test result for 50*50*50mm for RPC was equal to or very close to the cylinder test result mentioned in **(ASTM C1856, 2017).**

In SRPC, the compressive strength is high due to the presence of steel fibers (SF) that contribute to reduce the lateral tensile strain, which increases the energy absorption capacity under the compressive load. While the compressive strength of GRPC is lower despite the presence of glass fibers (GF), due to the modulus of elasticity of GF being small compared to SF **(Raza et al, 2020).**

4.2.2: Modulus of Rupture (f_r):

The modulus of rupture test is used to visualize the load that causes cracks in concrete in bending due to tensile stresses and is done by using a

simple beam with a Tow-point load. **Table (4-3)** and **Figure (4-2)** show the results of the modulus of rapture for all types of concrete, where an average was taken for three models with an age of 28 days for each type of concrete.

Table (4-3) Results of Flexural Strength Tests For NSC, GRPC and SRPC

Type of concrete	Modulus of rupture at 28 days (f_r) (MPa)
Conv. Concrete	3.38
GRPC	11.06
SRPC	8.97

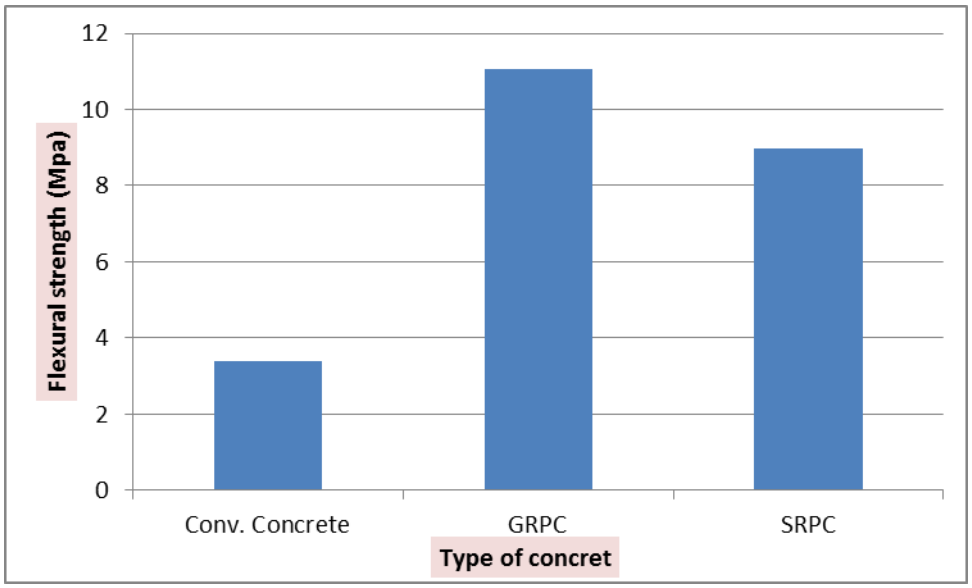

Figure (4-2) Results of flexural strength tests for conv. concrete, GRPC and SRPC

By testing prism models, it was noticed that the failure in conventional concrete was a brittle failure and sudden, where the model was divided into two pieces. While in fibrous RPC, the concrete behaves as a ductile material, where the failure was gradual until the maximum load, While the model

remains in one piece because the fibers act as bridges between the concrete particles and as shown in **Plate (4-1).**

Plate (4-1) Flexural strength tests failure for conv. concrete, GRPC and SRPC

From **Table (4-3)**, it is noted that the f_r value of GRPC is greater than the f_r of SRPC although the f'_c of SRPC is greater than that of GRPC. This indicates that the effect of GF by acting as bridges between concrete particles was better than SF because of its rough texture and strong adhesion to other concrete parts, which makes it a better hybrid material than steel fiber and this confirms the results of **Resif (2020)**. Note that the other previous studies (**Rahmani et al, 2011**& **Kushartomo and Ivan, 2017**& **Raza et al, 2020**) showed results opposite to these results, where the f_r for SRPC was usually greater than for GRPC, and the reason for the difference in results is due to the characteristics of the GF and SF used in this study differ from those used in previous studies.

4.2.3: Hardened Unit Weight:

Density is "a measurement of how much “stuff” is in a given amount of space", in other words, the quantities of air voids in the concrete, which

affect the compressive strength of the concrete. It is also a measure for calculating a dead load of concrete when designing structural members.

Table (4-4) presents the density values of the different concrete mixes used in this research at the age of 28 days.

Table (4-4) Results of density test for concrete mixes used

Test	Conv. concrete	SRPC	GRPC
Density, (kg/m^3)	2314	2340	2264

From **Table (4-4)** it is noted that the density of GRPC is the lowest despite its lack of voids, due to the presence of silica fume, which has a low density and does not contain coarse aggregates (heavyweight), as well as the lightness of glass fibers compared to steel fibers.

4.3: Test Result of Specimens:

4.3.1: Crack pattern and ultimate load:

Group A (Effect of Prismatic and Non-Prismatic Section):

This group consists of three specimens (P-C-1, NO-C-1, and NB-C-1), where the effect of the dimensions of the concrete section of columns and beams was studied.

4.3.1.1: Specimen P-C-1 (Control):

Specimen P-C-1 was considered the control frame of this group where it used conventional concrete with constant dimensions of the columns and beam.

When the loads were gradually applied, a flexural crack appears in the middle of the beam at a load of **43 kN**, as shown in **Plate (4-2)**.

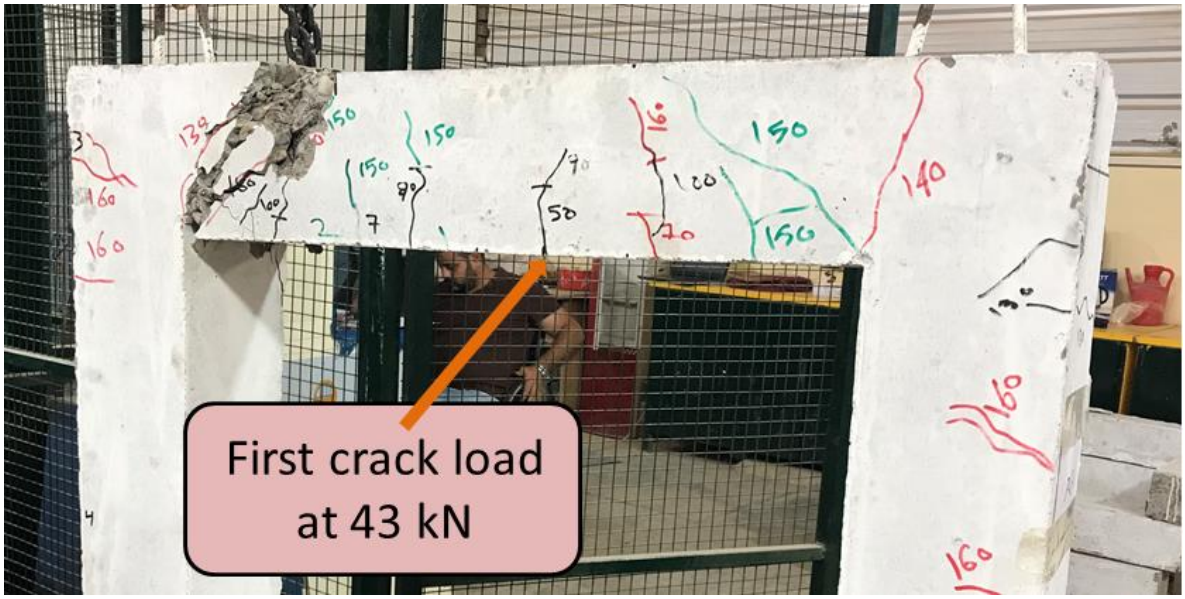

Plate (4-2): First cracks of the P-C-1

As the load continues, the first crack increases in width and extends towards the top surface of the beam, in addition to the appearance of additional bending cracks. When the load has reached **130kN**, a shear crack appears in the left joint from the bottom of the inner corner of the beam and column to the left load point applied. A crack appeared on the outside of the right joint transversely. At load **140kN**, a shear crack appears in the right joint and when carrying **160kN** cracks appear on the outer face of both columns and then a shear failure occurs on the left side of the frame as a diagonal failure from the inner face of the joint to the loading point, as shown in **Plate (4-3)**.

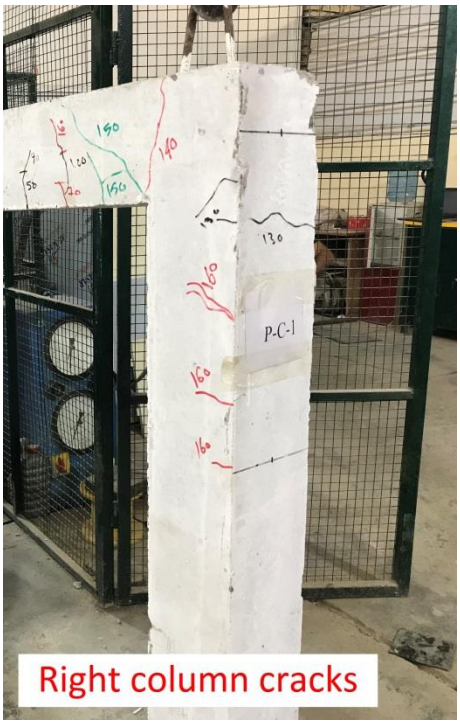

- All numbers in kN.

Plate (4-3) Failure crack and cracks patterns of the P-C-1

4.3.1.2: Specimen NO-C-1:

The specimen NO-C-1 was prismatic in the beam and non-prismatic in the columns (tapered) at width only, as it has an aspect ratio of the large width to the small width is **1.3**.The small width was at the bottom of the column, while the large width was at the joint of the beam and column.

The first crack appeared at the **46kN** load directly below the left loading position, as shown in **Plate (4-4)**. The increase in the amount of first crack load of this specimen was **7%** over the control frame, due to the change

in the geometric shape of the columns, which causes the decreases in beam length.

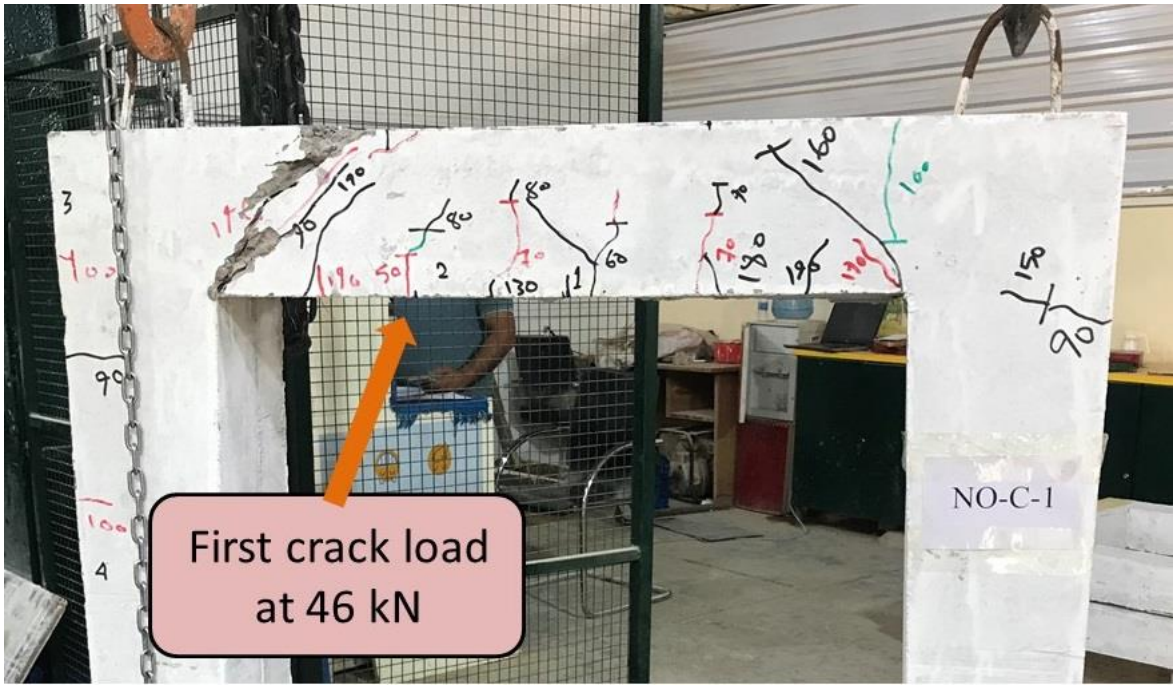

Plate (4-4): First cracks of the NO-C-1

With the increase in loads, new bending cracks appeared in the beam, and when the load reached **90kN**, cracks appeared on the outer face of the columns in the zone near the joint and for both the right and left columns. As the loads continue to be applied, shear and negative bending cracks appeared at load **100kN** and when reaching load **200kN**, the specimen failed on the left side, as a shear failure and the angle of the crack failure have an inclination with horizontal line more than of P-C-1 specimen as shown in **Plate (4-5)**.

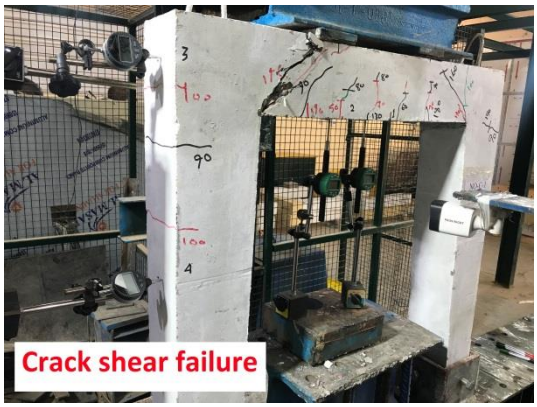

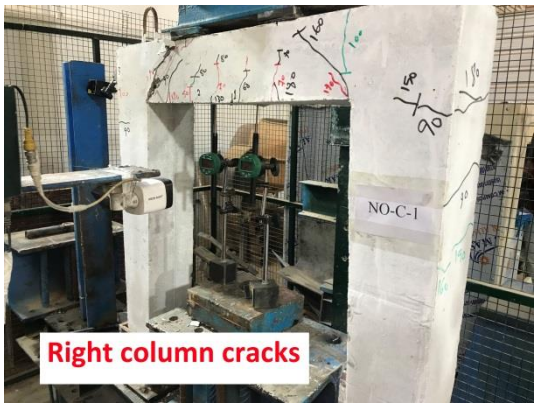

- All forces in kN.

Plate (4-5) Failure crack and cracks patterns of the NO-C-1

Note that there was an increase in the ultimate load for this specimen by 25% compared to the control frame, and the reason for this increase was the decrease in the length of the shear span by 10% as a result of the large upper part of the column as a result of using a non-prismatic section in the columns. For the smallest value of the shear span, the applied load is directly transferred to supports by the compression struts due to arch action, which increases shear strength. On the other hand, when the shear span increases, the effectiveness of the compression strut in transferring the load is decreased resulting in a decrease in the ultimate strength of the specimens. **(Qissab and Dhaiban, 2015)**

4.3.1.3: Specimen NB-C-1:

Specimen NB-C-1 was a concrete frame with a non-prismatic (tapered) beam in-depth, where the ratio of large depth to small depth was **1.3**. The large depth was at the edges of the beam (beam-column joint) and the small depth was in the middle of the span.

At the beginning of the load applied, the first visible crack appeared at **30kN** load as a flexural crack. The first crack was located below the beam in a zone between the middle of the beam and the left load-applying point, as shown in **Plate (4-6).** The first crack load of this specimen was **30%** less than the control frame of this group, due to the small depth of the beam in the first crack zone as a result of using a non-prismatic section of the beam.

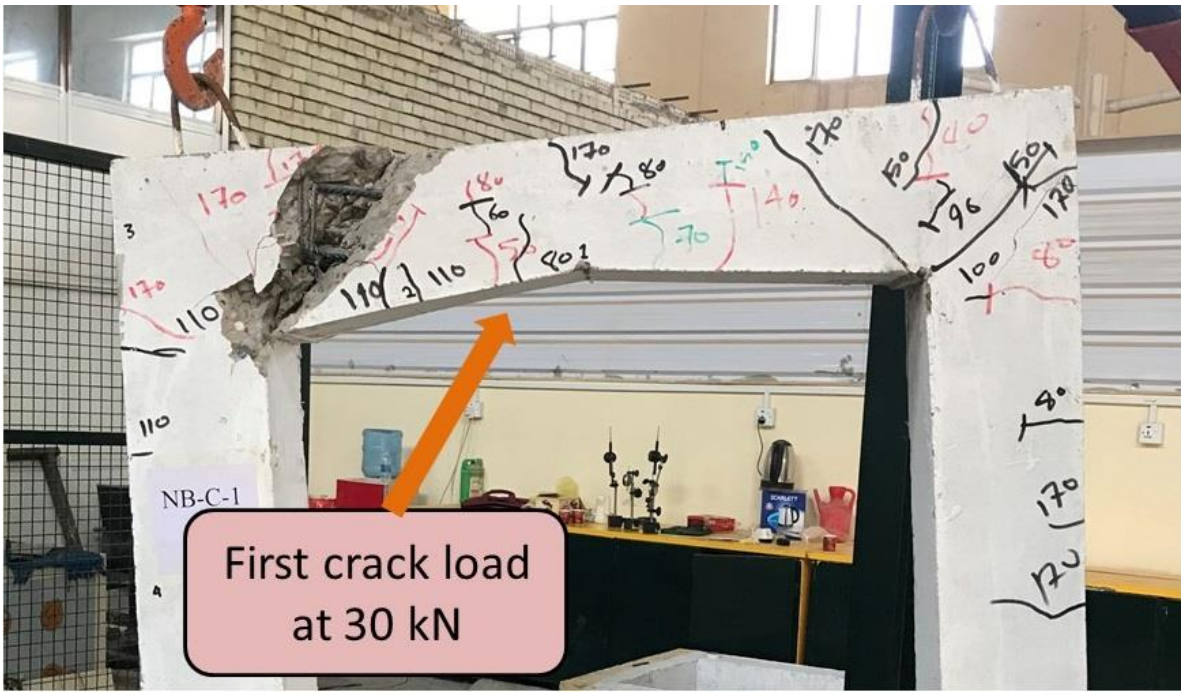

Plate (4-6): First cracks of the NB-C-1

After the appearance of the first crack and the continuation of the loads applied, additional bending cracks appeared. While reaching the loads **80kN** and **90kN**, a crack appeared on the outer face of the right column and a diagonal crack in the right joint from the inner corner to the outer corner, respectively. The NB-C-1 reached the ultimate load at **185kN** with the shear mode failure. **Plate (4-7)** shows the crack pattern and crack failure of this specimen.

Plate (4-7) Failure crack and cracks patterns of the NB-C-1

The ultimate load of this specimen was increased by **16%** over the ultimate load of the control frame and the reason was due to an increase in the beam depth at the end by **13%** due to the non-prismatic beam.

The failure behavior of the P-C-1 and NO-C-1 specimens was fragile, as a sudden failure of shear occurs. While the behavior of the NB-C-1 specimen was less fragile, as many cracks appear and a large deformation occurs compared to other specimens before failure, because the presence of non-prismatic sections develops arch-action theory and makes the distribution of damage along the taper before the formation of diagonal shear cracks, and this is the reason for the appearance of cracks in the shear region at a load of **90 kN** in this specimen, while in P-C-1 they appear at a load of **130 kN**, and this confirms the results of previous research on the non-prismatic beams. **(Qissab and Dhaiban, 2015)**

Summary of Group A (Effect of Prismatic and Non-Prismatic Section):

A summary of the first crack loads, the ultimate loads, the percentages of increase and decrease in the loads compared to the control frame, and the type of failure for the specimens of this group were presented in the **Table (4-5)**.

Table (4-5) Summary of the first crack loads and ultimate loads for the group (A)

Sp. Names	P_{cr} (kN)	P_{cr} increases (%)	P_u (kN)	P_u increases (%)	Type of failure
P-C-1 (control)	43	------	160	------	Shear failure
NO-C-1	46	7%	200	25%	Shear failure
NB-C-1	30	-30%	185	16%	Shear failure

Group B (Effect of Type of Concrete):

This group includes two specimens (NB-S-1 and NB-G-1), where the effect of the type of concrete on the strength of the concrete frame was studied. The effect of glass fibers in the reactive powder concrete on the behavior concrete frame was studied and also compared with the reactive powder concrete with steel-fiber and conventional concrete.

In this group, the specimen "NB-C-1" in group (A) was considered as a control frame for this group.

4.3.1.4: Specimen NB-S-1:

The specimen NB-S-1 was similar to the control frame of this group (NB-C-1) in the dimension of sections, but steel fiber reactive powder concrete was used in its formation.

The first crack visible for this specimen appeared at a load of **68 kN** in the middle of the beam under bending stresses only. As shown in **Plate (4-8)**. The effect of the presence of SF in the RPC of the concrete frame was evident by increasing the load causing the first crack by (**127%**), where the SF has a high energy absorption capacity due to its high elastic modulus, which reduces the lateral tensile strain therefore, SRPC resists cracking better than conventional concrete. **(Raza et al, 2020)**

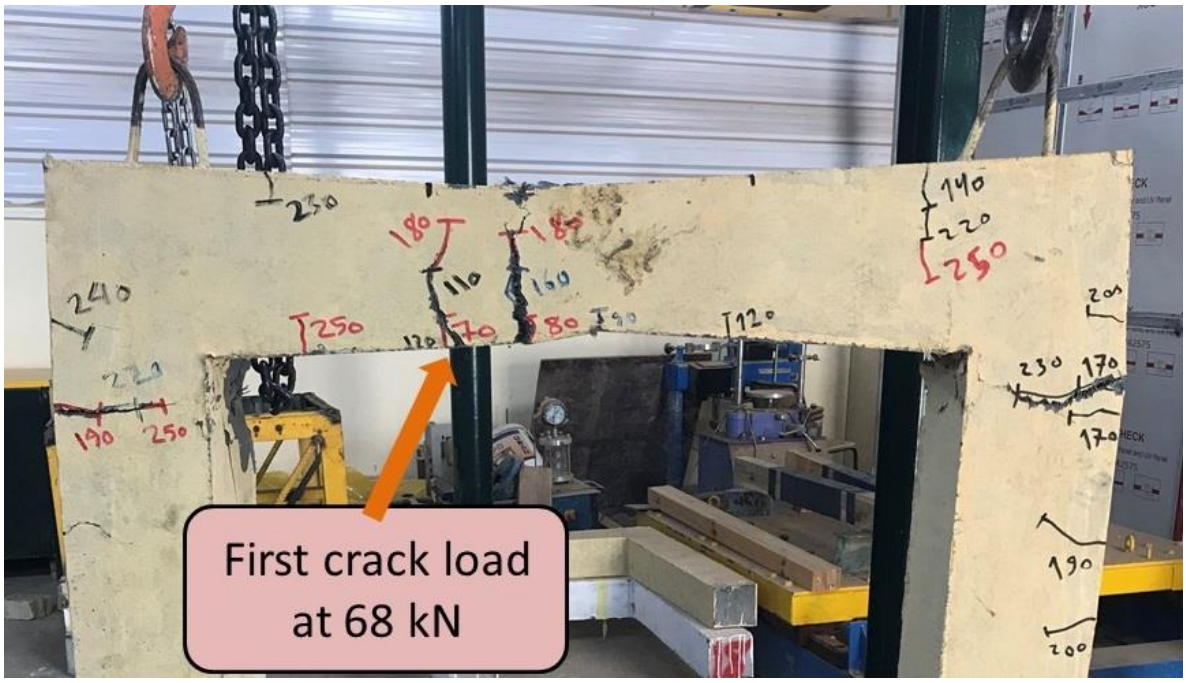

Plate (4-8): Location of the first cracks of the NB-S-1

As the continued applied loads, additional bending cracks appeared, and when the loads reached **170kN** and **190kN**, the left and right columns started cracking, respectively. When carrying was **265kN**, a crushing occurred in the right and left joints due to the creation of plastic hinges at the joints. With the stability of the load applied, the specimen collapse occurred at **270kN** in the middle of the beam under the effect of the bending stresses. The load of the first plastic hinge and the load of the collapse of the specimen were close because the negative moments were slightly larger than the positive moment. **Plate (4-9)** shows the crack pattern of the frame and the crushing of the right and left joints and the failure of the bending beam.

It is noted that the number of cracks in this specimen is slight due to the smallness of the steel fibers, which works to reduce the formation of cracks effectively at the initial loads, so the cracks are concentrated in the areas with high stresses only. **(Raza et al, 2020)**

Plate (4-9) Failure crack and cracks pattern of the NB-S-1

The presence of RPC with SF in the concrete frame improves the shear strength of the concrete due to the properties of RPC, **(O'Neil and Dowd, 1995)** and this was reflected in its effect on the frame, so the type of failure changes from a shear failure in the control frame to a flexural failure, and the ultimate load increases by **46%**.

4.3.1.5: Specimen NB-G-1:

The specimen NB-G-1 was similar to the control frame of this group (NB-C-1) in the dimension of sections, but glass fiber reactive powder concrete was used in its formation.

The first visible crack of NB-G-1 was observed in the bending region only at **39 kN** loading, where its location in the frame is shown in **Plate (4-10)**. The first crack load of this specimen was increased by **30%** more than the control frame due to the presence of GF in the RPC. It was also **42%** less than NB-S-1 because the glass fiber has a high aspect ratio **(857%)** compared to the steel fiber with an aspect ratio **(60%)**, therefore the resistance of GRPC to initial stresses is less than SRPC. **(Raza et al, 2020)**

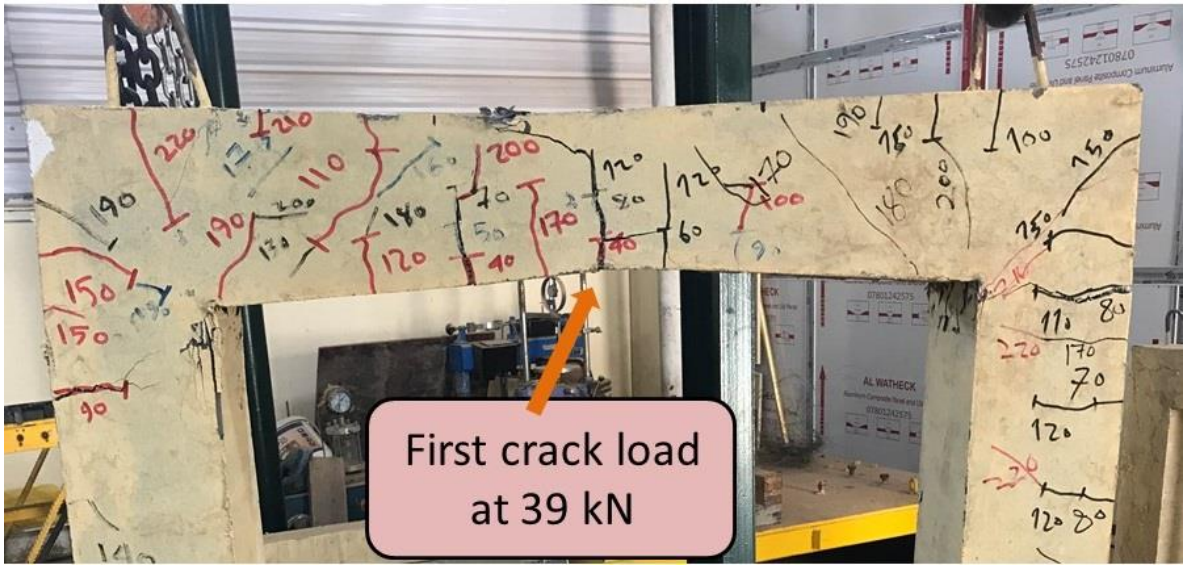

Plate (4-10): Location of first cracks of the NB-G-1

The right and left columns started cracking when loading **70kN** and **90kN** respectively, while the left and right joints started cracking when loading **170kN** and **180kN** respectively. Two plastic hinges are formed on both joints at a load of **260kN** and then a frame failure occurs in the middle of the beam at the same load applied but shortly after (The negative moment was very close to the positive moment, so the difference between the first plastic hinge and the collapse of the frame were very close). The ultimate load of this specimen was more than the control frame **(41%)** and less than the NB-S-1 **(4%)** because GRPC has a lower modulus of elasticity than SRPC due to the stiffness of SF being higher than that of GF **(Algburi et al, 2018).** **Plate (4-11)** shows the distribution of cracks and failure locations for this specimen.

Plate (4-11) shows the effect of GRPC on the behavior of the frame as it changed the type of failure from shear failure as in the case of NB-C-1 to bending failure. In addition to increasing the number of cracks in a wider area of the frame and not concentrating them in specific places as happened in NB-S-1, the aspect ratio of GF is greater than that of SF. Therefore, voids gather at the bottom of the fibers and thus do not prevent cracks from developing at initial loads as happens with SF. At the same time, the presence of fibers prevents the expansion of cracks by acting as reinforcement bridges between the granules of the concrete parts. **(Raza et al, 2020)**

Plate (4-11) Failure crack and cracks patterns of NB-G-1

Summary of Group B (Effect of Type of Concrete):

A summary of the first crack loads, the ultimate loads, the percentages of increase and decrease in the loads compared to the control frame, and the type of failure for the specimens of this group were presented in **Table (4-6)**.

Table (4-6) Summary of the first crack loads and ultimate loads for the group (B)

Sp. Names	P_{cr} (kN)	P_{cr} increases (%)	P_u (kN)	P_u increases (%)	Type of failure
NB-C-1 (control)	30	------	185	------	Shear failure
NB-S-1	68	127%	270	46%	Flexural failure
NB-G-1	39	30%	260	41%	Flexural failure

**** Group C (Effect of Hybrid in Shear Region of Frame):***

This group contains two specimens (NB-25GLE-1 and NB-50GE-1), where the effect of hybridizing the frame with GRPC within the shear effect region in specific regions mentioned earlier in the third chapter was studied on the behavior of the frame and compared its results with NB-C-1 and NB-G-1. The specimens were painted yellow for hybrid concrete (GRPC), and white for conventional concrete, to distinguish between the two types of concrete during the testing.

According to **(ACI 318-19, 2019)**, the steel stirrups for the beams are placed at a distance (d) from the column face. Therefore, the effect of the presence of GRPC from the beam joint up to a distance of (d/2) was studied.

4.3.1.6: Specimen NB-25GLE-1:

The geometry of the specimen NB-25GLE-1 was similar to NB-C-1 and NB-G-1; however, it differs from them in that it has a hybrid concrete conventional concrete and GRPC. GRPC was in the lower part of the beam edges only by **25%** of the total concrete quantity of the beam to strengthen the shear strength of the beam with the least possible amount of GRPC.

The first crack of the NB-25GLE-1 appeared at load **30kN** under the left applying point load. **Plate (4-12)** shows the exact location of the first crack. The first crack load was equal to NB-C-1 because of the hybridization it does not fall within the cracked region.

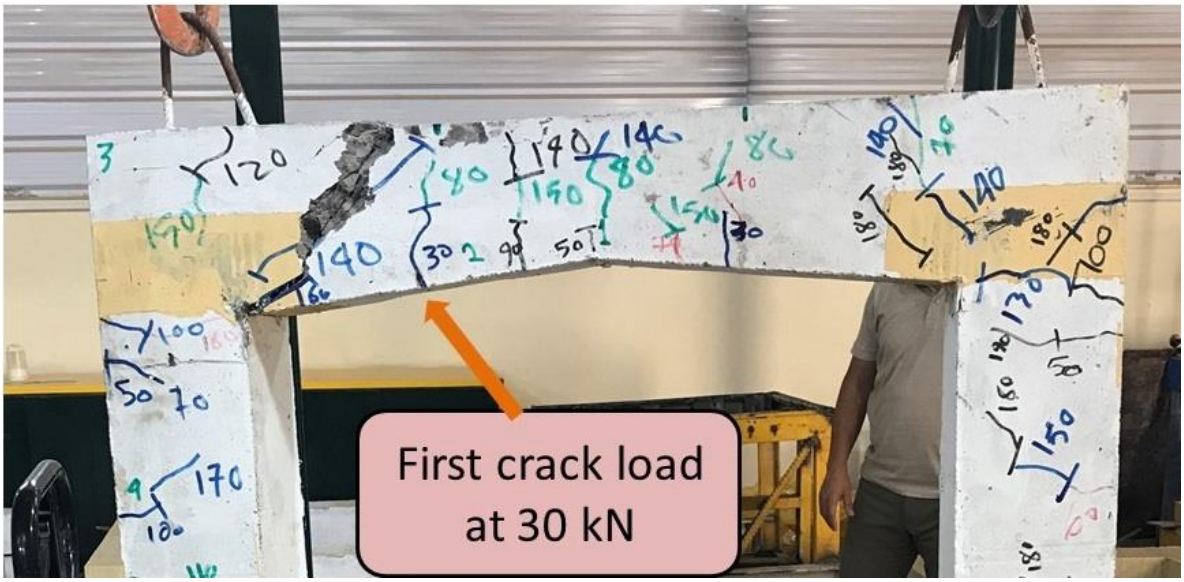

Plate (4-12): Location of First cracks for NB-25GLE-1

The right and left columns start cracking at a load of **50kN**, and as the load continues to be applied, the number of cracks and their width increase in the beam and columns. When the applied load was **205kN**, the frame suffers from a shear failure in the left part of the beam, where cracking began from the lower corner of the joint to the point of applying the load on the upper face of the beam, as shown in **Plate (4-13)**.

The presence of hybridization in the shear region increased the ultimate load of this specimen by **11%** over NB-C-1. The reason for that was due to the passage of part of the failure path within the hybridization region, especially at the beginning of cracking, as the presence of GRPC delayed the initiation of cracking. Also, the presence of GRPC in the region that is devoid

of reinforcing steel (the steel reinforcement is straight and not inclined with the inclination of the beam section) thus gives high shear strength compared to conventional concrete. And the ultimate load was less than NB-G-1 by **21%** because the hybridization region does not cover the whole failure path as in the NB-G-1 and this is also the reason why the failure does not change from a shear failure (NB-C-1) to a bending failure (NB-G-1).

Plate (4-13) Failure crack and cracks patterns of NB-25GLE-1

4.3.1.7: Specimen NB-50GE-1:

The specimen NB-50GE-1 was similar to NB-25GLE-1 but differs from it in that the hybridization region was at the edges of the beam where all the depths were hybrid not at the bottom part only. The hybridization percentage with GRPC was **50%** of the total amount of the beam. In order to study the effect of hybridization and its quantity on the ultimate load of the frame and compare it with NB-25GLE-1 and NB-G-1 to determine the best quantity of hybridization that was more effective and less expensive.

The first crack of NB-50GE-1 appeared when the applied load was **30kN** in the region that was subjected to bending stresses only, as shown in **Plate (4-14)**. The first crack load was equal to the NB-C-1 as well as the NB-25GLE-1 where the first crack occurred in the region of conventional concrete, whose properties were similar to the mentioned specimens.

Plate (4-14) Location of First cracks of the NB-50GE-1

After the appearance of the first crack, the frame suffered from several cracks, especially in the middle of the beam and the right joint, then when the applying load reached **50kN** and **80kN**, the right and left columns began to crack, respectively. Shear cracks appeared on the left side of the frame which begin from the inner corner of the joint to the point of application of the load when the loading reached **170kN**, which later caused the specimen to finally fail. The ultimate load for this specimen was **213kN**, as the frame collapsed as a result of shear failure despite a plastic hinge occurring at the frame joints. **Plate (4-15)** shows the crack pattern of the frame and the location and shape of the failure.

The use of hybridization in this way increased the ultimate load of the frame by **15%** more than the NB-C-1 and also increased it by **4%** more than the NB-25GLE-1. The behavior of the frame, although the same failure remained with NB-C-1 (shear failure), it changed, as the presence of hybridization slightly improved the shear strength of the frame, which exceeded the load of the first plastic hinges at the corners, but was not sufficient to exceed the load of the last plastic hinge and the type of failure changed to a flexural failure.

Plate (4-15) Failure crack and cracks patterns of the NB-50GE-1

Summary of Group C (Effect of Hybrid in Shear region of frame):

A summary of the first crack loads, the ultimate loads, the percentages of increase and decrease in the loads compared to the control frame, and the type of failure for the specimens of this group were presented in **Table (4-7)**.

Table (4-7) Summary of the first crack loads and ultimate loads for the group (C)

Sp. Names	P_{cr} (kN)	P_{cr} increases (%)	P_u (kN)	P_u increases of NB-C-1 (%)	P_u decreases of NB-G-1 (%)	Type of failure
NB-C-1 (control)	30	------	185	------	------	Shear failure
NB-G-1	39	------	260	------	-------	Flexural failure
NB-25GLE-1	30	0%	205	11%	-21%	Shear failure
NB-50GE-1	30	0%	213	15%	-18%	Shear failure

Group D (Effect of hybridized in flexural region of frame):

This group includes three specimens (NB-100G-1, NB-50GL-1, and NB-50GU-1). The effect of hybridization of the conventional concrete frame with GRPC in the flexural zones on the behavior of the concrete frame was studied. The beam was hybridized with different quantities and locations to determine the best location and the least amount of GRPC. The frame was painted yellow for GRPC and white for conventional concrete to distinguish between the two types during testing.

4.3.1.8: Specimen NB-100G-1:

The specimen NB-100G-1 was similar to the NB-C-1 in the geometry, but it differs in that the all beam material was GRPC and the columns were conventional concrete. This specimen was taken to study the effect of hybridization with GRPC on the ultimate load of the frame and the type of failure.

The first crack of this specimen started at a load of **40kN** in the middle of the beam as a pure bending crack as shown in **Plate (4-16).** The increase in the first cracking load of this specimen was **33%** more than that of the NB-C-1 due to the effect of GRPC present in the cracked region, and this appears clearly when the cracking load was very close to the first crack load of the NB-G-1.

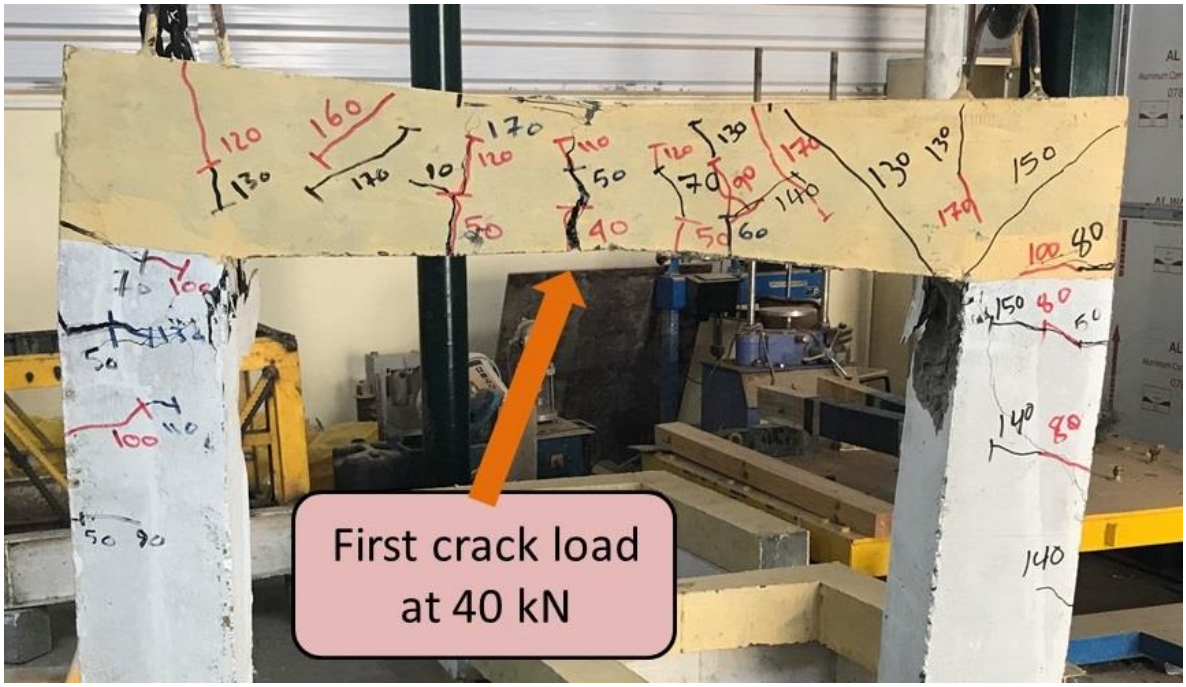

Plate (4-16): Location of first cracks of the NB-100G-1

The first crack gradually increases in width when the loads continue to be applied, and new cracks were formed especially in the flexural region of the beam while both columns started cracking at **50kN** loads. The plastic hinge formed in both the right and left joints when loads of **225kN** were applied, but the frame did not collapse until creating the last plastic hinge in the middle of the beam causing the specimen to collapse. **Plate (4-17)** shows the model cracks and failure locations.

Hybridizing the frame in a similar way to the NB-100G-1 increases the ultimate load by **22%** more than NB-C-1 as the presence of GRPC increases the resistance of the frame to shear stresses and changes the type of failure from a shear failure as in the NB-C-1 to flexural failure after formed plastic hinge at joints. At the same time, the presence of GRPC only in the beam region reduces the ultimate load by **13%** less than NB-G-1.

Plate (4-17) Failure crack and cracks patterns of the NB-100G-1

4.3.1.9: Specimen NB-50GL-1:

This specimen was similar to the NB-100G-1 but differs from it in that the hybridization with GRPC was in the lower half of the beam only (from the centerline of the beam to the lower face of the beam). This specimen was taken to strengthen the bottom of the shear crack track (the beginning of the shear crack initiation) and also to strengthen the tensile region for a positive moment and the compressive region for a negative moment and to find the development in the behavior of the frame.

The specimen started cracking when **40kN** loads were applied in the middle of the beam as a pure bending crack, as shown in **Plate (4-18)**. The increase in the first crack load was **33%** more than that of NB-C-1 and equal to NB-100G-1 and NB-G-1 due to the first cracking onset of this specimen composed of GRPC.

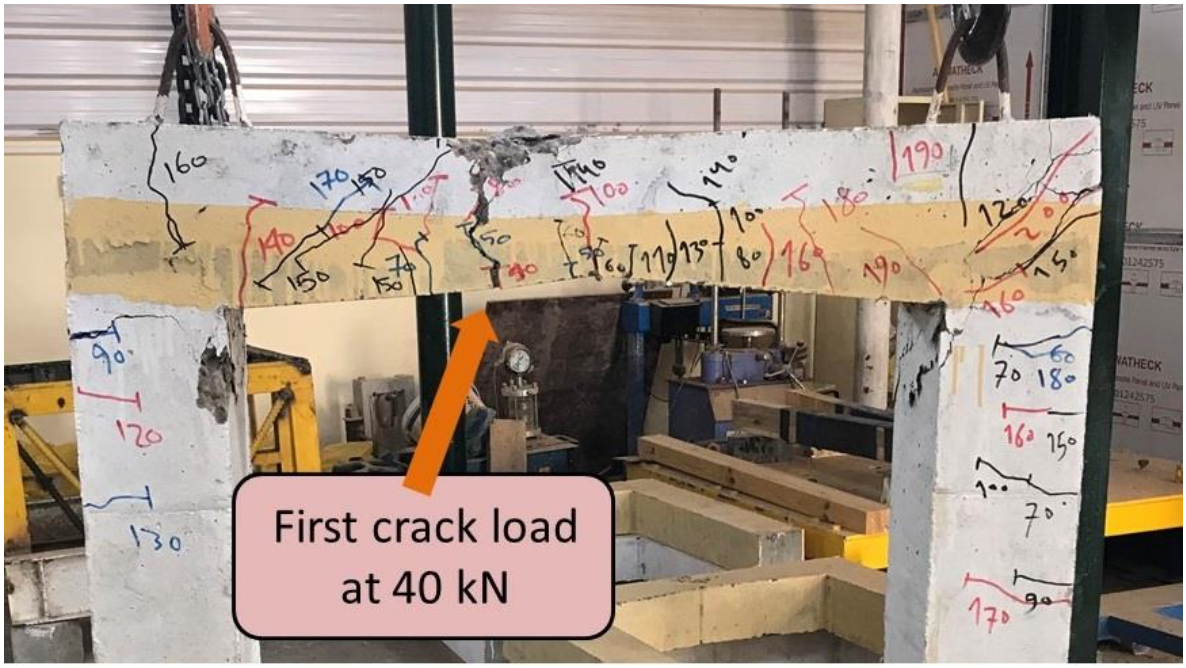

Plate (4-18): Location of First cracks of the NB-50GL-1

The right and left columns started cracking when loads applied **60kN** and **90kN** respectively and continued cracking until the specimen failed at **220kN** loads where the ultimate load was reached. The right joint began to reach the load of the first plastic hinge, and after a very short time, the left joint reached the plastic hinge, then there was a decrease in the loading gauge slightly, followed by the final failure of the specimen in the middle of the beam due to the bending stress, as shown in **Plate (4-19)**.

Plate (4-19) Failure crack and cracks patterns of the NB-50GL-1

Hybridization in this specimen increases the frame's ultimate load by **19%** more than NB-C-1, and the presence of GRPC in the positive moment tension region in addition to its presence in the shear region increases the frame strength by **7%** when compared to the NB-25GLE-1 and changes the type of failure from shear failure to bending failure. Reducing the amount of hybridization by half compared to the NB-100G-1 results in a reduction of the ultimate load strength of the frame by only **2%**.

4.3.1.10: Specimen NB-50GU-1:

This specimen differs from NB-50GL-1 in that the hybridization with GRPC was only in the upper half of the beam (from the centerline of the beam to the upper surface of the beam) while the lower half was conventional concrete. This specimen was taken to determine the effect of strengthening the compressive region in the positive moment and the tension region in the negative moment.

The first crack of this specimen appeared when **28kN** loads were applied in the middle of the beam as a flexural crack, as shown in **Plate (4-20)**. The first crack load was very close or equal to NB-C-1, where the crack appeared below the beam in the conventional concrete region, and the load was not affected by the presence of GRPC in the upper part of the beam.

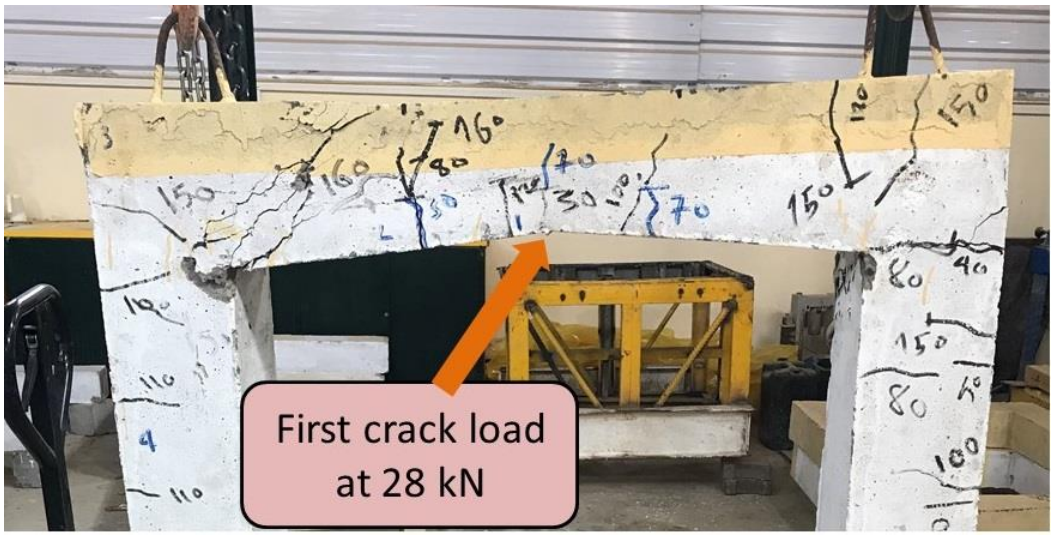

Plate (4-20): Location of First cracks of the NB-50GL-1

The ultimate load for the NB-50GU-1 was **193kN**, where the plastic hinges formed firstly in the right and left joints, but remain standing, and a collapse of the frame occurs due to a shear failure on the left side of the beam. **Plate (4-21)** shows the failure locations of the specimen.

Plate (4-21) Failure crack and cracks patterns of the NB-50GU-1

Frame hybridization as in the NB-50GU-1 increased the ultimate load by **4%** more than NB-C-1 and reduced it by **12%**, **14%**, and **26%** less than NB-50GL-1, NB-100G-1, and NB-G-1 respectively. It was noted that the hybridization in this way did not resist the shear stresses in an optimal way, as happened in the NB-50GL-1, due to the presence of hybridization in the upper part of the beam does not prevent micro-shear cracks from forming during the casting stage, as in the case of the NB-50GL-1, where the micro-cracks cause weakness of the specimen. The micro-cracks expand in conventional concrete with low loads, unlike the GRPC, which resists these cracks and prevents their expansion in the future at high loads.

Summary of Group D (Effect of Hybrid in flexural region of frame):

A summary of the first crack loads, the ultimate loads, the percentages of increase and decrease in the loads compared to the control frame, and the type of failure for the specimens of this group are presented in **Table (4-8)**.

Table (4-8) Summary of the first crack loads and ultimate loads for the group (D)

Sp. Names	P_{cr} (kN)	P_{cr} increases (%)	P_u (kN)	P_u increases of NB-C-1 (%)	P_u decreases of NB-G-1 (%)	Type of failure
NB-C-1 (control)	30	------	185	------	-------	Shear failure
NB-G-1	39	------	260	------	-------	Flexural failure
NB-100G-1	40	33%	225	22%	-13%	Flexural failure
NB-50GL-1	40	33%	220	19%	-15%	Flexural failure
NB-50GU-1	28	-7%	193	4%	-26%	Shear failure

Group E (Effect of Loading Type on Frame):

This group includes eight specimens and was similar to the specimens mentioned in groups (A, B, C, D), but in this group, the loads were applied repeatedly (loading and unloading) by nine cycles. Where in each cycle the load was applied gradually up to approximately **65%** of the ultimate load for a similar specimen under a monotonic load. Then the load was gradually removed until zero loads, then it was left for two minutes to rest, and then a new cycle begins, and so on until the ninth cycle. Two readings of the load and its corresponding deformation are taken at each loading stage, as well as two readings for each unloading stage, in order to draw a non-linear curve when studying the load-deflection curve and deflected shape of the whole frame. The tenth cycle, the specimen was loaded until failure. **Figure (4-3)** shows a diagram of the loading and unloading method for this group.

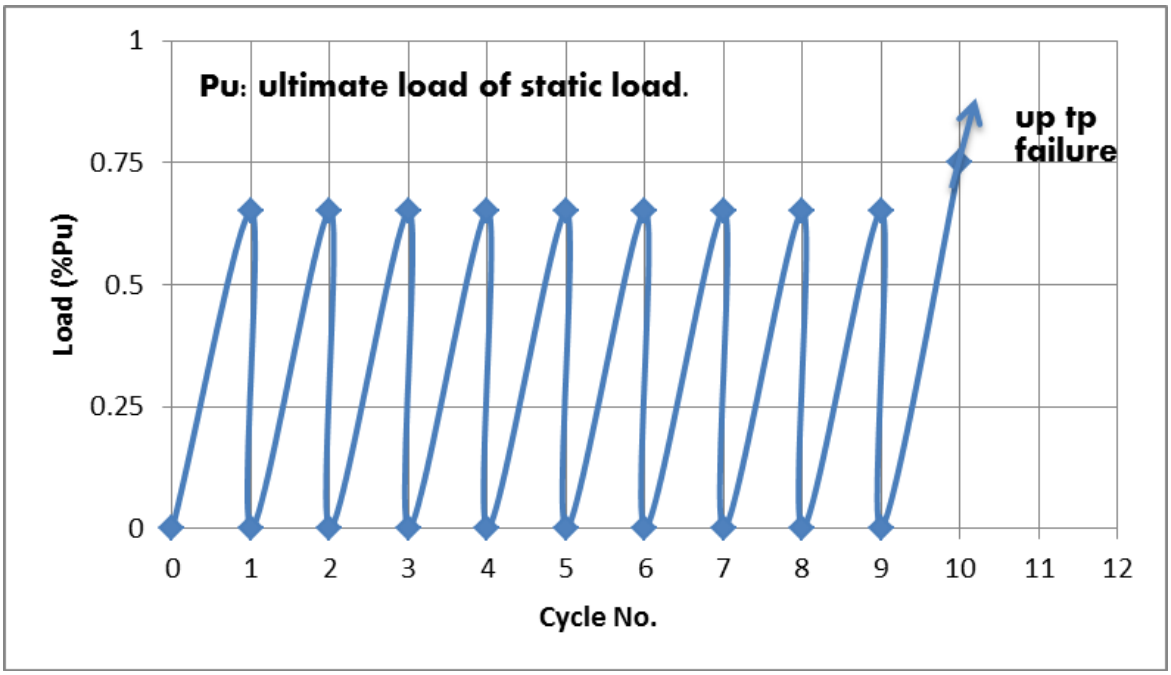

Figure (4-3) The procedure of applied repeated load

4.3.1.11: Specimen NB-C-2:

This frame was similar to the NB-C-1 but tested under repeated loads (loading and unloading) where the loads are gradually applied up to **120kN**, which was equivalent to **65%** of the ultimate load for NB-C-1, after which the load was removed to end the first cycle. Repeating this procedure for nine cycles and then the load was applied until the specimen fails.

When testing this specimen and during the first cycle, the model started to crack, especially in the middle of the beam and the right column at loads of **34kN**, and cracks continued to appear in this cycle and subsequent cycles, especially in the first cycles, while the last cycles, the cracks remained the same and no new cracks appeared.

The final load of NB-C-2 was **135kN** as the frame failed due to shear failure on the left side of the beam which was the same failure in the monotonic load specimen and as shown in **Plate (4-22)**. The ultimate load for this specimen was 27% less than that of NB-C-1 due to the effect of the repeated load where the repeated load of a composite material causes degradation due to the accumulation of discrete micro-damage (e.g. fiber fractures, fiber/matrix debonds, matrix cracks) or macro-crack propagation. Also, it caused a modification in the mechanical parameters of the concrete, which caused a change in the structural responses of the members. This reason applies to all specimens in which the ultimate load decreases as a result of repeated loads.

Plate (4-22) Failure crack and cracks patterns of the NB-C-2

4.3.1.12: Specimen NB-S-2:

This frame was similar to the NB-S-1, but under repeated load, which was similar to the procedure of the testing of specimen NB-C-2, but the maximum load for the first nine cycles was **180kN,** which was equivalent to **67%** of the ultimate load for NB-S-1.

The first crack of this specimen appeared in the first cycle and when **90kN** loads were applied in the middle of the beam as pure bending cracks. As the loads continued to be applied, some other cracks appeared, but they are not many, and with the loading and unloading cycles, the cracks remained almost the same until the last cycle where the specimen failed.

The failure of the NB-S-2 was similar to the failure of the specimen under monotonic load (NB-S-1) where the left and right plastic hinges formed followed by a mid-span beam failure (flexural failure). The ultimate load of

the NB-S-2 was **265kN**. **Plate (4-23)** shows the cracks and failures of the specimen.

Plate (4-23) Failure crack and cracks patterns of the NB-S-2

The effect of the repeated load on the frame with SRPC was less than the frame with conventional concrete, where the percentage of decrease in the ultimate load between the frame under repeated load to the frame under monotonic load was **2%** for SRPC while for frame with conventional concrete was **27%.** So, the SRPC improves the resistance of concrete to repeated loads by **25%**, and therefore it can be used for members exposed to fatigue stresses. The reason for this was the presence of steel fibers in the RPC, which increases the elastic modulus of the mixture as a result of its imprisonment of the concrete particles and thus increases the energy absorption capacity.

4.3.1.13: Specimen NB-G-2:

The NB-G-2 specimen was similar to the NB-G-1, but under repeated load testing, the maximum load for the first nine cycles was **170kN**, which was **65%** of the ultimate load of the NB-G-1. After that, the unloading process begins, then the specimen was carried until failure.

The specimen started cracking in the first cycle of applying loads in the left and right columns, as well as in the beam that first suffered from cracks at the flexural zone. As the beam started cracking when loading of **40kN**, while the columns withstood until the load of **100kN**, where both columns cracked together.

In the last cycle of repeated load, the frame collapsed due to the shear failure on the right side of the beam. The diagonal crack begins from the inner corner of the joint to the position of the load applying where the ultimate load for this specimen was **255kN**. Even though the specimen suffered from plastic hinges at the right and left joint together, followed by a beginner failure of the beam due to bending stresses. **Plate (4-24)** shows the crack pattern and failure crack of the NB-G-2.

The effect of repeated load on the ultimate load of a frame with GRPC was very slight, where the difference in the ultimate load of repeated load to monotonic load was only 2%. The effect of glass fiber on the RPC in the concrete frame appears very clear, as it works to connect the concrete mosaic well and prevents the breaking of the bonds between the concrete parts as a result of the impact of repeated loads.

Plate (4-24) Failure crack and cracks patterns of the NB-G-2

4.3.1.14: Specimen NB-25GLE-2:

This specimen was similar to the NB-25GLE-1, but under repeated load testing, where maximum loads were applied in each of the first nine cycles of **130kN** was equivalent to **63%** of the ultimate load of the NB-25GLE-1.

The first crack occurred in the first cycle when **20kN** loads were applied in the middle of the beam as a flexural crack, while the right and left

columns also cracked in the first cycle when **60kN** and **80kN** loads were applied, respectively

The ultimate load for this specimen was **173kN**, where the specimen collapses when a shear failure occurred on the left side of the beam. Where the shear crack initiation from the inner corner of the left joint to the point of applying loads, as shown in **Plate (4-25)**. Before the collapse, the plastic hinge started in the right and left joints, followed by a beginning of failure in the middle of the beam as a bending failure.

The effect of repeated loading on the hybrid frame with GRPC as the NB-25GLE-2 was obvious, where the ultimate load of the frame decreases by **11%** less than that of the NB-25GLE-1. At the same time, the presence of hybridization with GRPC improves the effect of repeated loading on the ultimate load by **16%** of the frame without hybridization.

The behavior of this specimen before failure differs from that of NB-25GLE-1, as the failure of the NB-25GLE-1 was a shear failure, while in the NB-25GLE-2 plastic hinge joints occurred and a beginning bending failure beam before the shear failure occurred. This was due to the hybridization of the frame with GRPC in the zone subjected to shear stresses, where the effect of repeated load on GRPC was less than conventional concrete as was detected in the NB-G-2. Therefore, plastic hinges at joints occurred in the parts of joints containing conventional concrete only, and then the onset of failure occurred in the middle of the beam containing conventional concrete only, and then shear failure occurred that passes through part of the GRPC.

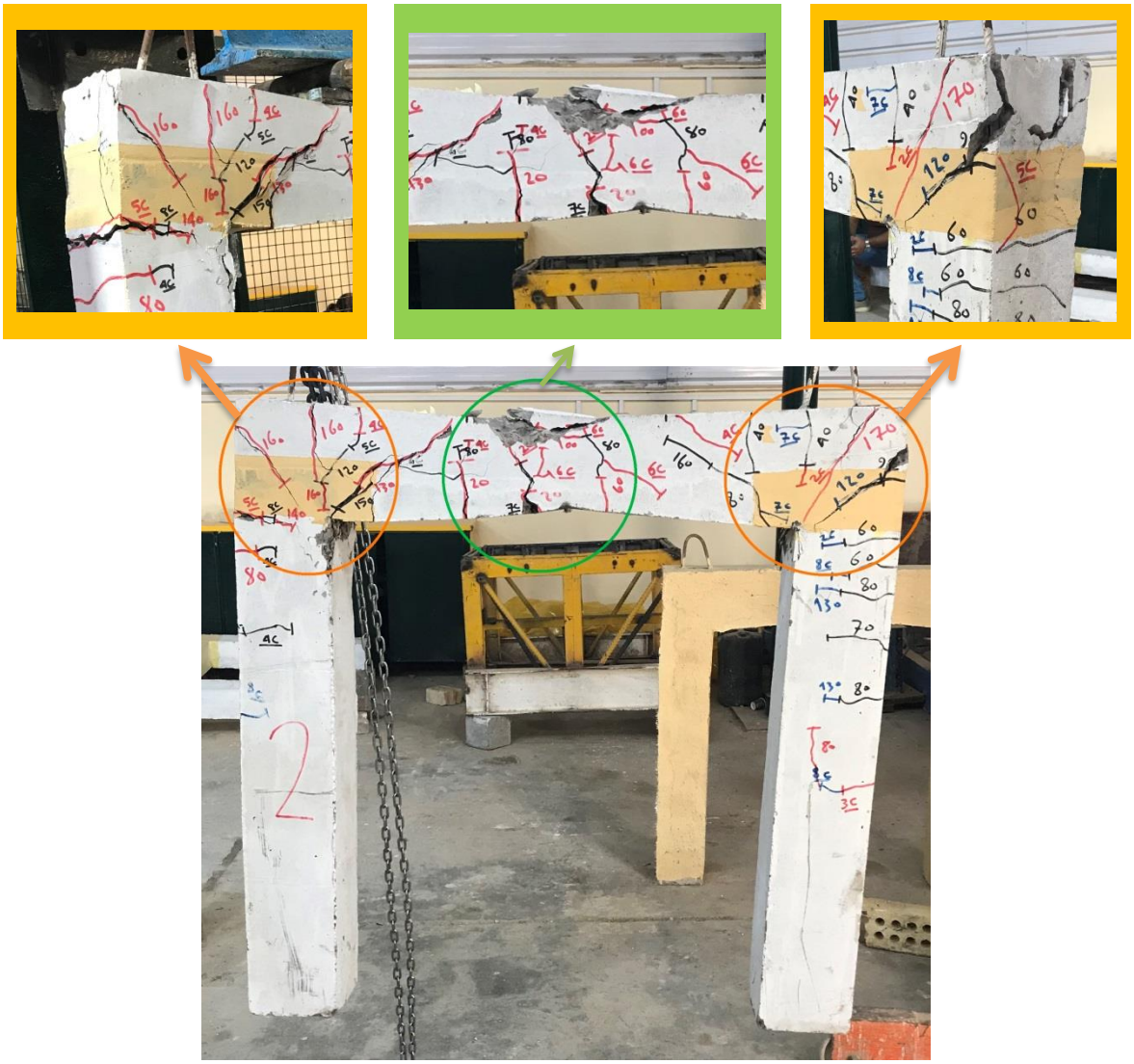

Plate (4-25) Failure crack and cracks patterns of the NB-25GLE-2

4.3.1.15: Specimen NB-50GE-2:

The NB-50GE-2 specimen was similar to the NB-50GE-1 in terms of frame dimensions as well as proportion and locations of hybrid with GRPC but was tested under repeated load as in the specimens of this group, where the maximum load applied in each of the first nine cycles was **140kN**, which was equivalent to **66%** of the ultimate load of NB-50GE-1.

When applying loads and during the first cycle, the beam cracked in the middle at a load of **30kN** and when loads continued to be applied, the left and right columns were cracked together at a load of **60kN**.

Continuously following cycles of loading and unloading, the specimen suffered several cracks, and when the last cycle was reached, the specimen failed at an ultimate load of **180kN** as a shear failure on the left side of the specimen. The failure crack started from the inner corner of the joint to the point of applying the load as a diagonal crack, as shown in **Plate (4-26)**.

Plate (4-26) Failure crack and cracks patterns of the NB-50GE-2

The percentage decrease in the ultimate load for the NB-50GE-2 was **15%** less than that of NB-50GE-1 and this was due to the effect of repeated load. The stages of failure in this specimen were different from the NB-25GLE-2, despite the use of the GRPC in the two specimens at the joints. The reason for this was that in the specimen NB-25GLE-2, the GRPC was in half of the joints, while the second half was conventional concrete, which was

considered weak in repeated load, while the NB-50GE-2 does not contain any conventional concrete at the joints.

4.3.1.16: Specimen NB-100G-2:

The NB-100G-2 specimen was similar to the NB-100G-1 but under repeated load testing where a maximum load of **145kN** (equivalent to **64%** of the ultimate load of the NB-100G-1) was applied in each of the first nine cycles and in the tenth cycle, the load was applied up to failure.

Cracks began to appear throughout the cycles of applying loads and until reaching the tenth cycle and at a load of **215kN**, the specimen started with plastic hinges in the right and left joints together, followed by a failure of shearing on the left side of the beam, as shown in **Plate (4-27)**.

Plate (4-27) Failure crack and cracks patterns of the NB-100G-2

The effect of repeated load on this specimen was small compared to other hybrid specimens, as the percentage of decrease in the ultimate load

does not exceed **4%**, because the cracking that causes the failure of the specimen passes all through the hybridization region.

4.3.1.17: Specimen NB-50GL-2:

This specimen was similar to the NB-50GL-1, but under repeated load testing, the maximum load in each of the first nine cycles was **145kN**, which was **66%** of the ultimate load for the NB-50GL-1.

After the end of the loading and unloading cycles and the accompanying cracks in the beam and columns, and when the last cycle began, the cracks began to be wider until the ultimate load was reached, which was determined at **210kN**, where the right and left joints have plastic hinges, followed by flexural failure at mid-span of the beam. **Plate (4-28)** shows the failure cracks and cracks patterns of the NB-50GL-2.

Plate (4-28) Failure crack and cracks patterns of the NB-50GL-2

The ultimate load for this specimen decreases by **5%** less than NB-50GL-1 and this was the result of the effect of repeated load. The failure in this specimen was similar to the failure of the specimen under monotonic load, and this indicates that the hybridization in this way strengthens the weak regions most affected by the repeated load (shear region), as happened in NB-25GLE-2.

4.3.1.18: Specimen NB-50GU-2:

This specimen was designed to be similar to the NB-50GU-1 and was tested under repeated load where the maximum load was applied in each of the first nine cycles, **130kN** to be equivalent to **67%** of the ultimate load of the NB-50GU-1 while in the tenth cycle, a load was applied until the specimen fails.

The first crack of this specimen appeared at **40kN** loads in the middle of the beam and then cracks continued to appear, especially in the first loading cycles. In the last cycle and when the load reached **170kN**, the right and left joints have plastic hinges then the specimen collapsed when a shear failure occurred on the left side of the beam. **Plate (4-29)** shows the failure of this specimen, where it is noticed that total cracking is observed in the shear zone in conventional concrete only and the loss of some of its parts when lifting the load. At the same time, in GRPC the concrete was not completely crushed due to the presence of GF that act as reinforcing bridges between concrete parts.

The ultimate load for this frame was reduced by **12%** due to repeated load, which was a high percentage compared to other frames hybrid with GRPC in different ways, because of the failure initiation from conventional concrete.

Plate (4-29) Failure crack and cracks patterns of the NB-50GU-2

Summary of Group E (Effect of type of load):

A summary of the maximum first nine cycle loads **($P_{max.Re}$),** percentage of the maximum first nine cycle loads to the ultimate load of similar specimens tested under monotonic load **($P_{max.Re}/P_{u.mon}$),** the ultimate loads **($P_{u.Re}$),** percentage of the decrease of the ultimate load of specimen tested under repeated load to the monotonic load **($\frac{P_{u.Re}-P_{u.mon}}{P_{u.mon}}$)**, and the type of failure for the specimens of this group were presented in the **Table (4-9).**

Table (4-9) Summary of the first crack loads and ultimate loads for the group (E)

Sp. Names	($P_{max.Re}$) (kN)	($P_{max.Re}/P_{u.mon}$) *100 (%)	$P_{u.\,Re}$ (kN)	$\frac{P_{u.Re} - P_{u.mon}}{P_{u.mon}}$ (%)	Type of failure
NB-C-2 (control)	120	65%	135	-27%	Shear failure
NB-S-2	180	67%	265	-2%	Flexural failure
NB-G-2	170	65%	255	-2%	Shear failure
NB-25GLE-2	130	63%	173	-16%	Shear failure
NB-50GE-2	140	66%	180	-15%	Shear failure
NB-100G-2	145	64%	215	-4%	Shear failure
NB-50GL-2	145	66%	210	-5%	Flexural failure
NB-50GU-2	130	67%	170	-12%	Shear failure

4.3.2: Load-Deflection Curve at Mid Span of Beam:

The results of the load-deflection curves at the beam mid-span for the tested frames were taken in groups according to the parametric study for the purpose of discussing the results and making comparisons among the frames.

4.3.2.1: Load-Deflection Curve for Group (A): (changing the cross-section of the beam and columns)

Figure (4-4) shows the relationship between the applied load and the deflection at the mid-span of the beam for the tested frames in this group. The deflection behavior was similar for all specimens, where the load-deflection curve was linear until the first crack, and then it behaved non-linearly. The

inclination of the NO-C-1 load-deflection curve is lower than that of the control frame (P-C-1), due to the small length of the beam that more affects the deflection. While the NB-C-1 frame was less stiff than the control frame due to the small depth of the beam that affects the moment of inertia of the beam.

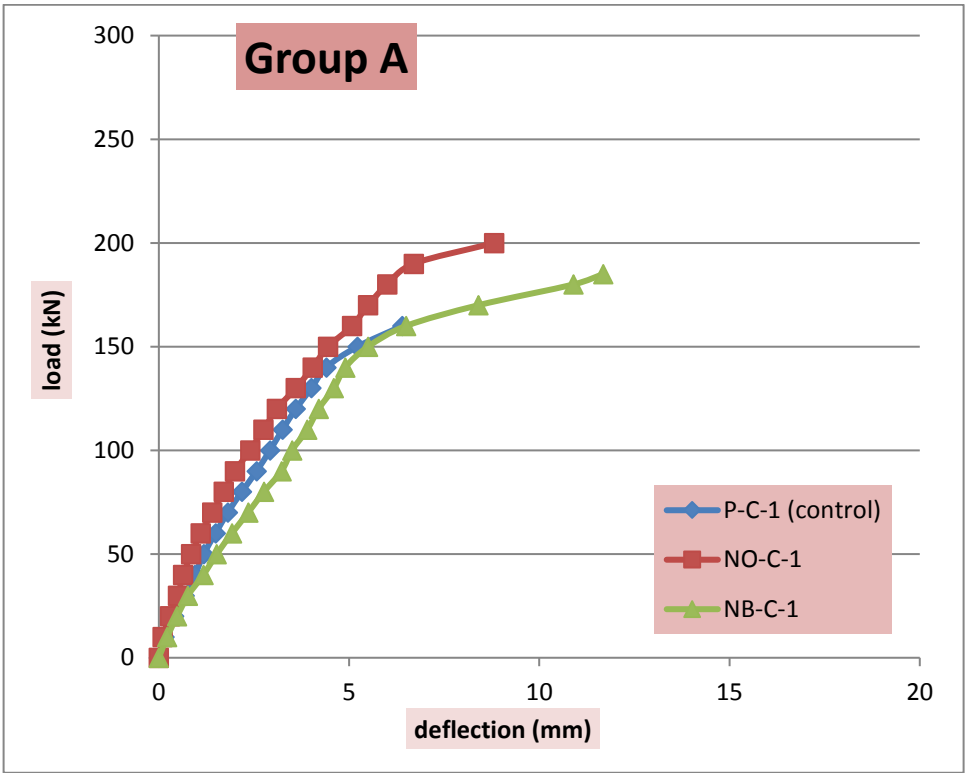

Figure (4-4): Load-deflection curves at mid-span beam for group (A)

4.3.2.2: Load-Deflection Curve for Group (B): (changing type of concrete frame)

The frame behavior of the load-deflection curve at the mid-span of the beam in this group changes according to the change of the type of concrete as shown in **Figure (4-5)**. The use of frame with the conventional concrete has a linear load-deflection curve behavior up to **35kN**, after which the relationship becomes non-linear where a higher increase in deflection commensurate to the

applied load up to **140kN** load, where deflection starts with a very high increase until the specimen fails. For the frame with the SRPC and GRPC specimens, the load-deflection relationship for NB-S-1 and NB-G-1 was applicable until the load **170kN**, after which the NB-G-1 begins to deform more than the NB-S-1 Because the modulus of elasticity of steel fibers was higher than that of glass fibers

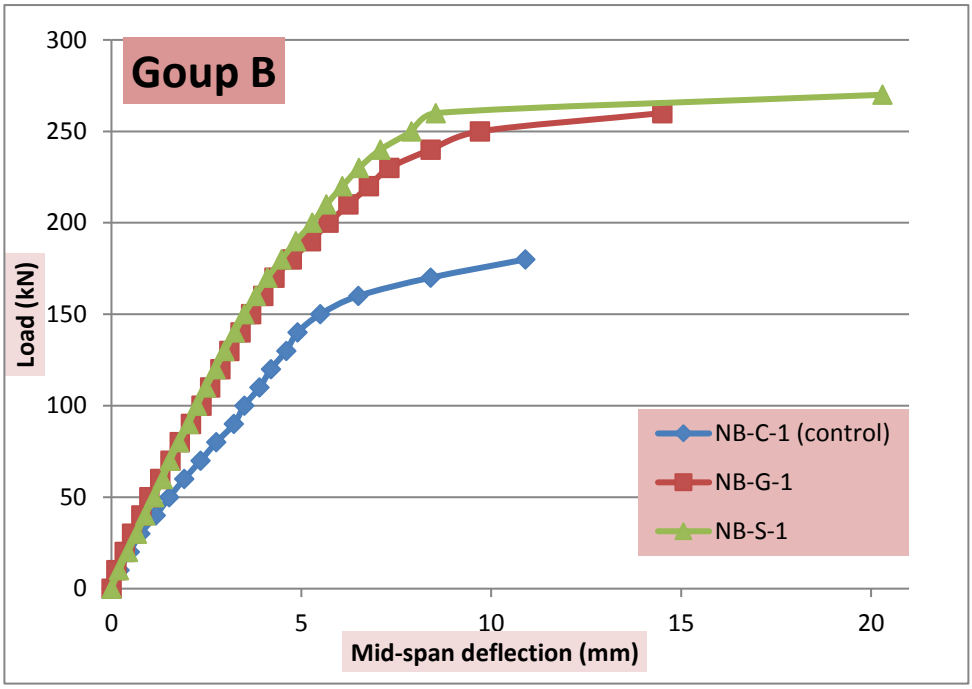

Figure (4-5): Load-deflection curves at mid-span beam for group (B)

4.3.2.3: Load-Deflection Curve for Group (C): (hybridization of conventional concrete with GRPC for shear)

The deflection behavior of the NB-50GE-1 was similar to that of the control frame, but it has a higher ductility before failure than it. The NB-25GLE-1 shows slightly stiffer, although the general deflection behavior was similar for the three specimens, where a load-deformation curve appears with

an inclination of almost the same pattern up to 80% of the ultimate load, after which the deflection increases rapidly with a slight increase in loads, as shown in **Figure (4-6)**.

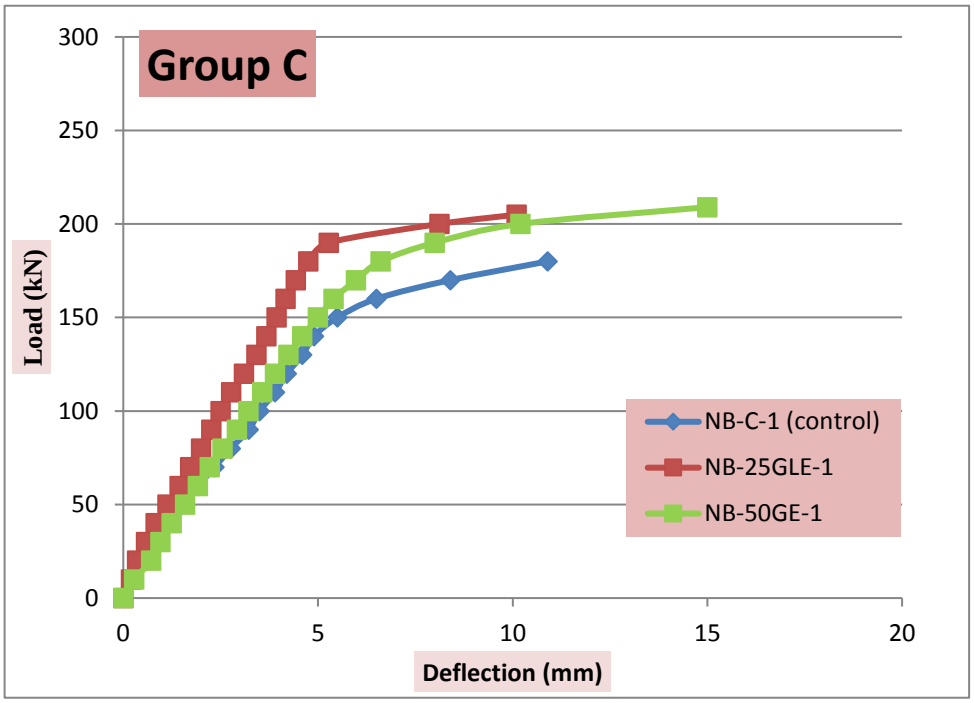

Figure (4-6): Load-deflection curves at mid-span beam for group (C)

4.3.2.4: Load-Deflection Curve for Group (D): (hybridization of conventional concrete with GRPC for bending)

The NB-50GU-1 frame has a load-deflection curve completely similar to the control frame, while the NB-50GL-1 frame has a similar curve to the control frame up to **73%** of the ultimate load of this specimen, after which the increment in deflection of the control frame increases more than before. For the NB-50GL-1 frame, it continues in the same previous increase, and here is the effect of having GRPC in the lower half of the beam. As for the specimen NB-100G-1, it has a curve with a more inclined angle with the horizontal line than the other specimens of this group, and this indicates more stiffness of the

frame, and this was the result of increasing the amount of hybridization with GRPC. **Figure (4-7)** shows the relationship between the applied load and the deflection at the mid-span of the beam for this group specimens.

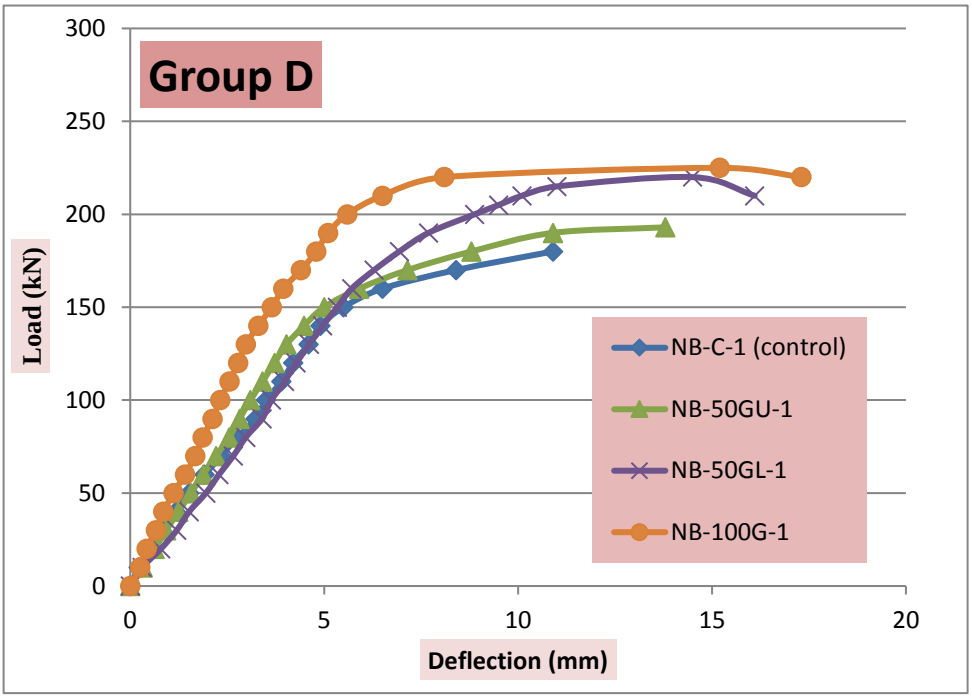

Figure (4-7): Load-deflection curves at mid-span beam for group (D)

4.3.2.5: Load-Deflection Curve for Group (E): (type of loading)

The load-deflection curves at the beam mid-span of the specimens tested under repeated load are shown in **Figure (4-8)**. It was noticed that in the unloading stage after the first cycle, the deformation does not return to zero due to the occurrence of cracks in the frames and overtaking the elasticity stage, and the specimens deal with the plasticity stage.

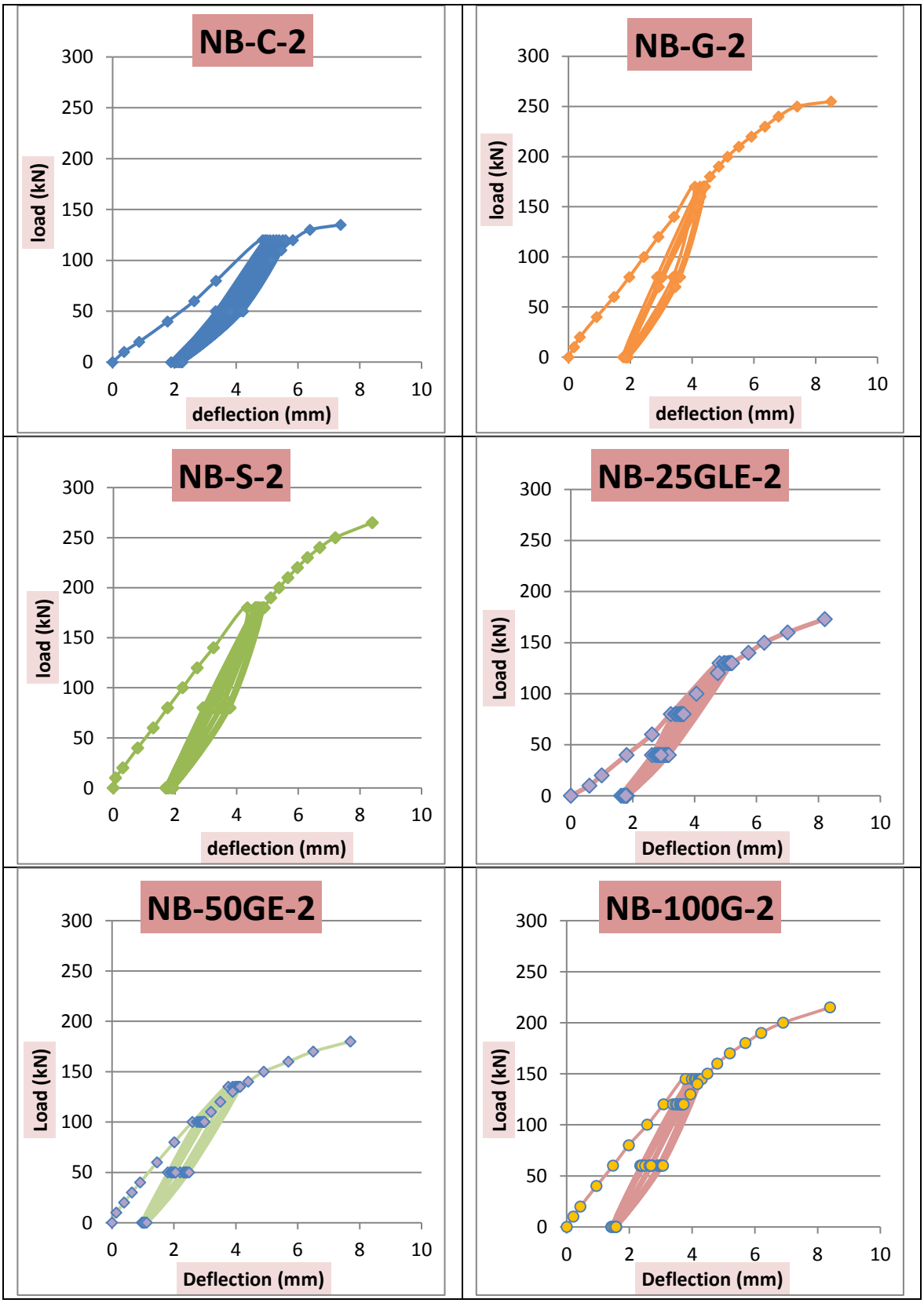

Figure (4-8): Load-deflection curves at mid-span beam for group (E)

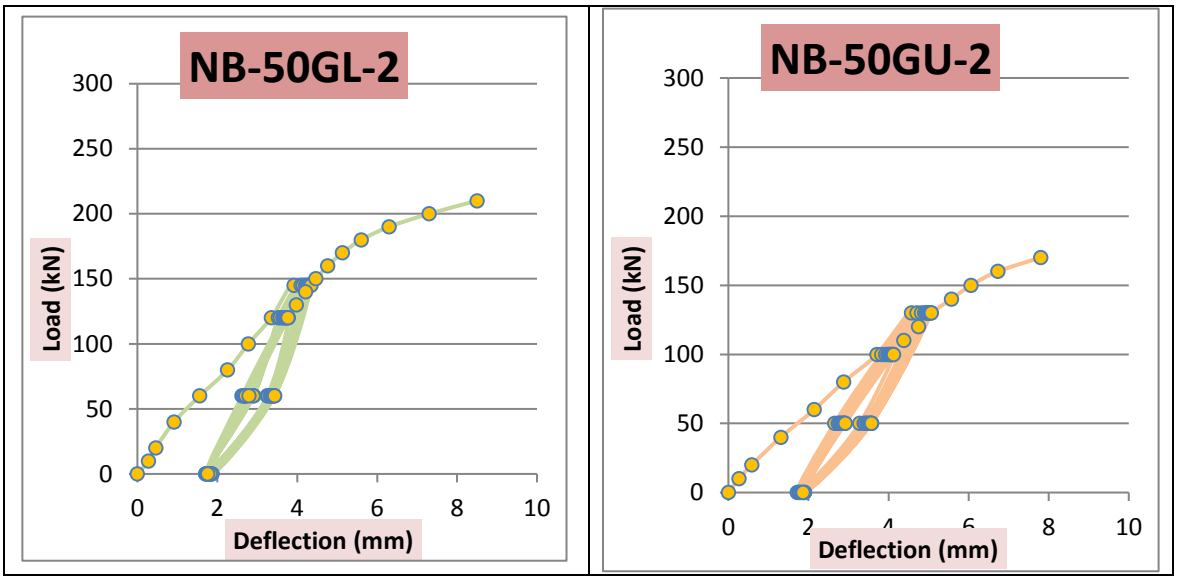

Figure (4-8): Continued

The deflection at the maximum load for each of the first nine cycles was almost equal for all specimens except for the control frame of this group (NB-C-2), which increases after each cycle. The reason for this was the presence of fibers in RPC (glass or steel fibers) that have a high modulus of elasticity compared to conventional concrete, which gives some properties of elasticity even after cracking of the concrete.

4.3.3: Deflection Shape of Frame:

To show the behavior of the total deformation frame during load applied, two-dial gages were placed below the beam and two-dial gages next to the left column. The deformations were read and drawn using the Excel program with each gradual load applied, and a mirror was made for the drawing to clarify the total deformations of the frame. The overview and discussion of the results were divided into five sub-sections according to the change of a parametric study of the thesis, which was as follows:

4.3.3.1: Deflection Shape of Frame for Group (A): (changing the cross-section of the beam and columns)

The deformation of the whole frame relative to the load increase for the specimens tested in this group was shown in **Figure (4-9)**. The use of non-prismatic sections increases deformations before failure. In the NO-C-1 specimen, the deflection of the beam was more than the control frame (P-C-1), especially in the loads close to the collapse loads, while the NB-C-1 specimen notices a high deformation in the beam as well as the columns. Therefore, this feature was taken advantage of by the specimens that fail in shear (as in the specimens of this study) by making the specimen less fragile, and this confirms the results of previous research on the non-prismatic beams. **(MacLeod, 1994)** and **(Qissab and Dhaiban, 2015).**

In **Figure (4-9),** the deflection of the beam below the point of applying load appears higher than the middle of the beam, especially in specimen NB-C-1. This is illogical, as the deformation in the middle of the beam should be higher. The reason for this is that when calculating the deformation of the beam, two dial gages were used to calculate the deformation for one-half of the beam only, as was referred to in chapter three. When the failure of the specimens was a shear failure in the left side where the dial gages were placed, the deformation close to the position of the shear failure was more deformation, and this appeared clearly when generalizing the deformation for the second half of the beam. This is the same reason why the deformation at the top of the column is outward and not inward as in the logical remainder specimens. This situation was repeated in some other specimens with shear failure.

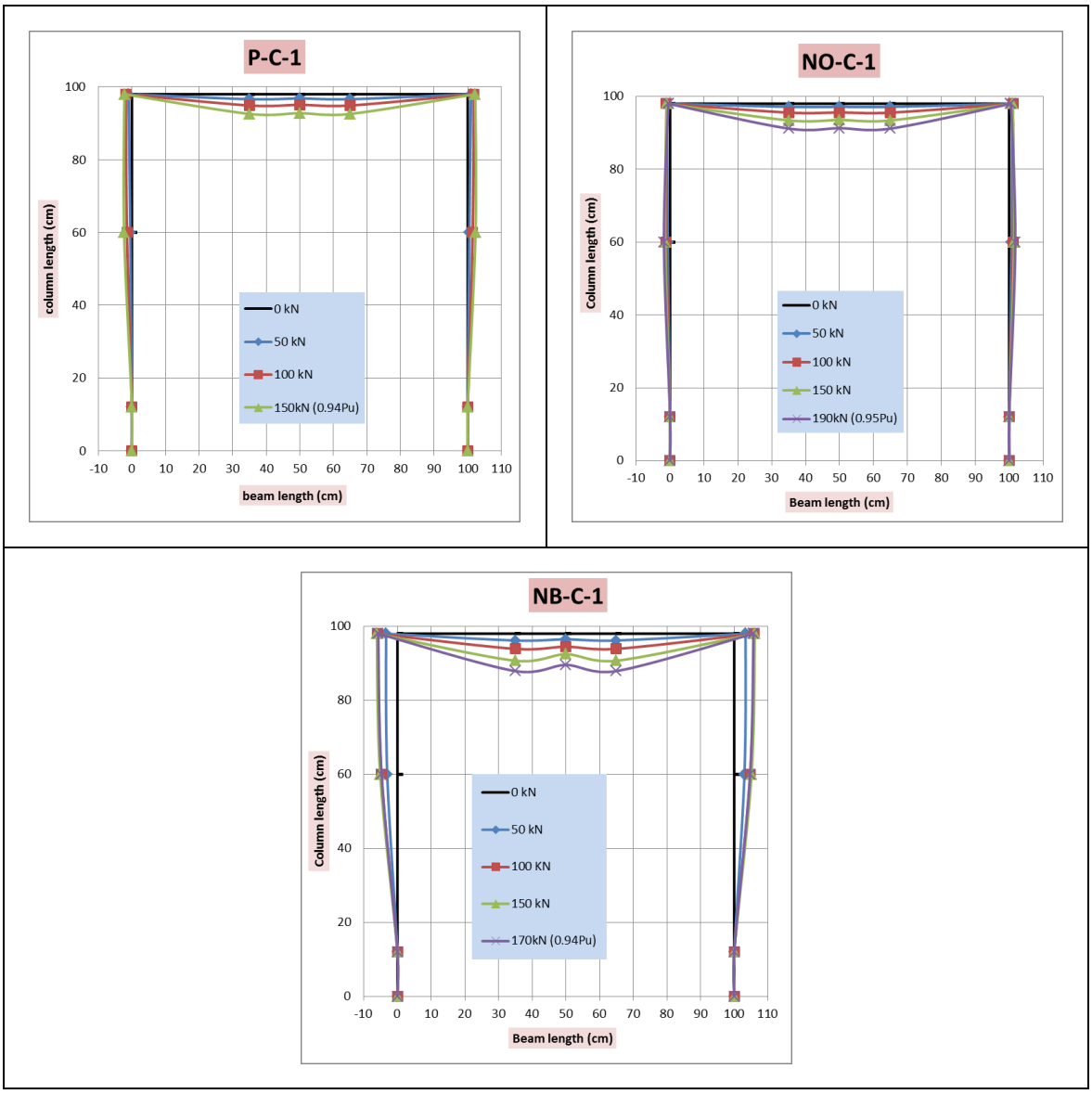

Figure (4-9): Deflected shape for group (A) (All deformation values are multiplied by 10)

4.3.3.2: Deflection Shape of Frame for Group (B): (changing type of concrete frame)

The deflected shape of this group was shown in **Figure (4-10)**. The deformation of the columns of specimens NB-S-1 and NB-G-1, especially in the middle of the column, was less than the control frame, due to the effect of

RPC, which makes the columns stiffer than columns with conventional concrete.

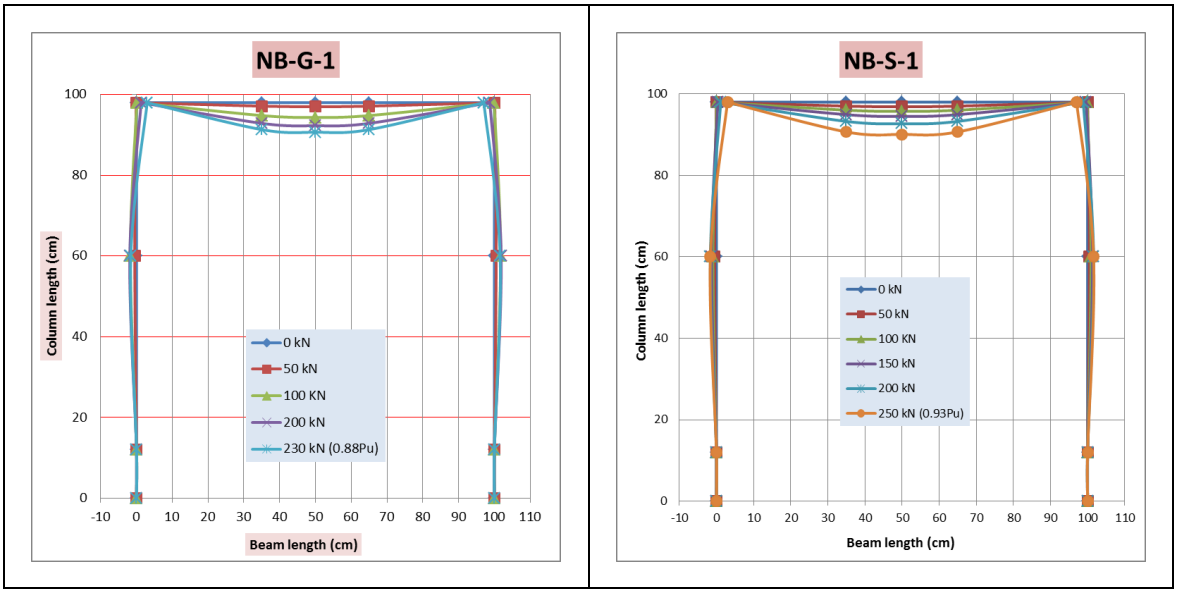

Figure (4-10): Deflected shape for group (B) (All deformation values are multiplied by 10)

4.3.3.3: Deflection Shape of Frame for Group (C): (hybridization of conventional concrete with GRPC for shear)

Figure (4-11) shows the deflected shape of all the tested frames with the applied loads of this group. The beam deformation was observed below the loading points higher than the middle of the beam in the stages close to the ultimate load, unlike other specimens. The reason for this was the fact that these specimens collapsed due to the shear failure on the left side of the beam, so the deformation of the region close to the failure was higher than the middle of the beam.

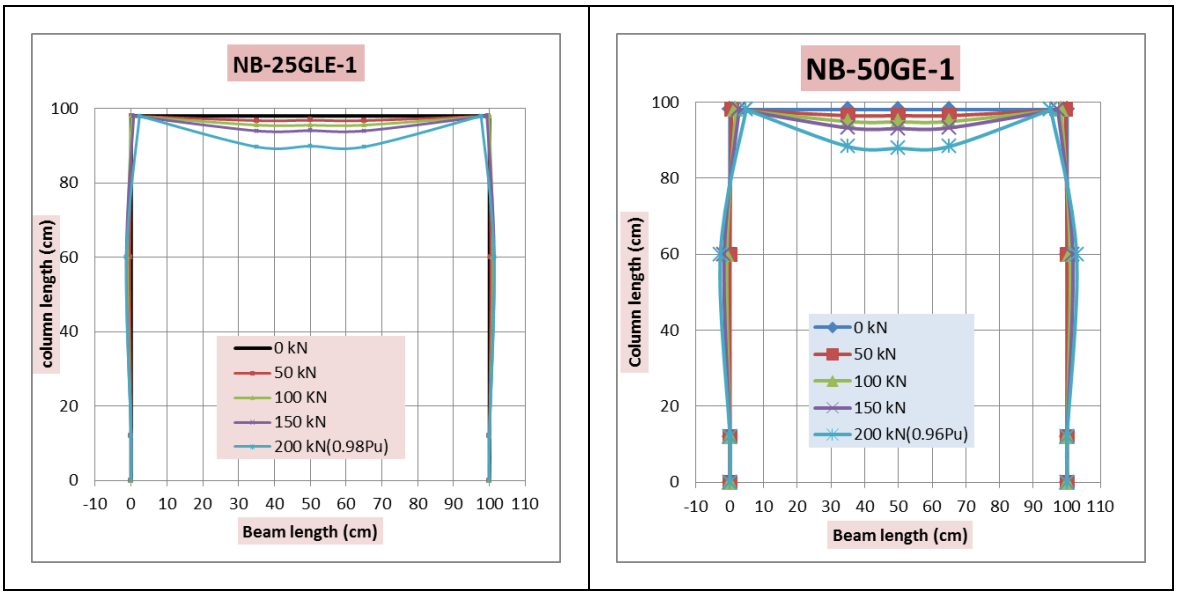

Figure (4-11): Deflected shape for group (C) (All deformation values are multiplied by 10)

4.3.3.4: Deflection Shape of Frame for Group (D): (hybridization of conventional concrete with GRPC for bending)

The effect of the amount and location of hybridization with GRPC appears clearly in the deflected shape of the frame, as shown in **Figure (4-12)**. When the hybridization was in the full beam, as in NB-100G-1, the deflection was low in the beam and high deformation in the columns due to the weak strength of the columns (conventional concrete). When hybridized by 50% of the beam and in its upper part, the deflection in the beam was high compared to other specimens. While in the NB-50GL-1 the deflection in the beam was less than that of NB-50GU-1 due to the presence of GRPC in the tensile region of the positive moment, which works to reduce the deflection of the beam due to the presence of glass fibers that act as bridges between the parts of the concrete, thus reducing its movement and deformation.

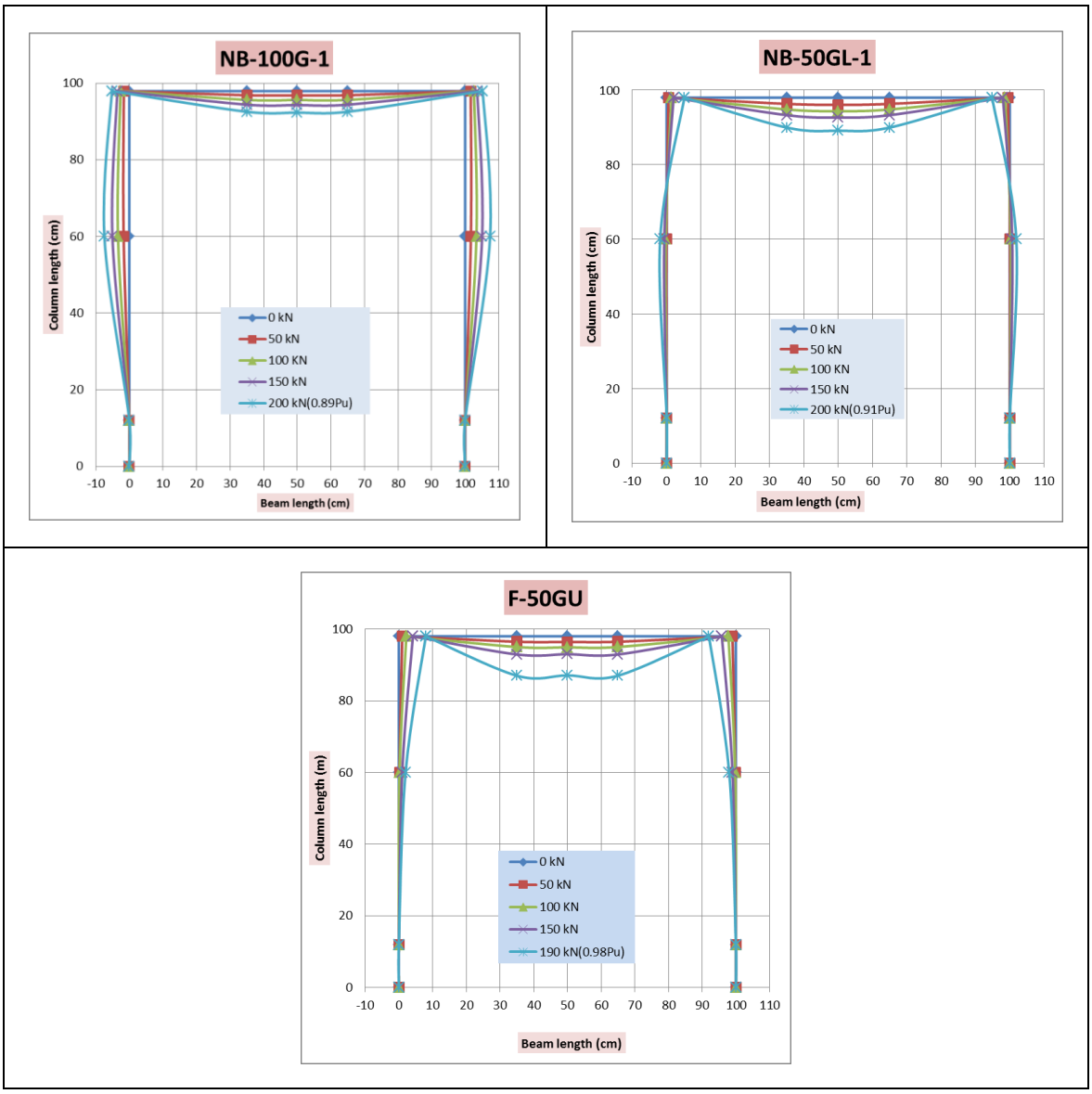

Figure (4-12): Deflected shape for group (D) (All deformation values are multiplied by 10)

4.3.3.5: Deflection Shape of Frame for Group (E): (type of loading)

Figure (4-13) shows the deformation of the whole tested frames under repeated load. The behavior of all specimens was similar, where the deformation was low for all the first loading cycles, and the deformation increased in the last cycle loaded. The deformation of the columns in all the hybrid specimens with GRPC as well as the NB-G-2 specimen was relatively

low and it was similar to the control frame (NB-C-2). As for specimen NB-S-2, it has a high deformation of columns due to the high modulus of elasticity of SRPC due to the high modulus of elasticity of steel fibers.

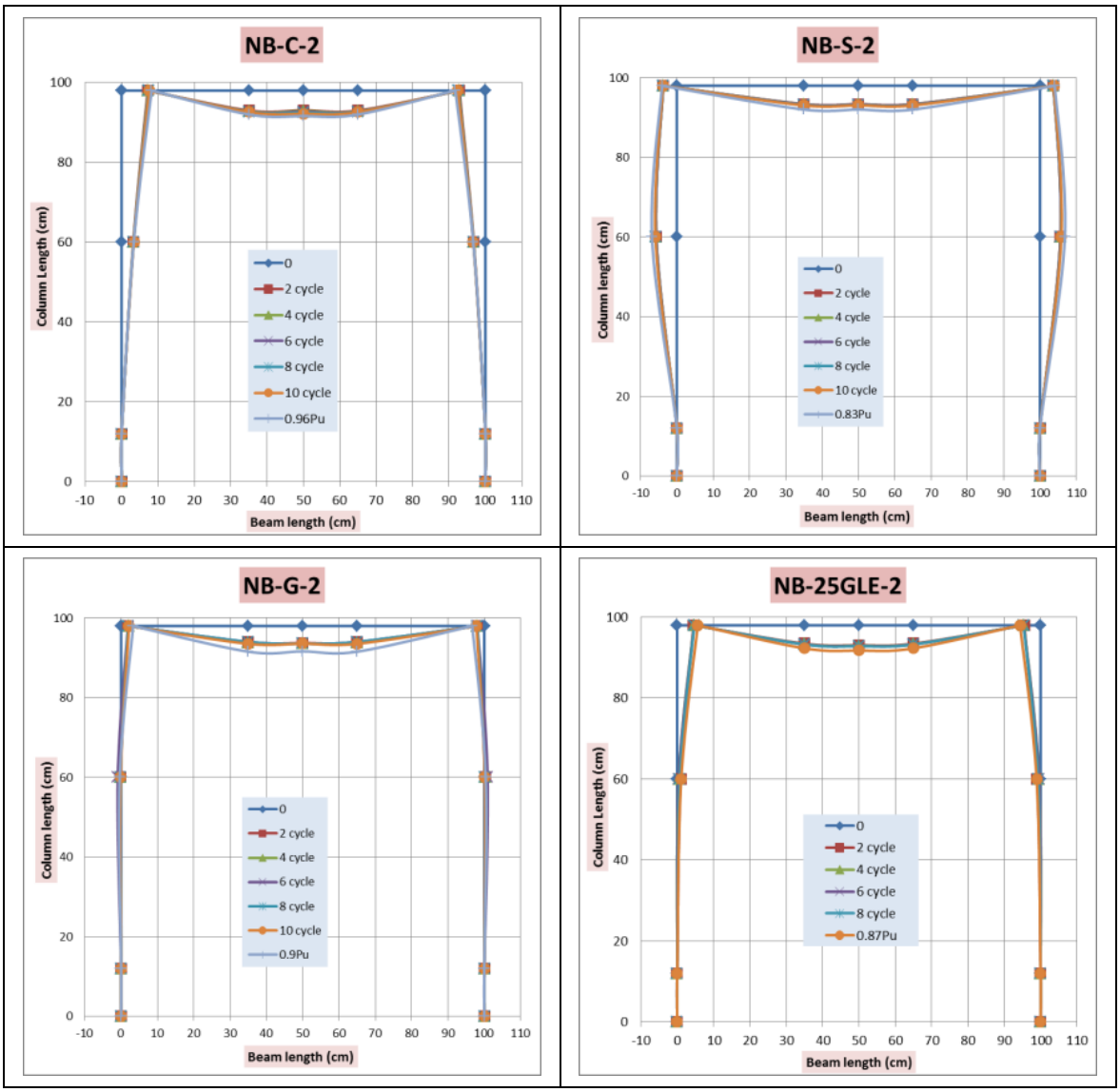

Figure (4-13): Deflected shape for group (E) (All deformation values are multiplied by 10)

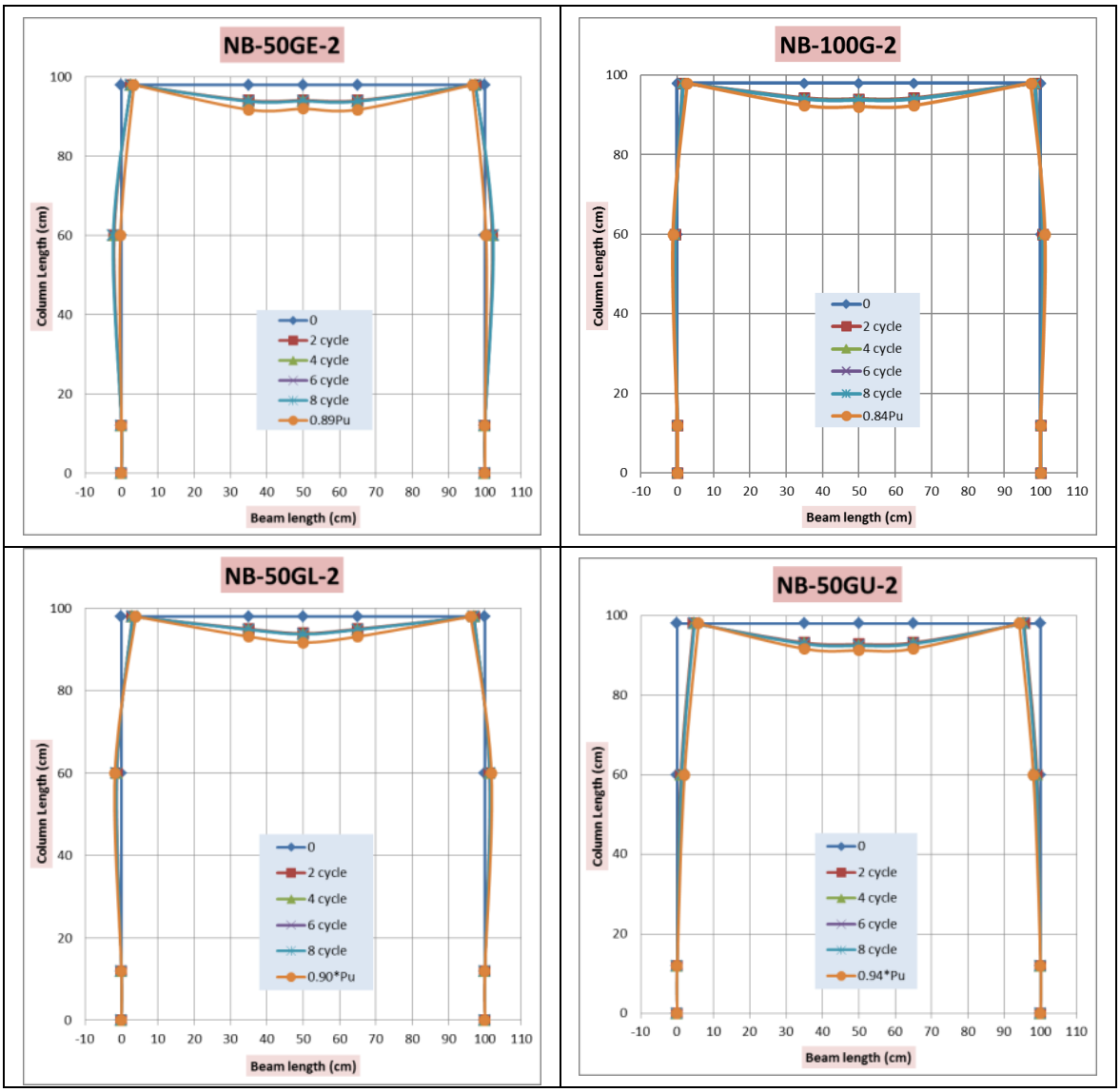

Figure (4-13): Continued

4.3.4: Load Crack Width Relationship:

The development of the crack width by increasing the applied loads for the tested specimens was divided into five groups according to the parametric study for the purpose of studying them and making comparisons between the specimens. All results were compared with **(ACI 224R-01)** where the maximum crack width is 0.41 mm.

4.3.4.1: Load Crack Width Relationship for Group (A):

The effect of using non-prismatic sections appears very clearly on the crack width before failure. This confirms the results of **(MacLeod, 1994)** and **(Qissab and Dhaiban, 2015)**, which showed that the use of non-prismatic sections increases the ductility before failure, and this appears through increasing the crack width of non-prismatic frames. **Figure (4-14)** illustrates the relationship between load and crack width for the crack in the middle of the beam for specimens P-C-1, NO-C-1, and NB-C-1.

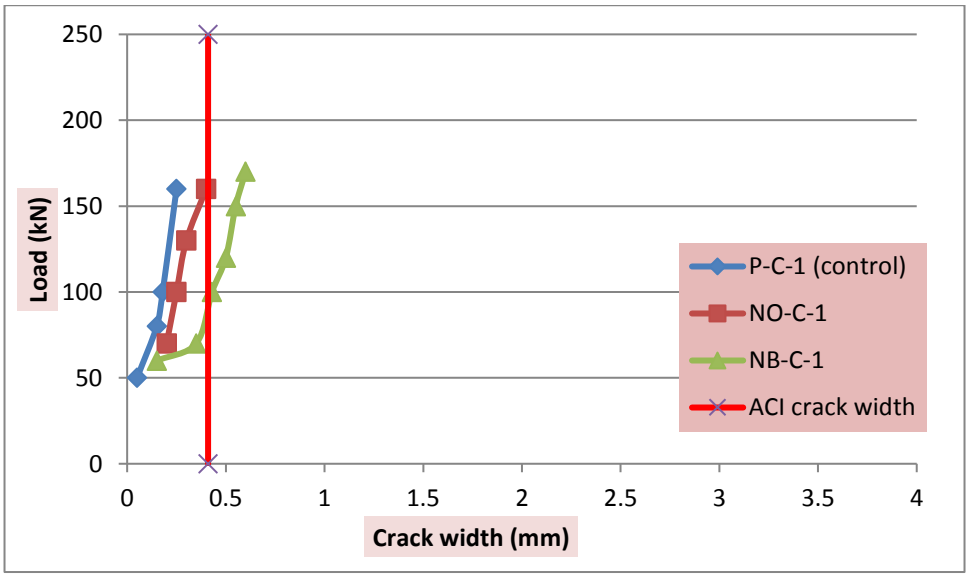

Figure (4-14) Load-crack width for group (A)

4.3.4.2: Load Crack Width Relationship for Group (B):

Figure (4-15) shows the load-crack width for the NB-C-1, NB-S-1, and NB-G-1. The crack width of NB-S-1 appears more than the other specimens due to the aspect ratio of the steel fibers, which makes the concrete's resistance to cracks very high, so we find few cracks, but with a high crack width, and this is the opposite of GRPC, in which the glass fibers

have a high aspect ratio, so they have many cracks and a limited crack width since the deformation is distributed over a wider region.

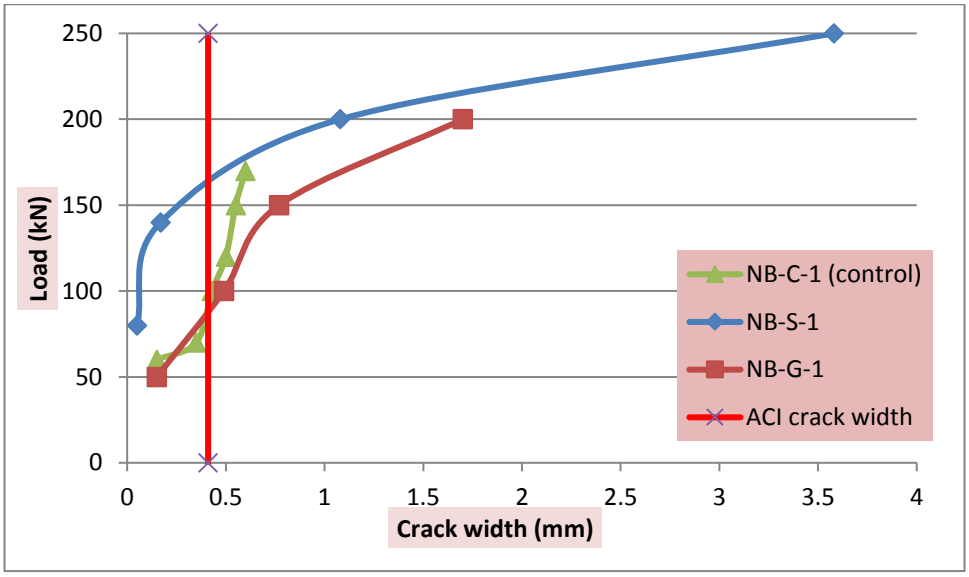

Figure (4-15) Load-crack width for group (B)

4.3.4.3: Load Crack Width Relationship for Group (C):

Crack width by the load change for specimens NB-C-1, NB-25GLE-1, and NB-50GE-1 was shown in **Figure (4-16)**. The presence of GRPC at the edges of the beam appears to increase the crack width in the middle of the beam crack due to the presence of GRPC, It strengthens the edges of the beam and reduces the deformation, so the deformations are more concentrated in the middle of the beam and make the crack width wider.

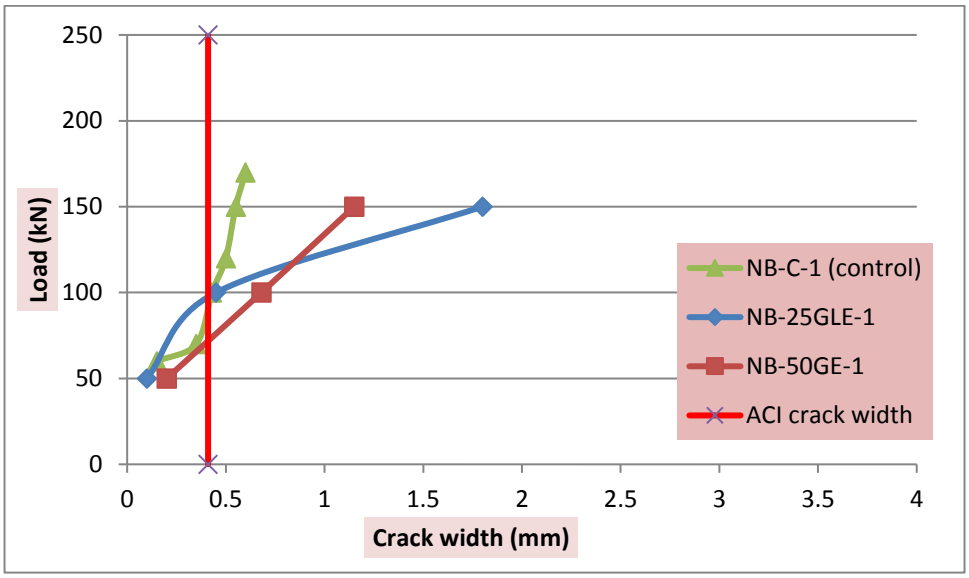

Figure (4-16) Load-crack width for group (C)

4.3.4.4: Load Crack Width Relationship for Group (D):

The crack width with variable load of the specimens of this group was close except for NB-50GU-1 which has a crack width more than the others. **Figure (4-17)** shows the relationship load-crack width for the specimens of this group.

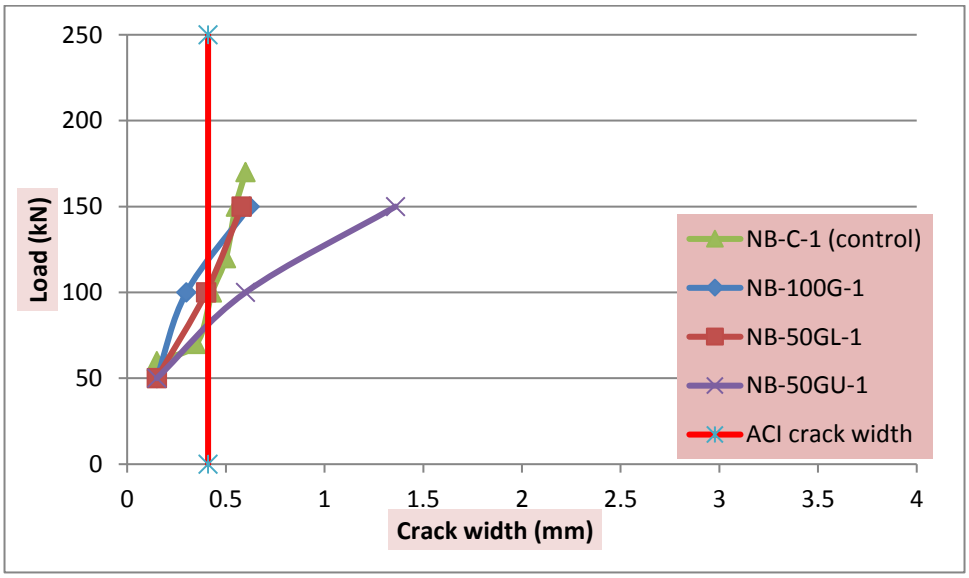

Figure (4-17) Load-crack width for group (D)

4.3.4.5: Load Crack Width Relationship for Group (E):

The crack width behavior of the tested frame under repeated load varies according to the material of each frame. In some specimens, the crack width was close in all cycles except for one or two cycles that were different while in other specimens, the crack width increases as the number of loading and unloading cycles increases. **Figure (4-18)** shows the crack width at the maximum loading per cycle.

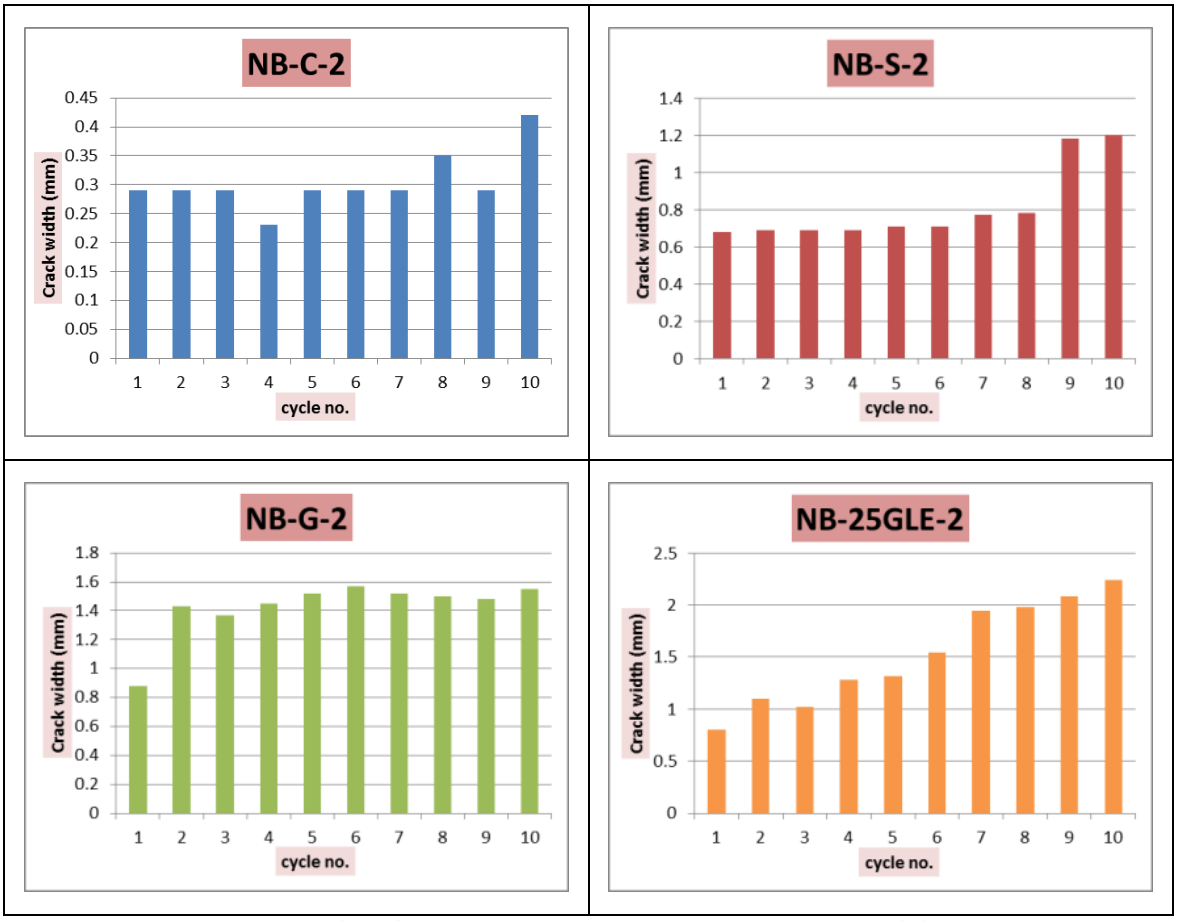

Figure (4-18) Crack width-cycle numbers for group (E)

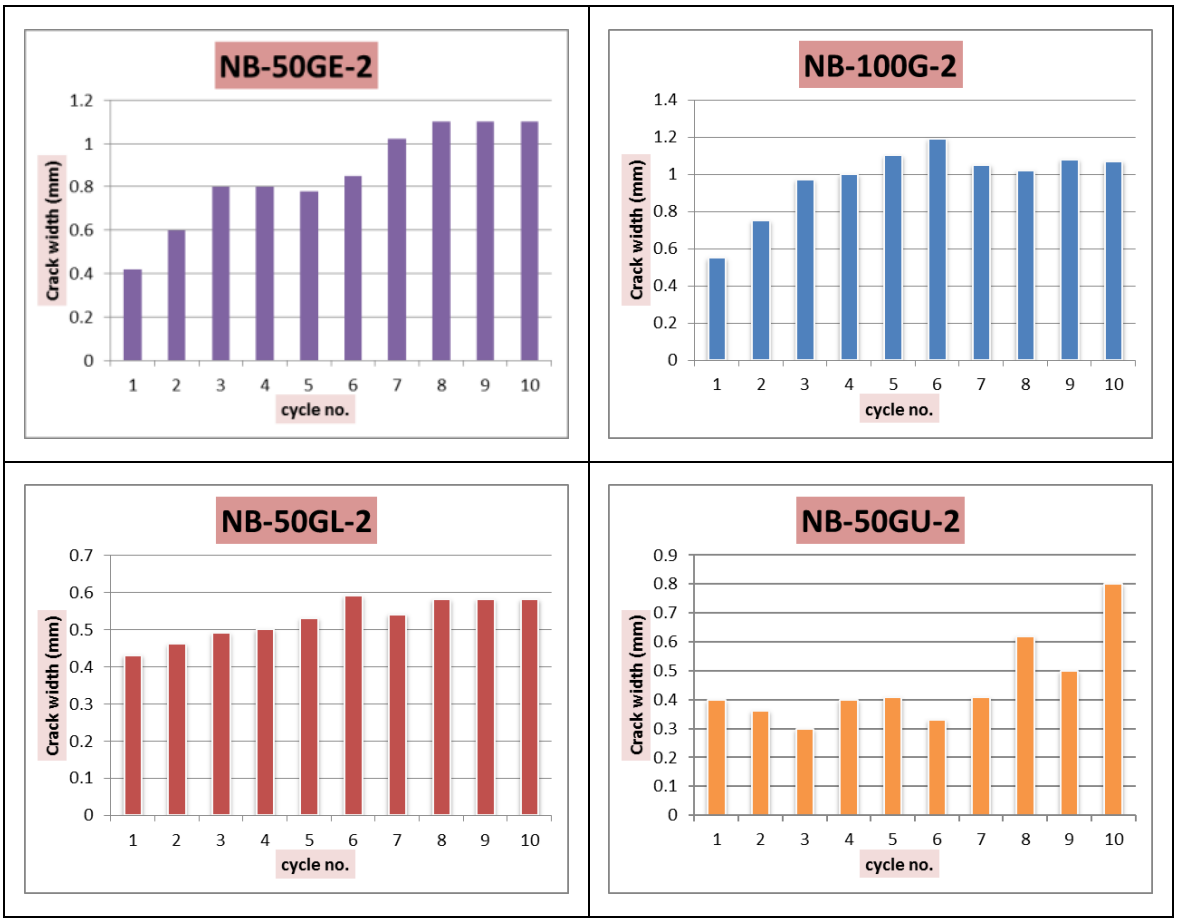

Figure (4-18) Continued

4.3.5: Stiffness of Frame:

Stiffness is the force required to produce one unit of deformation in a member. The initial stiffness can be calculated by determining the slope of the load-deflection curve at the servicing stage (the ratio of the load at 65% of the ultimate load of the specimen to the corresponding deflection) **(AL-Khafaji et al- 2018)**. In comparison, the elastic load is determined by the first crack load **(Moosa and Ali- 2022).**

In this study, for organizational purposes, this section is divided into two subsections according to the method of applying the load (monotonic load and repeated load), in which the initial stiffness is addressed.

4.3.5.1: Stiffness of Frames Under Monotonic Load:

In this section, the initial stiffness of the specimens tested under monotonic load (the first four groups) is discussed. The initial stiffness was calculated by dividing the service load of the specimen (0.65 of ultimate load) by its corresponding deflection (deflection in the middle of the beam). The initial stiffness results are presented in **Table (4-10).**

Table (4-10) Stiffness results of the specimens tested under monotonic load

Name Sp.	0.65 P_u (kN)	Deflection at 0.65P_u (mm)	Stiffness (K_i) (kN/mm)	$\frac{K_i^{*} - K_c^{**}}{K_c}$ (%)	Note
Group A					
P-C-1	104	3.05	34.1	-------	Control
NO-C-1	130	4.75	27.4	-20	
NB-C-1	120	4.2	28.6	-16	
Group B					
NB-C-1	120	4.2	28.6	--------	Control
NB-S-1	176	4.33	40.6	42	
NB-G-1	169	4.26	39.7	39	
Group C					
NB-C-1	120	4.2	28.6	--------	Control
NB-25GLE-1	133	3.5	38	33	
NB-50GE-1	138	4.53	30.5	7	
Group D					
NB-C-1	120	4.2	28.6	-------	Control
NB-100G-1	146	3.51	41.6	45	
NB-50GL-1	143	5.07	28.2	-1	
NB-50GU-1	125	3.88	32.2	13	

* Initial stiffness of specimens.

** initial stiffness of control specimen of each group.

Table (4-10) shows a decrease in the initial stiffness of the specimens NO-C-1 and NB-C-1 of Group A by **20%** and **16%** compared to P-C-1, respectively. These results confirm the results of previous research, in that the presence of a non-prismatic section reduces the stiffness of the member as a result of the formation of cracks in the shear direction before shear failure. **(Tena-Colunga et al, 2008) (Balduzzi, 2016)**

In Group B, the effect of the SRPC and GRPC on the frame stiffness appears very clearly, as the initial stiffness increases by 42% and 39% for specimens NB-S-1 and NB-G-1 compared to NB-C-1, respectively. The reason for the increase in stiffness in NB-S-1 above that of NB-G-1 is that the modulus of elasticity of steel fibers is higher than glass fibers, and thus the energy absorption capacity of SRPC is higher than GRPC. **(Algburi et al, 2018)**

In Groups C and D, the effect of hybridization with GRPC on the frame stiffness appears variable according to the quantity and location of hybridization, ranging from a decrease of 1% to an increase of 45%, as shown in **Table (4-10).**

4.3.5.2: Stiffness of Frames Under Repeated Load:

To study the effect of repeated loading on the frame stiffness, the initial stiffness was calculated in each loading cycle for each specimen. The maximum load for each cycle was divided by its corresponding mid-span beam deflection, and comparisons were made between the loading cycles. **Figure (4-19)** displays the changes in frame stiffness with loading cycles for all specimens.

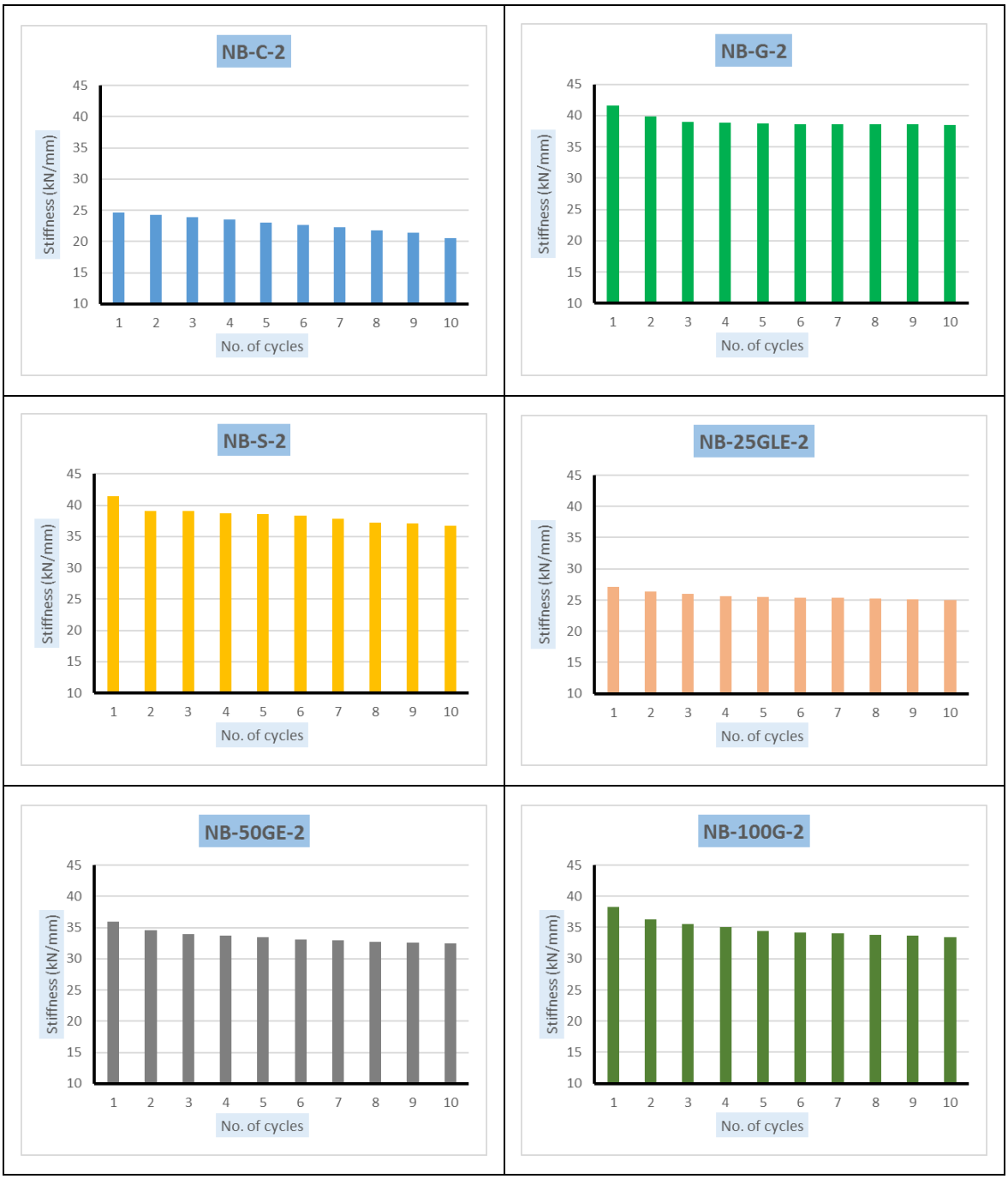

Figure (4-19) Frame stiffness of specimens under repeated load

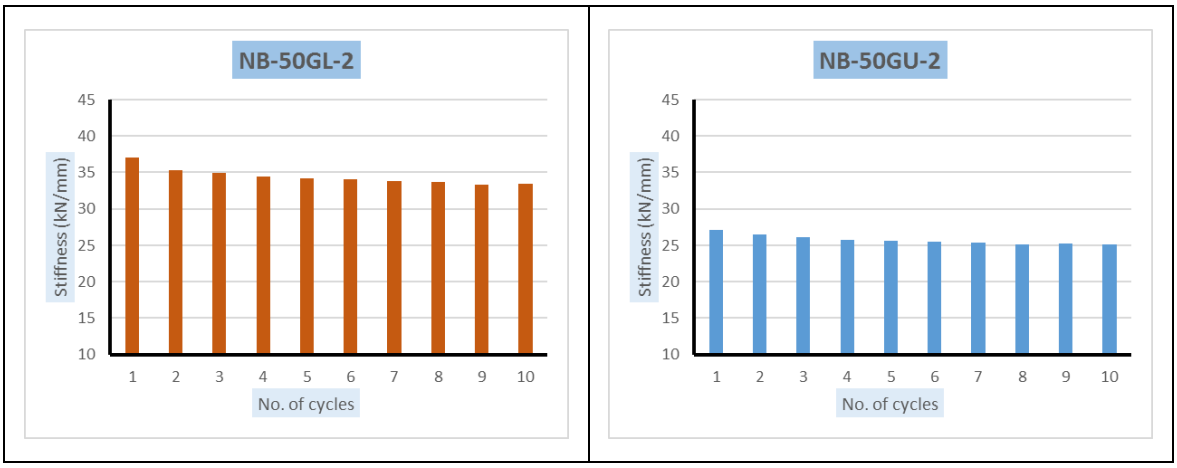

Figure (4-19) Continued

Figure (4-19) shows that the initial stiffness decreases with the progression of the loading and non-loading cycles for all specimens. The reason for this is that the elasticity stage is exceeded and cracks occur in the beam and columns for all specimens in the first cycle of loading.

CHAPTER FIVE

Chapter Five

Numerical Applications Using ABAQUS Program

5.1: Introduction:

This chapter uses a numerical simulation (Finite Element Method (FEM)) to increase the parametric study of the plane frame, as it is a practical and cost-effective method. FEM developed using the ABAQUS program was used.

In this study, ABAQUS/CAE2017 represents the concrete plane frame of prismatic and non-prismatic sections, with conventional concrete and RPC, using one type of concrete or hybrid concrete under monotonic load.

5.2: Modeling of Reinforced Concrete Frame:

This section presents the details of the materials used in the Abaqus program to simulate the experimental specimens, as it deals with the element selected, the interaction between the different types of materials, the boundary conditions for support, loading, and the meshing convergence of the concrete frame model.

5.2.1: Element Selection:

In the Abaqus, many different elements can be used, each one has its characteristics. A three-dimensional element with eight nodes (C3D8) was used to simulate solid concrete and bearing steel loading, as shown in **Figure (5-1-a)**. This element is capable of modeling nonlinear geometric and

materials as well as high deformation **(Abaqus, 2014) & (Hibbitt et al, 2016)**. While simulating the main reinforcing steel of the beam and columns, as well as the shear reinforcement for the beam and column, a linear three-dimensional of two node truss elements (T3D2) were used, as in **Figure (5-1-b).**

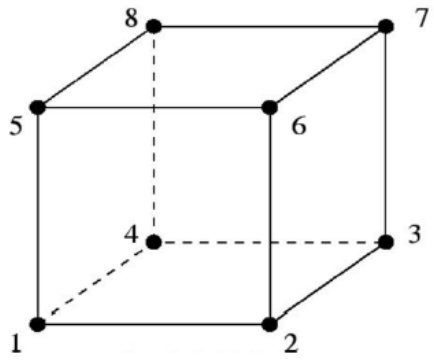

a. 3D brick element (C3D8)

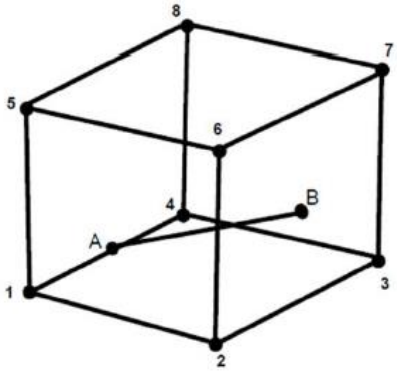

b. 2 node 3D truss element (T3D2)

Figure (5-1): The geometry ABAQUS elements used in this study (Zebalah, 2020)

5.2.2: Modeling of Material in ABAQUS:

In order to accurately simulate the models in the ABAQUS program, the material properties are entered in the elasticity and plasticity stages. The elastic stage includes entering the material's elastic modulus data and Poisson's ratio. As for the plasticity stage, the ABAQUS provides a set of different models according to the behavior of the materials after the elasticity stage. In this study, concrete damage plasticity (CDP) is used for concrete, and its details will be discussed in the next paragraph. As for reinforcing steel, bilinear plastic behavior is used, while the loading steel plate is represented in the elasticity stage only.

5.2.2.1: Modeling of Concrete:

The ABAQUS program provides three models for the purpose of providing low confining pressure for concrete after the elasticity stage (concrete damage plasticity (CDP), Concrete Smeared Cracking, and Concrete brittle cracking).

"Concrete smeared cracking model applied with ABAQUS/Standard and offers significant simplifications for concrete structures which are supposed to represent compressive crushing or tensile cracking. While, a concrete brittle cracking Model is used for structures under dynamic load and it is only available in ABAQUS/Explicit" **(Zebalah, 2020).** On the other hand, the CDP estimates the response of concrete structures and quasi-brittle materials under static, repeated, and dynamic loads and can be found in ABAQUS/Standard and ABAQUS/Explicit. Accordingly, the most suitable model for conventional concrete and RPC is CDP.

"Compressive crushing and tensile cracking are the two failure mechanisms assumed by the CDP model. This model also accounts for material stiffness loss and the influence of stiffness recovery under cyclic load. Damage plasticity is used to identify concrete phenomena in compression and tension using the CDP model". **(Abdulameer, 2022)**

1. **Elastic Stage:**

At this stage, data for the modulus of elasticity and Poisson's ratio are entered. Poisson's ratio for concrete ranges between (0.15-0.25) **(Anson and Newman, 1966)**. As for the modulus of elasticity, it is calculated according to the type of concrete, as **equation (5-1)** is used for RPC **(Grayeabl, 2007)**, while conventional concrete uses an **equation (5-2) (ACI 318-19, 2019)**.

$E = 3840\sqrt{f_c'}$ (MPa) . . . . . (5-1)

$E = 4700\sqrt{f_c'}$ (MPa) . . . . . (5-2)

2. Concrete Damage Plasticity (CDP):

At this stage, the concrete is represented by three steps: plasticity parameter, compression behavior, and tensile behavior. See Appendix D.

5.2.2.2: Modeling of Steel Reinforcement:

The characteristics of the reinforcing steel bars used in the Abaqus program were represented by data of bars for elasticity and plasticity stages. The elastic stage is described by elastic modulus and Poisson's ratio, which are 200,000 MPa and 0.3 respectively. While the plasticity stage is represented by stresses and strains corresponding to it for the yield and ultimate stages and obtained by experimental tests, where it is used to model the plastic behavior (bilinear behavior) of reinforcing steel.

5.2.2.3: Modeling of Loading Plate:

Only the elastic stage is used to describe the properties of the load plates which are 200,000 MPa and 0.3 for modulus of elasticity and Poisson's ratio, respectively.

5.2.3: Modeling of Interaction:

In the Abaqus program, when representing two or more different parts of the materials, the program requires that there is a certain restriction between the materials connected together. In this study, there are three types of interactions according to the observed experimental behavior of the tested frame, which are as follows:

5.2.3.1: Interaction Between Steel Reinforced Bars and the Surrounding Concrete:

In this analysis, an embedded region constraint is used to connect the elements of the reinforcing steel rods and the surrounding concrete element, as shown in **Plate (5-1)**. "Embedding allows for the proper connection of each node of the reinforcement element to the nearest concrete node. This bonding type doesn't include the slip effects of concrete beam reinforcements, but that effect has been partially considered by defining concrete tension softening". **(Malm, 2006)**

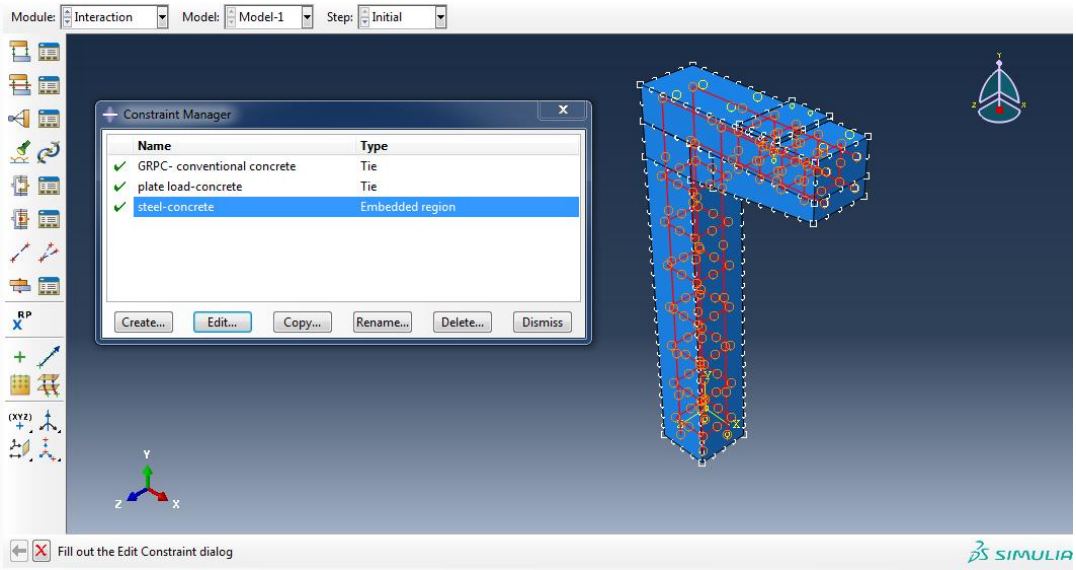

Plate (5-1) Interaction between reinforcement of steel bars and the concrete surrounding

5.2.3.2: Interaction Between Conventional Concrete and GRPC:

By testing the specimens experimentally, no isolation is observed between conventional concrete and hybrid concrete (GRPC), so it can be assumed that there is complete contact between the two types of concrete. When simulating this case with the Abaqus, a full restriction of contact is

imposed by the use of the "Tie contact technique". A tie constraint ties two separate surfaces together so that there is no relative motion between them. This type of constraint allows us to fuse together two regions even though the meshes created on the surfaces of the regions may be dissimilar **(Abaqus V, 2014).** **Plate (5-2)** shows the connection between the two types of concrete.

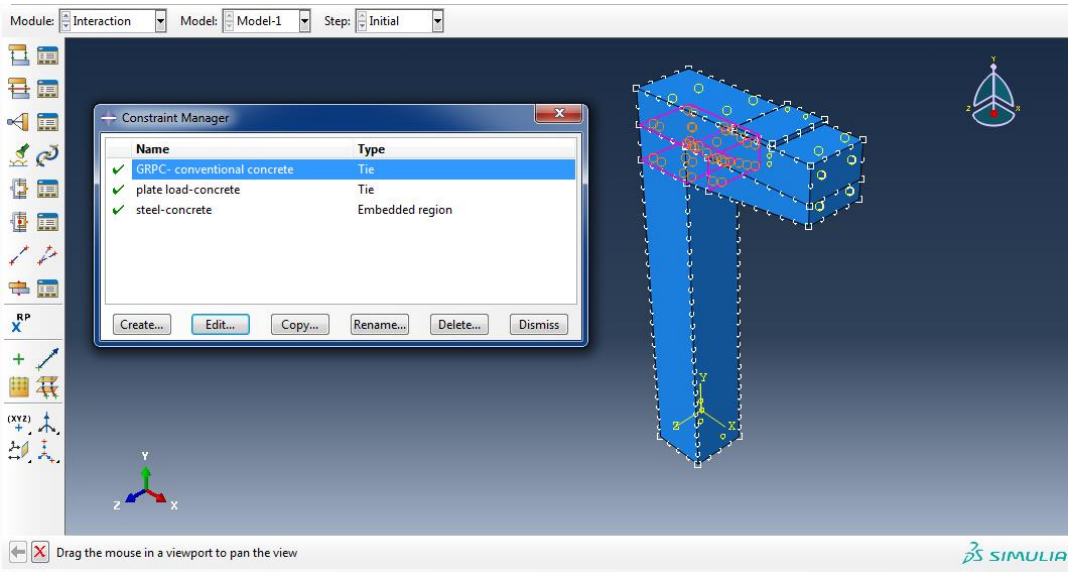

Plate (5-2) Interaction between conventional concrete and GRPC

5.2.3.3: Interaction of Frame with the Loading Steel Plates:

The loading steel plate is also connected to the concrete frame using the "Tie contact technique" to eliminate stress concentration around the loading points. "The tie constraint module does not allow to the concrete surface to be separated from the plates, meaning the components cannot be moved during loading". **(Zebalah, 2020)**

5.2.4: Boundary Condition:

In this study, half of the model is used to reduce the analysis duration as well as save CPU by adding symmetry boundary conditions in the x-

direction. Abaqus provides special boundary conditions to add symmetry, as shown in **Plate (5-3)**.

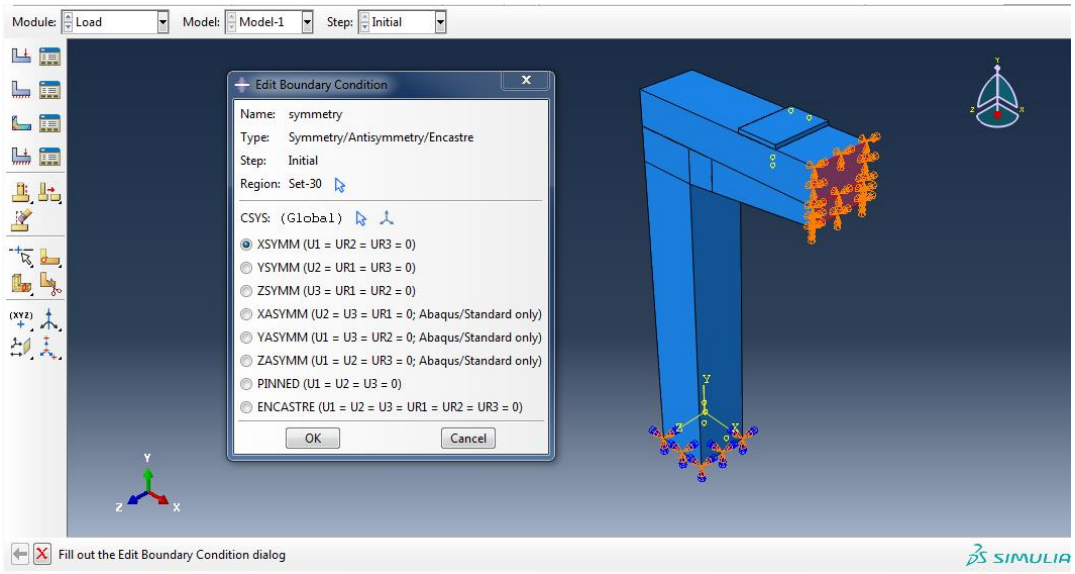

Plate (5-3): Boundary conditions of the symmetry of the frame in ABAQUS

By testing the specimens experimentally, no movement of the supports is noticed, whether it is horizontal or rotational, due to the presence of a cup support at the bottom of the column (as mentioned in the third chapter). Therefore, when simulating the model in the Abaqus, the linear movement in the direction of x, y, z is restricted, as well as the rotational movement in the direction of x, y, z. As shown in **Plate (5-4).**

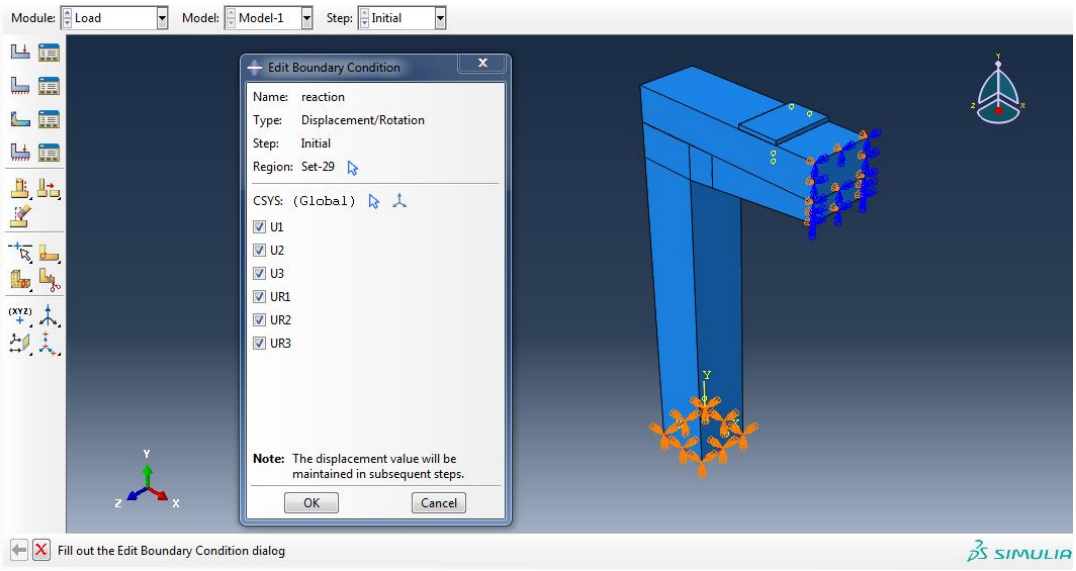

Plate (5-4): Boundary conditions of the reaction of the frame in ABAQUS

5.2.5: Mesh Size Convergence:

After determining the type of element for each material in the concrete frame, the optimal number of elements (mesh density) used in the simulated model is determined. Choosing the appropriate mesh size is an important step in the finite element model, as it is considered one of the factors affecting the behavior of the model.

Six different mesh sizes are studied to simulate the prismatic concrete frame with conventional concrete (P-C-1) to choose the appropriate model for the mesh that meets the minimum finite element number and good convergence. **Plate (5-5)** shows a trial finite element mesh with number (1236, 1359, 2178, 3540, 7416, and 14604) for a half-frame concrete.

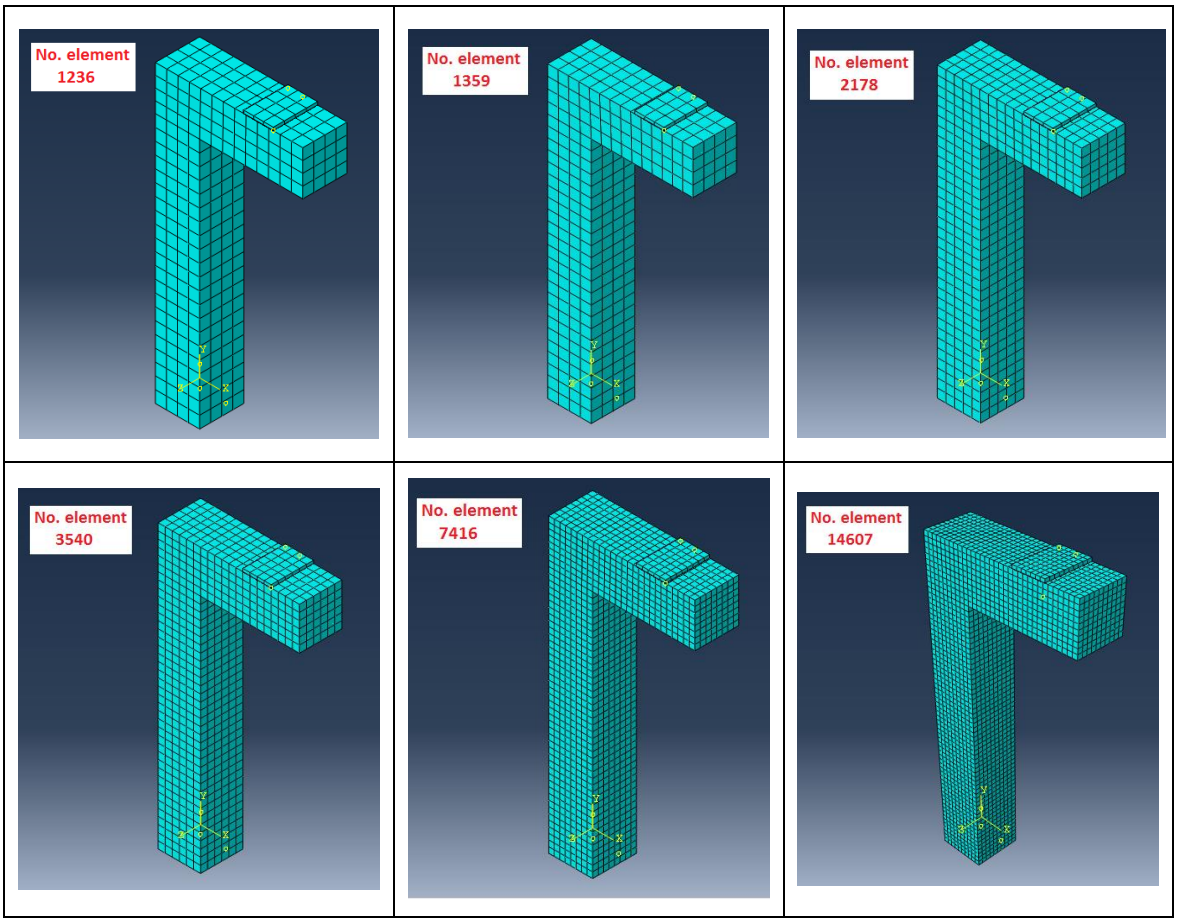

Plate (5-5): trial meshes for the half frame

As shown in **Figure (5-2),** the deflection at the midspan of the beam at a load of 50 kN approaches the deflection resulting from the experimental test by increasing the number of elements, as it is observed when the number of elements (3540) is the best because by increasing a large number of elements, the approach is relatively small. Therefore, in this study, a mesh size similar to the mesh size of a frame with (3540) elements will be adopted.

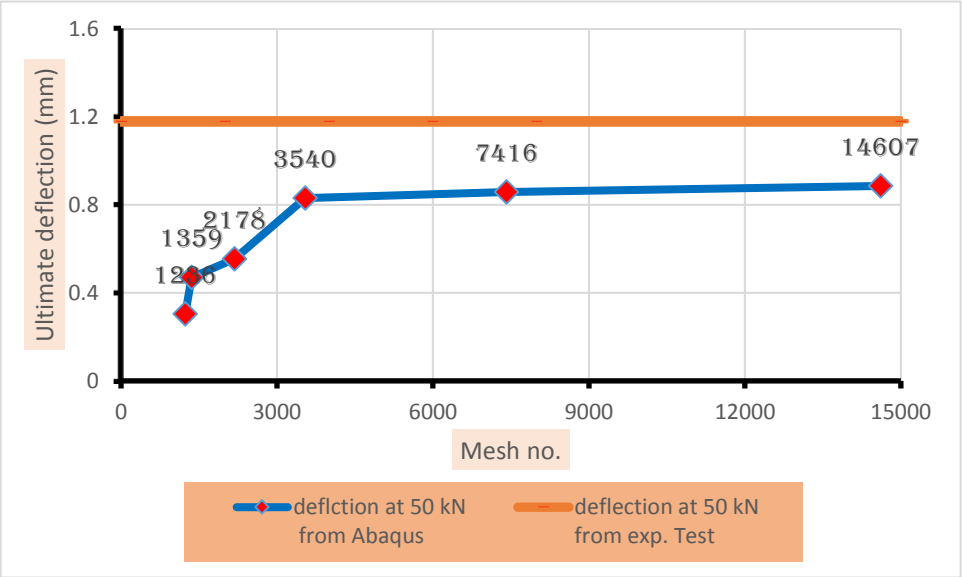

Figure (5-2): Ultimate deflection and number of the element's curves

5-3: Numerical Results:

5-3-1: Checking Abaqus Modeling:

For the purpose of approving the Abaqus model before representing new parametric study cases, an acceptable agreement must be obtained between the results of the experimental program and the simulated model analysis. In this study, the load-deflection curves for the beam mid-span and the ultimate load of the models, and the ultimate deflection in the middle of the beam are determined, in addition to the type of failure and cracks as determinants of the acceptance of the simulated model.

The parametric study concerning to study the change of the percent of the non-prismatic sections and the hybridization ratio in conventional concrete with GRPC under monotonic load only. So, the results of the descriptive analysis are compared with the results of the experimental specimens tested under monotonic load only.

5-3-1-1: Load-Deflection Curve at Beam Mid-Span Response:

The relationship in load-deflection curves in the middle of the beam for some experimental specimens and numerical analysis are presented in **Figures (5-3) to (5-10). Figures (5-11) and (5-12)** display the curve of the coefficient of determination (R^2) between the deflection of the experimental test and the deflection of the numerical analysis for the models P-C-1 and NB-C-1, as examples. It was found that R^2 is equal to 0.98% and 0.97% for models P-C-1 and NB-C-1, respectively. All of these figures indicate a good agreement between the results of the experimental specimens and the numerical analysis of the Abaqus program. **Plates (5-6) to (5-9)** show the deformation shape of the simulated frame in the Abaqus program.

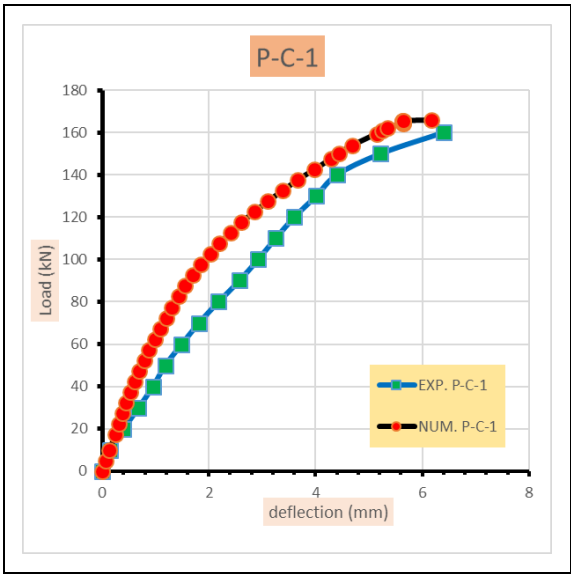

Figure (5-3) Load-deflection curve for experimental and numerical results of P-C-1

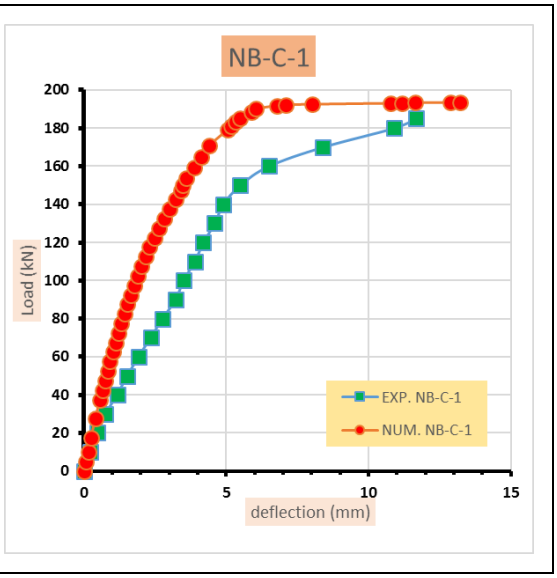

Figure (5-4) Load-deflection curve for experimental and numerical results of NB-C-1

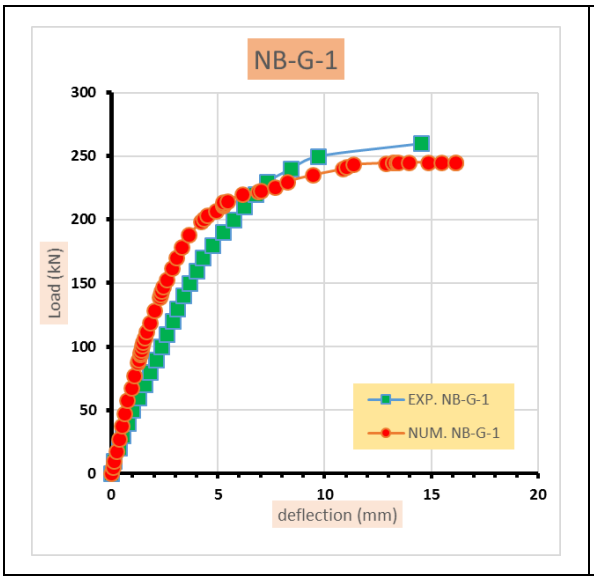

Figure (5-5) Load-deflection curve for experimental and numerical results of NB-G-1

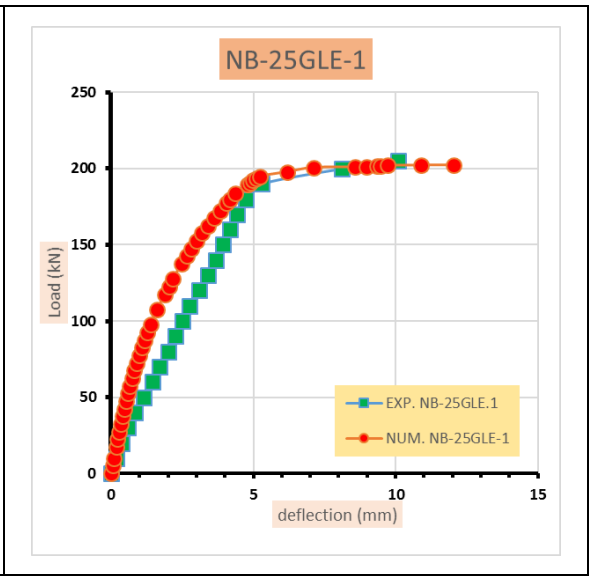

Figure (5-6) Load-deflection curve for experimental and numerical results of NB-25GLE-1

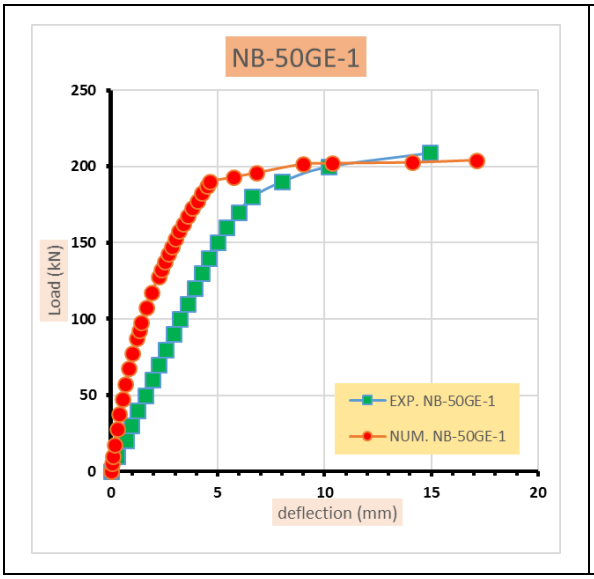

Figure (5-7) Load-deflection curve for experimental and numerical results of NB-50GE-1

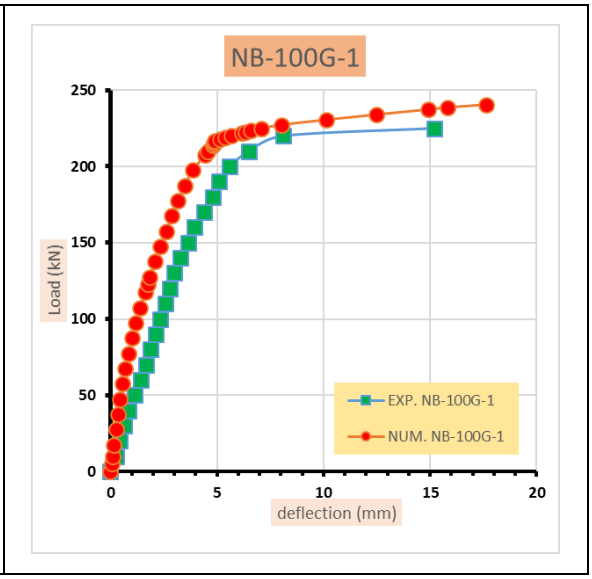

Figure (5-8) Load-deflection curve for experimental and numerical results of NB-100G-1

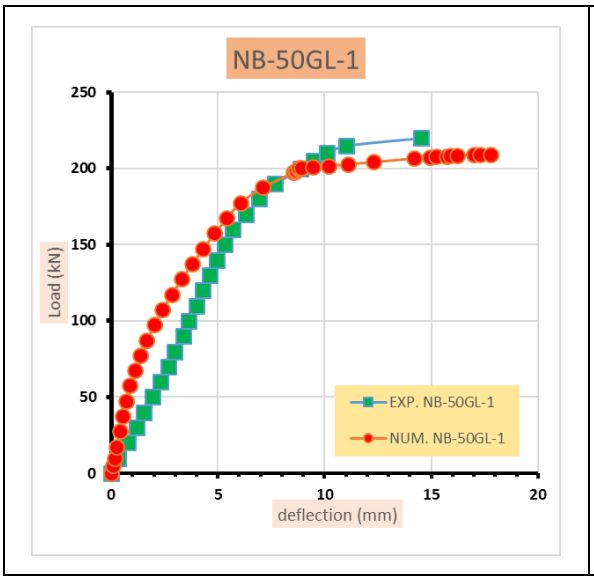

Figure (5-9) Load-deflection curve for experimental and numerical results of NB-50GL-1

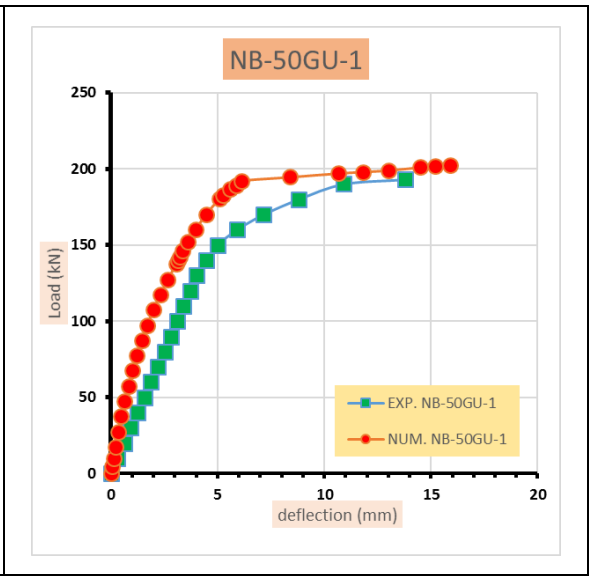

Figure (5-10) Load-deflection curve for experimental and numerical results of NB-50GU-1

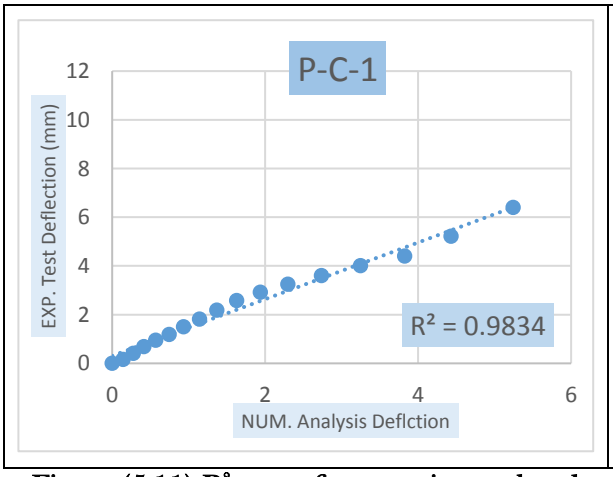

Figure (5-11) R^2 curve for experimental and numerical results of P-C-1

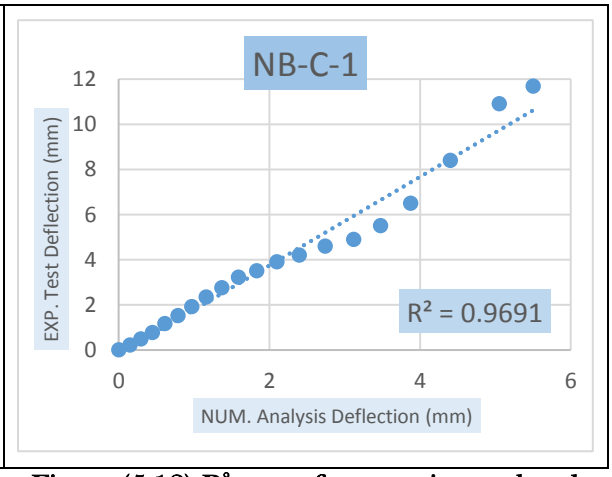

Figure (5-12) R^2 curve for experimental and numerical results of NB-C-1

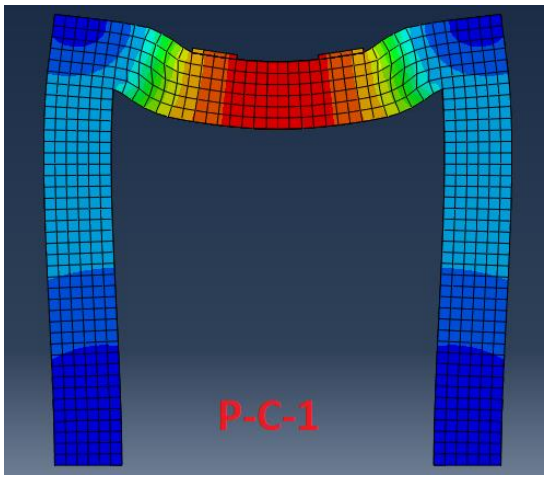

Plate (5-6) Deformation of the frame with Abaqus for P-C-1

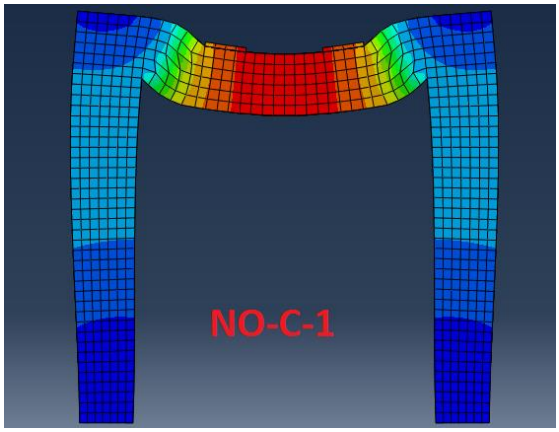

Plate (5-7) Deformation of the frame with Abaqus for NO-C-1

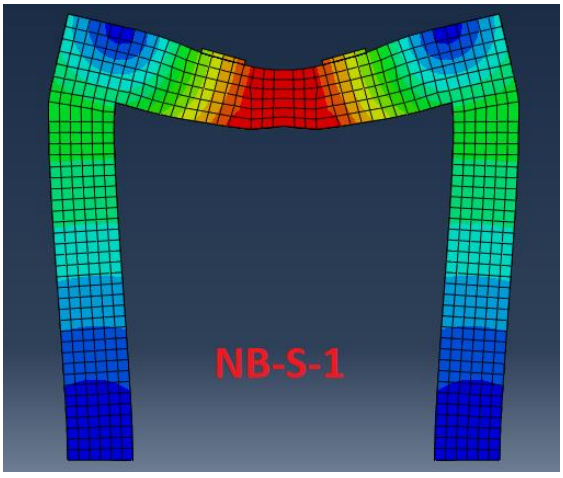

Plate (5-8) Deformation of the frame with Abaqus for NB-S-1

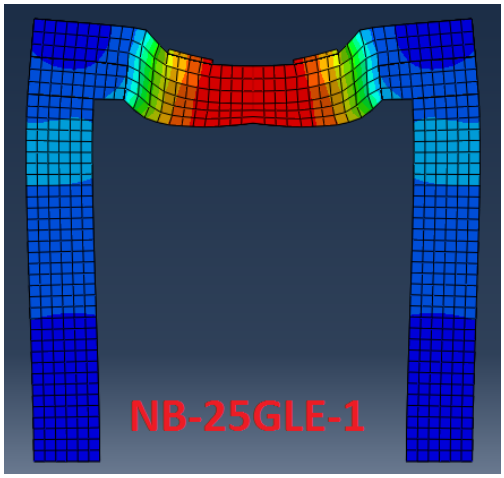

Plate (5-9) Deformation of the frame with Abaqus for NB-25GLE-1

From **Figures (5-3)** to **(5-10)** it is noted that the load-deflection curve in FE is stiffer than the curves of the experimental tests in the elasticity stage. The reason for this is that not all material properties in the experimental

program can be perfectly represented in FE as many factors are difficult to represent such as: (**Zebalah, 2020)**

1. In finite element, concrete is assumed as a homogeneous material when in actuality it is a heterogeneous material.
2. Microcracks are formed in the concrete after it is poured as a result of shrinkage, and this makes the concrete less stiffness, and this cannot be included in the FE.
3. Integration analysis is done using the Gaussian quadrature rule (Gauss points), which is an approximate method of integration that depends on specific points to achieve the balance, and therefore the possibility of reaching points other than chosen points for yielding limited firstly is possible.

5-3-1-2: Ultimate Load Compatibility and Ultimate Deflection:

The results obtained from the numerical analysis using the Abaqus program for the ultimate load and the corresponding deflection indicate an acceptable agreement with the experimental tests of the concrete frame. **Table (5-1)** shows that the ultimate load obtained from the numerical analysis is higher than the experimental test by **(4%-7%)** for models (P-C-1, NB-C--1, NB-100G-1, NB-50GU-1) While the other models, the ultimate load of the numerical analysis is less than the experimental test by **(1%-7%)**.

On the other hand, the deflection at the ultimate load is less compatible than the ultimate load, as the difference between the numerical analysis and the experimental test is (2%-23%), especially for the models with conventional concrete and hybrid with GRPC.

Table (5-1) Comparison between experimental and numerical in ultimate load and deflection

Name	Load			Deflection		
	EXP. (kN)	**NUM.** (kN)	**$\frac{\text{NUM.}}{\text{EXP.}}$** (%)	**EXP.** (mm)	**NUM.** (mm)	**$\frac{\text{NUM.}}{\text{EXP.}}$ (%)**
P-C-1	160	165.8	**1.04**	6.4	6.179	**0.97**
NO-C-1	200	196.1	**0.98**	8.81	7.32	**0.83**
NB-C-1	185	193.7	**1.05**	11.68	13.22	**1.13**
NB-G-1	260	245.1	**0.94**	16.14	14.83	**0.92**
NB-S-1	270	251.7	**0.93**	20.3	19.9	**0.98**
NB-25GLE-1	205	202.3	**0.99**	10.1	12.05	**1.19**
NB-50GE-1	209	204	**0.98**	14.93	17.12	**1.15**
NB-100G-1	225	240.5	**1.07**	15.2	17.65	**1.16**
NB-50GL-1	220	209.4	**0.95**	14.5	17.78	**1.23**
NB-50GU-1	193	202.2	**1.05**	13.8	15.88	**1.15**

5-3-1-3: Failure Type Compatibility:

Within the acceptance of the simulation of the numerical analysis model is the type of failure that must be similar to its experimental test counterpart. In the studied models, the type of failure was identical to all experimental specimens. **Plate (5-10) - (5-13)** shows the compressive and tensile damages of some models. Where the shear failure appears by the concentration of compressive and tensile damages in the shear region in models P-C-1, NB-C-1, and NB-25GLE-1 as showing in **Plates (5-10), (5-11), and (5-13)**, while the bending failure is in NB-G-1 as showing in **Plate (5-12),** which is what happened in the experimental test.

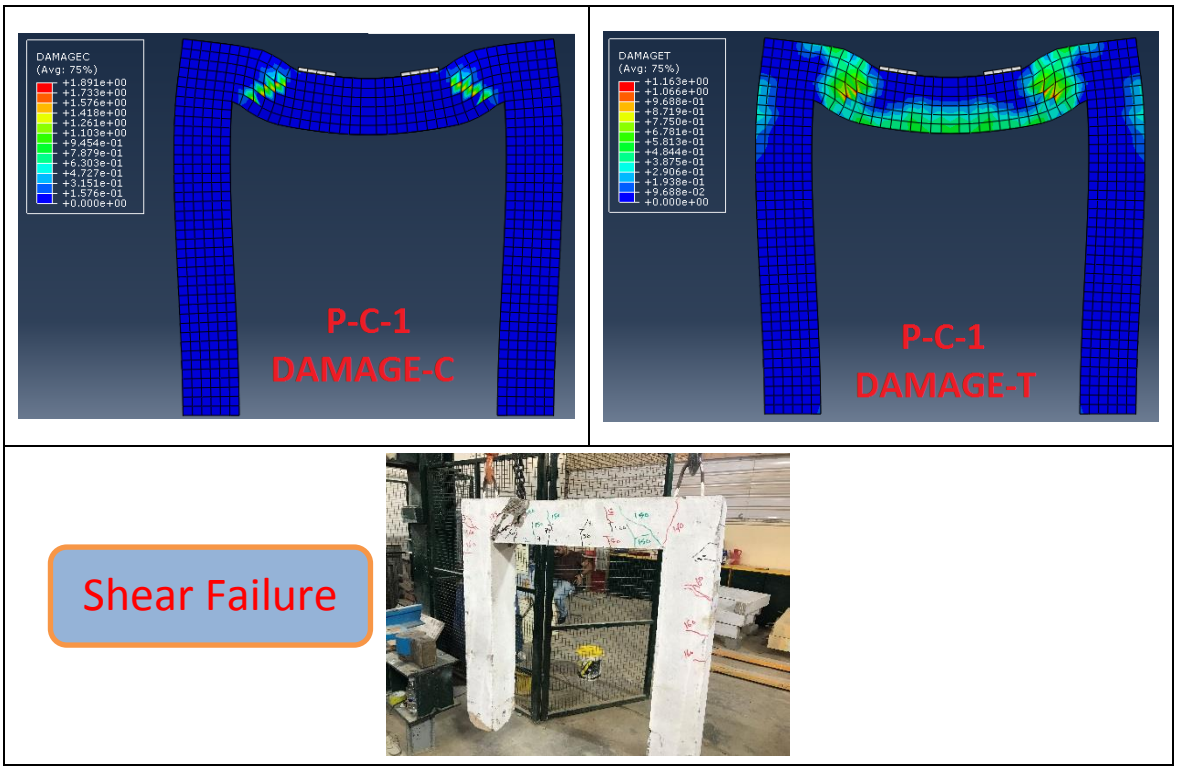

Plate (5-10) The compressive and tensile damages of P-C-1

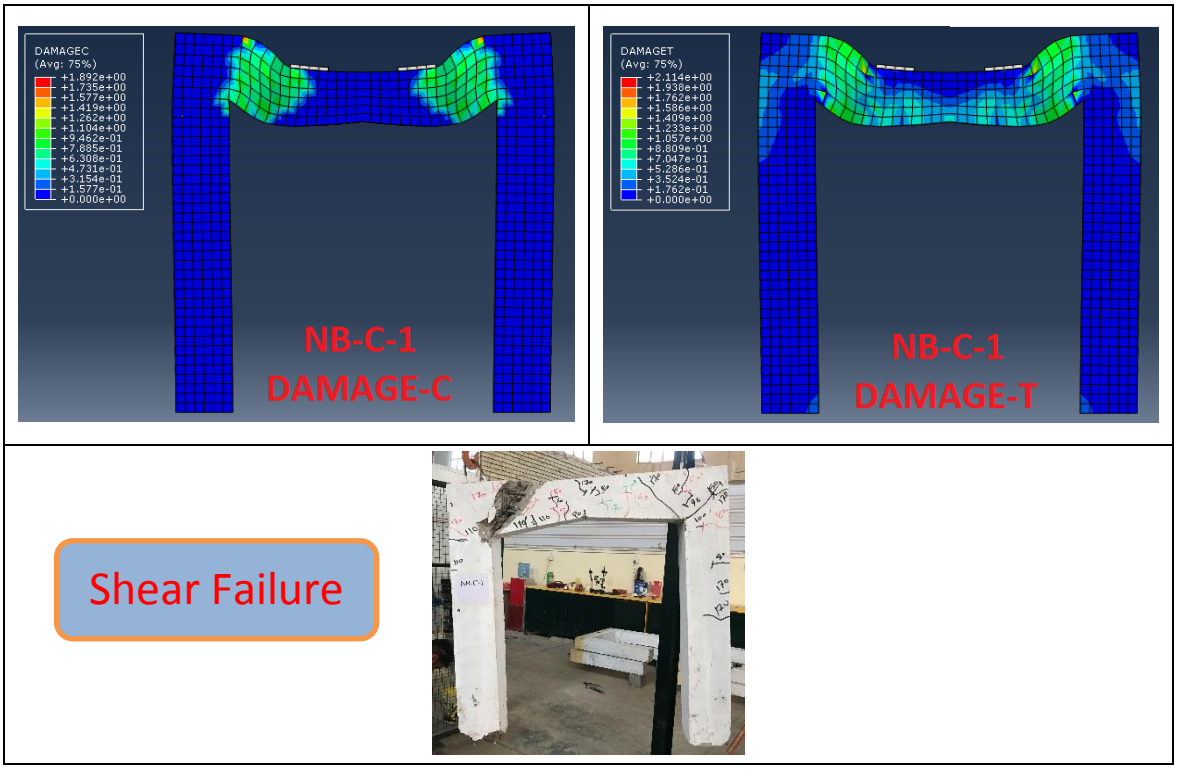

Plate (5-11) The compressive and tensile damages of NB-C-1

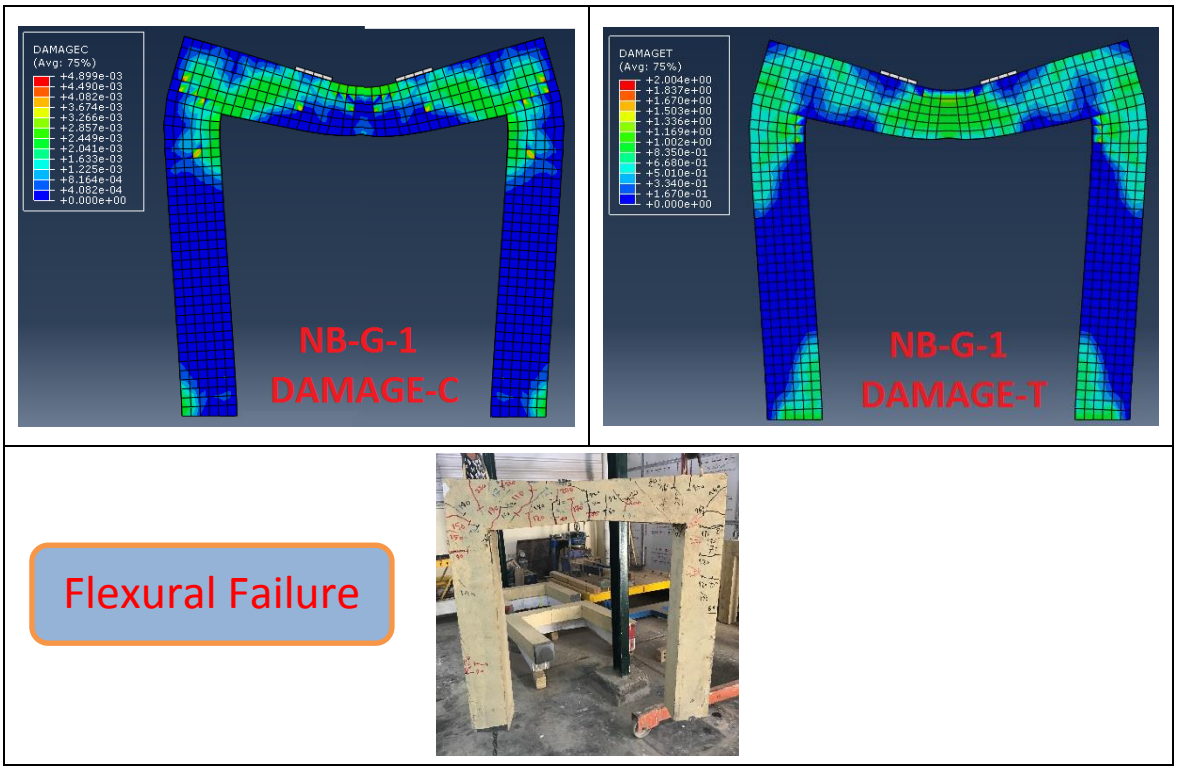

Plate (5-12) The compressive and tensile damages of NB-G-1

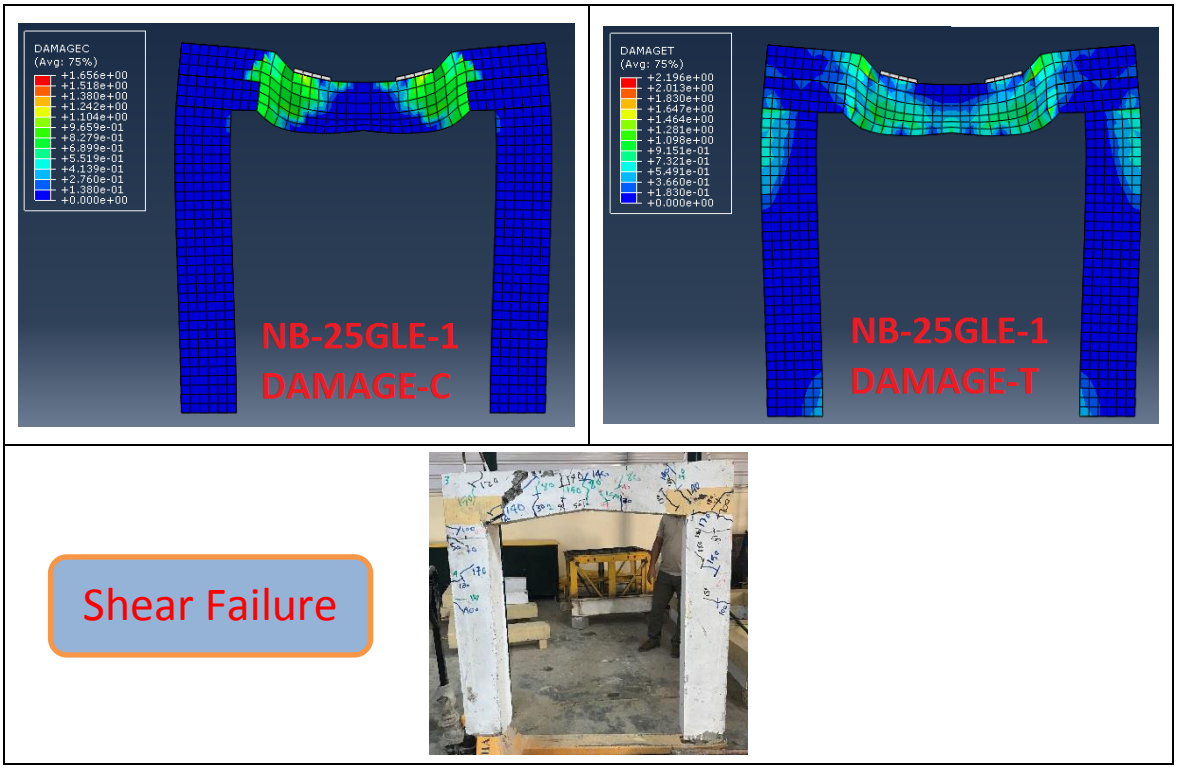

Plate (5-13) The compressive and tensile damages of NB-25GLE-1

Therefore, based on the results of the Abaqus and their compatibility with the results of the experimental tests, a good agreement can be judged between the Abaqus program and experimental work, and the Abaqus program can be used to create a new parametric study.

5-3-2: Parametric Study:

In this study, a new set of parametric studies that are close to the research was adopted to find out their effect on the behavior of the concrete frame, such as the study of changing the ratio of large depth to the small depth of beam in the frame along the length of the beam, the ratio of large depth to the small depth of beam in the frame in two-thirds of the beam, and the hybridization of conventional concrete with different proportions and locations of GRPC.

5-3-2-1: Non-Prismatic Frame in Whole Beam:

In this section, the change in the non-prismatic ratio of the beam in the concrete frame along the length of the beam (the ratio of the edge beam depth (h_2) to the middle beam depth (h_1)) was dealt with to study the effect of the change ratio on the behavior of the concrete frame. **Figure (5-13)** shows the dimensions of the section used. Conventional concrete with properties similar to that used in the experimental program.

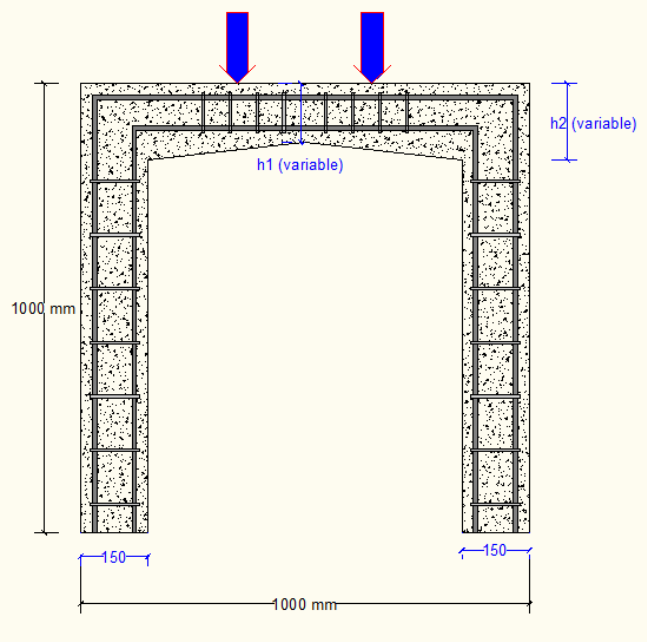

Figure (5-13) Dimension of frame used in non-prismatic in whole beam

Ten models were taken to describe the effect of the non-prismatic of the whole beam on the concrete frame, where the ratio starts at 1.1 and ends at 2. The ultimate load of the models and the corresponding deflection in the mid-span beam are presented in **Table (5-2)** and **Figure (5-14).**

Figure (5-14) shows an increase in the ultimate load by **13.8%** when using a non-prismatic section by 1.1, This means that the beam behaves non-prismatic even if the percentage of non-prismatic is very small. The ultimate load increases by increasing the ratio of the large depth of the beam to the small depth up to 1.5, which is **19.6%,** and then load is almost constant when the sectional non-prismatic ratio is increased.

Table (5-2) Results of the Non-Prismatic Frame in Whole Beam

Specimens Names	Edge beam depth (h_2) (mm)	Middle beam depth (h_1) (mm)	$\frac{h_2}{h_1}$	Ultimate load (P_u) (kN)	P_u increases (%)	Ultimate deflection (mm)
P-C-1 (Control)	150	150	1.0	165.8	-----	6.18
NB1.1-C-1	157	143	1.1	188.7	13.8	9.3
NB1.2-C-1	163	137	1.2	190.3	14.8	10.7
NB1.3-C-1	170	130	1.3	193.7	16.8	13.2
NB1.4-C-1	175	125	1.4	196	18.2	15.9
NB1.5-C-1	180	120	1.5	198.3	19.6	21.1
NB1.6-C-1	185	115	1.6	198.3	19.6	20.2
NB1.7-C-1	189	111	1.7	197.9	19.3	18.4
NB1.8-C-1	193	107	1.8	197.9	19.3	22.2
NB1.9-C-1	196	104	1.9	198.5	19.7	24.5
NB2.0-C-1	100	200	2.0	198	19.4	18.3

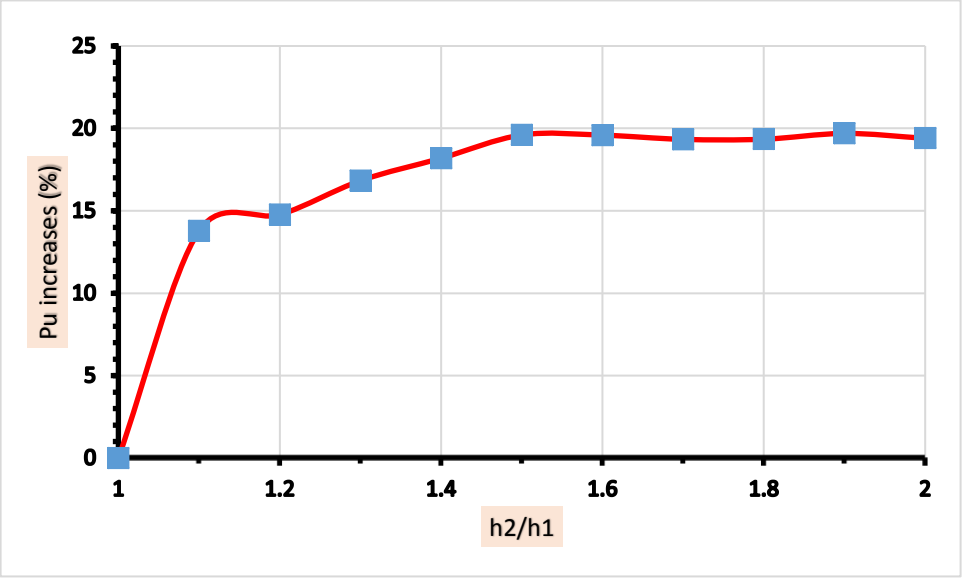

Figure (5-14) The ultimate load increases and the percentage of the non-prismatic section relation of the frame

5-3-2-2: Non-Prismatic Frame in Two-Thirds of The Beam:

In this section, the shape of the non-prismatic section of the beam was changed, and the inclined part of the non-prismatic section (tapering) was made in two-thirds of the two ends of the beam (the parts have maximum shear force), while the middle third was prismatic, as shown in **Figure (5-15).**

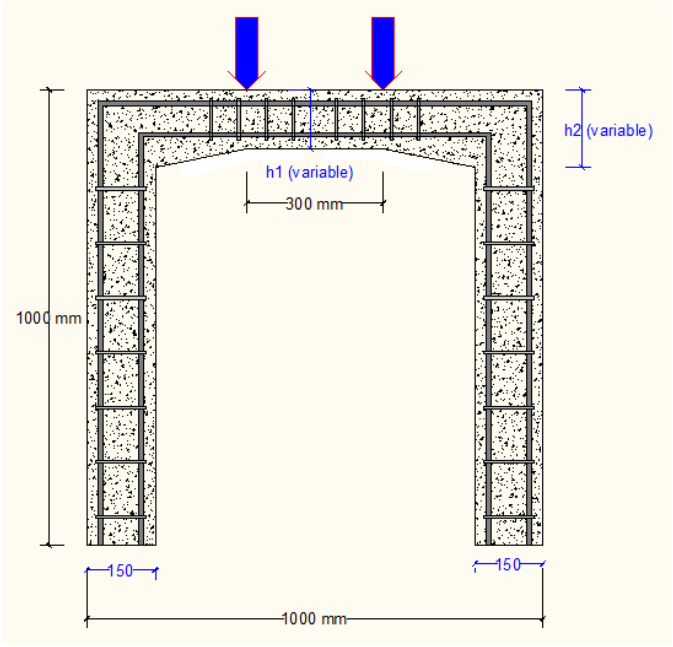

Figure (5-15) Dimension of frame used in non-prismatic in two-thirds of the beam

To study this form of non-prismatic beam section in the concrete frame, six models were analyzed with the ratio of the large depth at both ends of the beam to the small depth at the third of the beam (1.1, 1.2, 1.4, 1.6, 1.8, and 2.0). The ultimate load and the corresponding deflection are shown in **Table (5-3),** while the percentage increase in the ultimate load is presented in **Figure (5-16).** Where a significant increase in the ultimate load is observed with an increase in the h_2/h_1 ratio up to 1.4, and then the increase in the

ultimate load is slight, with the exception of the model with h_2/h_1 equal to 2.0, where there is a jump in the increase of the ultimate load.

Table (5-3) Results of the Non-Prismatic Frame in two thirds of the Beam

Specimens Names	Edge beam depth (h_2) (mm)	Middle beam depth (h_1) (mm)	$\frac{h_2}{h_1}$	Ultimate load (P_u) (kN)	P_u increases (%)	Ultimate deflection (mm)
P-C-1 (Control)	150	150	1.0	165.8	-----	6.18
NBT1.1-C-1	160	146	1.1	191.6	15.6	17
NBT1.2-C-1	170	142	1.2	205.9	24.2	33.7
NBT1.4-C-1	189	135	1.4	216.2	30.4	25.4
NBT1.6-C-1	205	128	1.6	220.1	32.8	22.5
NBT1.8-C-1	220	122	1.8	221.8	33.7	26.5
NBT2.0-C-1	234	117	2.0	234.7	41.5	34.9

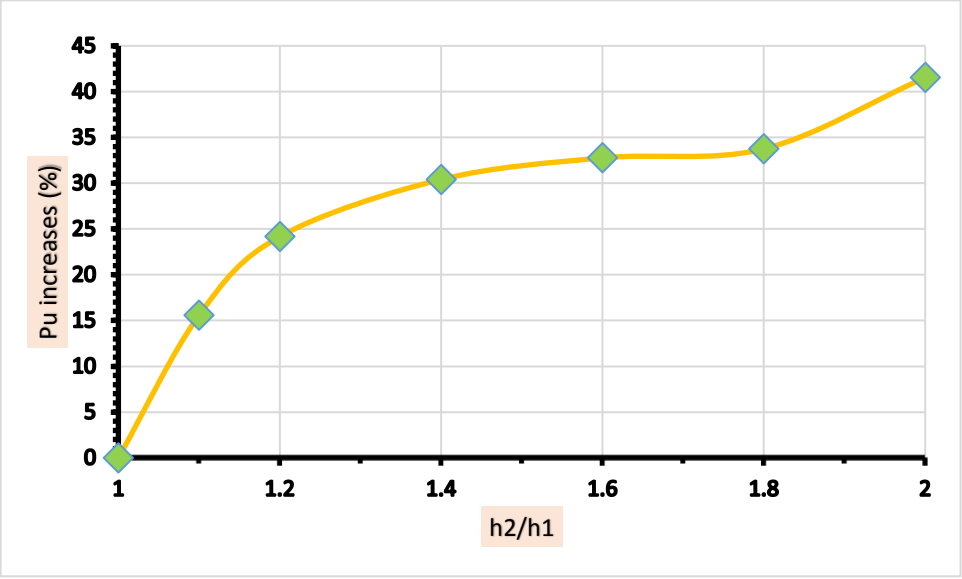

Figure (5-16) The ultimate load increases and the percentage of the non-prismatic section relation of the frame in two-thirds of the beam

It is noted that the ultimate load of NBT1.2-C-1 is greater than that of NB1.2-C-1, although h_2/h_1 is equal to 1.2 for both models. As well as the rest of the models, there is an increase in the ultimate load for the models with a non-prismatic section at the edges of the beam more than the models with a non-prismatic section along the beam for the same h_2/h_1. The reason for this is that NBT1.2-C-1 has a beam depth in the face of the column that is greater than the beam depth in NB1.2-C-1and this leads to an increase in the nominal shear strength produced by the concrete, and this applies to the rest of the models.

5-3-2-3: Hybrid Concrete Frame at The Edge of The Beam:

To expand the scope of the investigation on the effect of the hybridization ratios of concrete by GRPC on the behavior of the concrete frame, models (NB-23GLE-1, NB-40GLE-1, NB-57GLE-1, NB-74GLE-1) with hybridization ratios (23%, 40%, 57%, and 74% of the volume of the beam, respectively, were analyzed using the Abaqus program. **Figure (5-17)** shows the location and dimension of GRPC in the frame. The method of hybridization of these models differs from the specimens NB-25GLE-1 and NB-50GE-1 used in the experimental test because the hybridization covers the entire shear region horizontally.

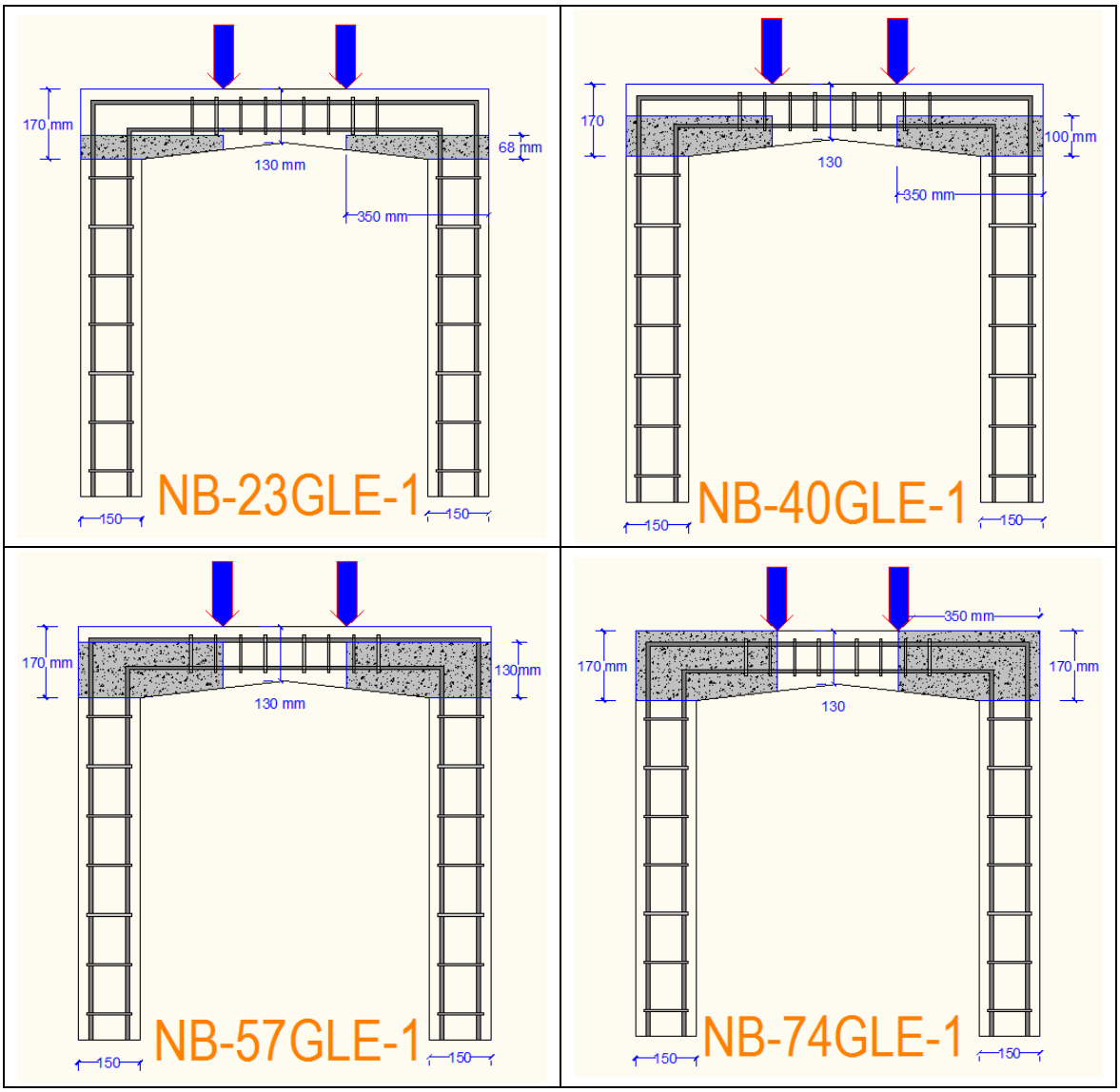

Figure (5-17) Details of NB-23GLE-1, NB-40GLE-1, NB-57GLE-1, and NB-74GLE-1

The ultimate load of the models, the corresponding deflection, and the percentage increase in the ultimate load for each model compared to the NB-C-1 are presented in **Table (5-4)** and **Figure (5-18),** respectively. **Figure (5-18)** shows a constant increase when the hybridization rate changes from 0% to 74% by about **6%**. While for the model NB-100G-1, a 24.2% increase in the ultimate load is noted. This is due to the presence of GRPC (for any of the quantities used) in the lower part of the edge beam, which strengthens the

shear strength in the frame and changes the failure type from shear failure to flexural failure at the middle of the beam, and the lack of hybridization in that region, so, all models behave similarly. While the NB-100G-1 contains GRPC in the center of the beam, so the ultimate load is higher than the rest, as it strengthens the flexural region.

Table (5-4) Results of the hybrid concrete frame at the edge of the beam

Specimens Names	Ultimate load (P_u) (kN)	P_u increases (%)	Ultimate deflection (mm)
P-C-1 (Control)	193.7	-----	13.22
NB-23GLE-1	205.5	6.1	14.3
NB-40GLE-1	205.1	5.9	17.7
NB-57GLE-1	205.7	6.2	14.3
NB-74GLE-1	205.8	6.2	14.9
NB-100G-1	240.5	24.2	17.7

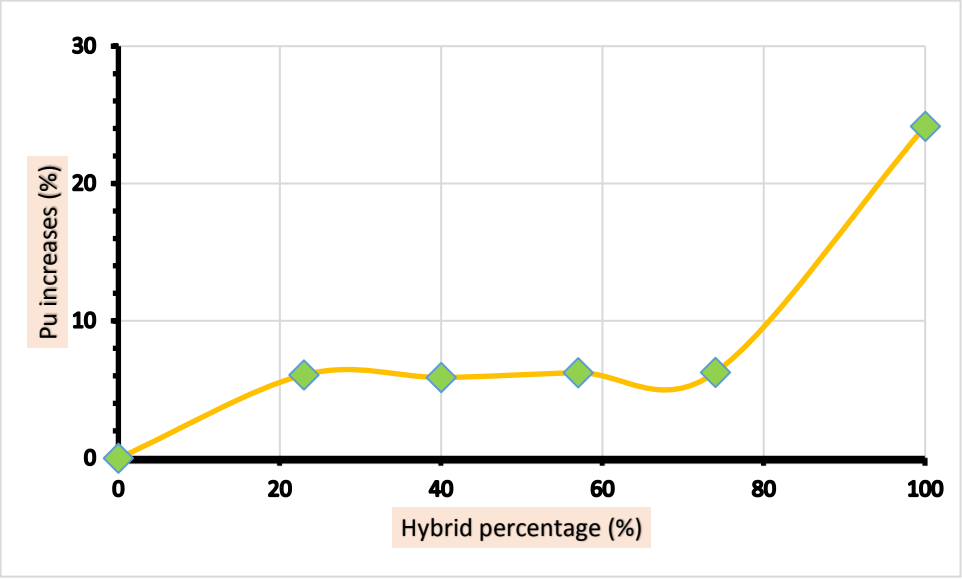

Figure (5-18) The ultimate load increases and the percentage of the hybrid concrete frame at the edge of the beam

5-3-2-4: Hybrid Concrete Frame in the Clear Span of The Beam:

In this section, the concrete was hybridized with GRPC along the clear span of the beam only. The depth of hybridization is variable according to the hybridization percentage. The models (NB-13GLM-1, NB-27GLM-1, NB50GLM-1, NB-62GLM-1) with hybrid percentages of 13%, 27%, 50%, and 62%, respectively, were analyzed using the Abaqus program. **Figure (5-19)** presents the dimensions and locations of hybridization in the concrete frame of this model.

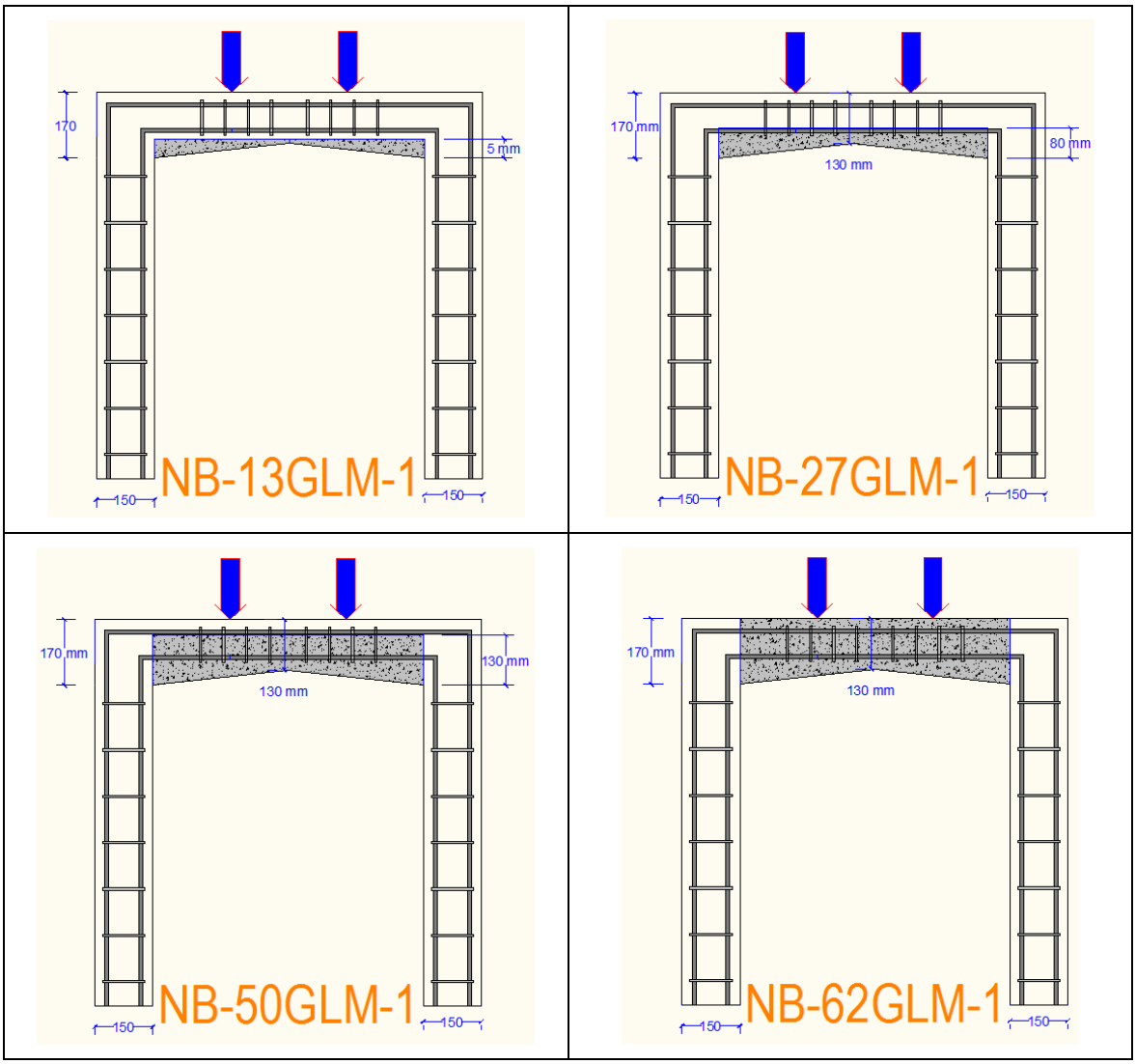

Figure (5-19) Details of NB-13GLM-1, NB-27GLM-1, NB50GLM-1, NB-62GLM-1

The ultimate load for hybrid frames in this way and the corresponding deflection are shown in **Table (5-5),** while the percentages of increase in the ultimate load for models compared with NB-C-1 are shown in **Figure (5-20).** A slight increase in the ultimate load is observed for hybrid models with a low percentage of GRPC, and the ultimate load increases with an increase in the hybridization percentage up to 62%, where the increase in the ultimate load is 16.9%, after which the curve of increases load becomes less inclined, as shown in **Figure (5-20).**

Table (5-5) Results of the hybrid concrete frame at the middle of the beam

Specimens Names	Ultimate load (P_u) (kN)	P_u increases (%)	Ultimate deflection (mm)
P-C-1 (Control)	193.7	-----	13.22
NB-13GLM-1	194	0.2	19.3
NB-27GLM-1	196.9	1.6	20
NB-50GLM-1	209.9	8.3	22.4
NB-62GLM-1	226.5	16.9	23.8
NB-100G-1	240.5	24.2	17.7

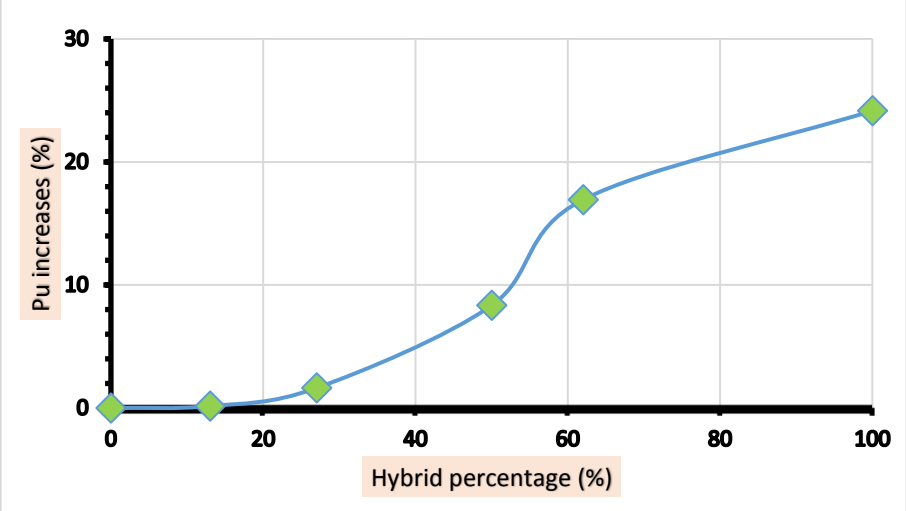

Figure (5-20) The ultimate load increases and the percentage of the hybrid concrete frame in the clear span of the beam

CHAPTER SIX

Chapter Six

Conclusions and Recommendations for Future Studies

6.1: Introduction:

In this chapter, the conclusions obtained from the results of the experimental program for the prismatic and non-prismatic concrete frame containing one or more types of concrete under monotonic and repeated load are presented. Also, the conclusions from the results of the numerical analysis using FEM (ABAQUS) are presented. Finally, some recommendations are proposed for future work related to the subject of the research.

6.2 Conclusions:

6.2.1: Conclusions of Experimental Work:

1. For the frame with hybrid concrete, the results of the tests indicate good compatibility between conventional concrete and RPC, as the hybridization with RPC improves the properties of the frame and gives full interaction, and no separation occurs between the two materials during the test.
2. The use of GRPC in the frame increases the first crack load of the frame **(27-30) %** more than the frame with conventional concrete, while the frame with SRPC increases by **(127-133) %.**

3. The visible first crack load is affected by the geometry of the section and the type of concrete used in the expected first crack position only, whereby the first crack load for all specimens with conventional concrete in the lower region of the beam is approximately equal even if GRPC has it in other regions.
4. The presence of glass fibers in RPC increases the crack propagation in the concrete frame at testing. In contrast, the presence of steel fibers reduces cracks. And the presence the GRPC does not prevent the appearance of cracks, but rather prevents their expansion and increases in width due to the presence of glass fibers in its concrete structure.
5. The presence of hybridization with GRPC develops the behavior of the concrete frame to resist the first crack when using RPC in the tensile zone of the positive moment.
6. The ultimate loads of the concrete frame increase by **25%** and **16%** for the non-prismatic frame in columns and beam respectively for the same amount of concrete used.
7. The use of GRPC and SRPC in whole frames increases the ultimate load by **41%** and **46%** respectively compared to a conventional concrete frame.
8. The hybridization position with RPC greatly affects the ultimate load of the frame, as hybridization in the lower half of the beam gives a higher ultimate load than frames with hybridization in the upper half of the beam and the edges of the beam.
9. Hybridization with RPC increases the ultimate load of the frame, where the increase is **(11%-22%)** when hybridizing by (25%-100%) of the beam.

10. The effect of repeated loading on the frame with RPC is less than that of the frame with conventional concrete, where the ultimate load decreases for both specimens of RPC with steel and glass fibers is only **2%**, while the decrease is **27%** of the frame with conventional concrete. Therefore, it is very useful when used in members subject to fatigue stress.
11. In the repeated load, the presence of hybridization improves the behavior of the frame in resisting the effect of the repeated load, and the improvements are according to the rate of hybridization and its location. Where, when hybridizing with (25%-100%), the improvement is (**26%-85%).**
12. The use of frame with RPC (glass fiber or steel fiber) improves the shear strength properties of concrete and changes the failure type of frame from shear failure (as in frame with conventional concrete) to flexural failure.
13. The shear failure occurred in the frame with whole conventional concrete and the hybrid frames in the shear zone as well as the hybrid frame in the upper half of the beam, While the hybrid frame in the lower half and hybrid frame in the entire beam show flexure failure.
14. The hybridization location with GRPC is very important as it determines the type of frame failure. The presence of GRPC at the beginning of the expected shear failure crack improves the shear strength of the frame. The presence of GRPC not along the shear failure path does not prevent the occurrence of shear failure but slightly improves the shear strength of the frame.
15. The test under repeated load did not significantly affect the type of failure of the hybrid specimens, as the shear failure of the specimens under monotonic load remained the same under the repeated load, and

the same is true of the flexural failure. Except for the frame with GRPC, the failure changed from a bending failure in the monotonic test to a shear failure in the repeated test.

16. The stiffness of the concrete frame decreases when a non-prismatic concrete frame is used in the beam and columns.
17. The results confirmed that the use of a non-prismatic concrete frame in the beam makes the shear failure less brittle.
18. The stiffness of the frame with the SRPC and GRPC in whole frame is higher than that of the frame with the conventional concrete for both types of loading (monotonic and repeated).
19. The deflection decreases when using hybridization with GRPC by 100% compared to the frame with conventional concrete only, and this is due to the effect of GRPC in the beam, which increases the stiffness of the beam.

6.2.2: Conclusions of Abaqus Analysis:

1. The analysis of the models using the finite element method by ABAQUS/CAE2017 is able to simulate the results of the experimental specimens with good agreement, as the difference in the ultimate load capacity does not exceed **7%**, while the corresponding deflection does not exceed **23%**.
2. From the Abaqus results, the ultimate load of the non-prismatic concrete frame increases **(12.8%-19.7%)** compared to the prismatic frame when the non-prismatic section is along the beam and with the ratio of the large depth of the beam to the small depth (1.1 - 2.0).

3. The best ratio of the large depth (at the edge of the beam) to the small depth (in the center of the beam) when the whole beam is not prismatic is 1.5.
4. From the results of the Abaqus, when using a non-prismatic section of (1.1 - 2.0) in the two-thirds of the two edges of the beam only, the ultimate load increases by **(15.6%-41.5%)** compared to the frame with a prismatic section.
5. The ultimate load of the non-prismatic frame with two-thirds of the two edges of the beam only is higher than the ultimate load of the frame with a non-prismatic whole beam for the same ratio of the large depth of the small depth of the beam. But this increase is at the expense of the clear length of the column, which in the first case is less than the second.
6. When hybridizing the concrete of the frame with GRPC for the parts of the beam subjected to shear stresses only, the ultimate load increases by a constant percentage of approximately **6%**, when hybridized by 18%-70%.
7. By hybridizing the frame beam with GRPC in its clear span only, the increase in the ultimate load is **(0.2%-16.9%)** when hybridizing by 13%-62%.
8. The best hybridization of the concrete frame is when it is in the clear span of the beam.

6.3: Recommendations for the Future Works:

1. Investigating the frame with GRPC and the hybrid frame (conventional concrete and GRPC) under horizontal load (monotonic and repeated load) to study the joint behavior in the presence of GRPC.

2. An investigation of the study of column hybridization with GRPC after designing the frame and making the columns the control of the failure.
3. Investigating experimentally the use of a large beam length in the frame and make the section non-prismatic only in the shear zone portion.
4. An investigation of feasible using beams without shear reinforcement and relying just on the strength of the GRPC.
5. An investigation of taking many cycles of loading (loading and unloading) thousands or hundreds of times with varying loads (many, few, many, and so on) to simulate the real life of the concrete structure.
6. Investigating the effect of fire on the hybrid frame with GRPC and comparing the results with a frame with conventional concrete and SRPC.

REFERENCES

References

1. Abaqus V., **"6.14 Documentation,"** Dassault Syst. Simulia Corp., vol. 651, pp. 2–6, 2014.
2. Abaqus v., **"ABAQUS Version 6.13, Analysis User‟s Manual,"** Dassault Syst. Simulia Corp., Provid. RI, 2013.
3. Abd AlRadha D. A., **"Behavior of Composite Reactive Powder Concrete Girder and Normal Concrete Deck Slab",** Ph.D. thesis, University of Babylon, Iraq, 2015.
4. Abdulameer T. A. M., **"Behavior of High Strength Light Weight Reinforced Concrete One-Way Ribbed Slabs"**, Ph. D. thesis, University of Babylon, Iraq, 2022.
5. ACI 116R-00, **"Cement and Concrete Terminology",** Reported by ACI Committee 116.
6. ACI 211.1-2004. **"Standard Practice for Selecting Proportions For Normal, Heavyweight, And Mass Concrete".**
7. ACI 224R-01, "**Control of Cracking in Concrete Structures**", ACI Committee 224, 2001.
8. ACI 318–19, 318M-19: "**Building Code Requirements for Concrete and Commentary"**, 2019.
9. ACI Committee 234R-06, **"Guide for the Use of Silica Fume in Concrete"**, reapproved 2012.
10. ACI Committee 318 **"Building Code Requirements for Reinforced Concrete (ACI 318-06) and Commentary-ACI318RM-06".** American Concrete Institute, Detroit, U.S.A., 2006.

11. ACI T1.1-01, **"Acceptance Criteria for Moment Frames Based on Structural Testing",** March 9, 2001.
12. AlAli S. S. H., Abdulrahman M. B., and Tayeh B. A., **"Response of Reinforced Concrete Tapered Beams Strengthened Using NSM-CFRP Laminates"** Tikrit Journal of Engineering Sciences (2022) 29 (1): 99-110. http://doi.org/10.25130/tjes.29.1.8.
13. Al-Amry, M. G., **"Experimental Investigation and Nonlinear Analysis of Hybrid Reinforced Concrete Deep Beams".** M.Sc. thesis, University of Babylon, Iraq, 2013.
14. Algburi A. H. M., Sheikh M. N., Hadi M. N. S. **"Mechanical properties of steel, glass, and hybrid fiber reinforced reactive powder concrete".** Front Struct Civ Eng. 2019;13(4):998–1006.
15. Al-Hassani H. M., Al-Kafaji J. M. and Ismael M. A., **"Flexural Behavior of Hybrid Tee Beams (Containing Reactive Powder Concrete and Normal Strength Concrete)"** Journal of Engineering and Development, Vol.19, No.2, march. 2015, ISSN 1813- 7822.
16. Al-hussainy, J. D. W., **"Behavior of R/C Portal Frames Strengthened by CFRP Products"**, M. Sc. thesis, University of Babylon, Iraq, 2015.
17. AL-Khafaji A. G. A., Al-Mamoori A. H. N., Aoun A. M. A., **"Improvement of flexural strength of precast concrete spliced girder using reactive powder concrete in splice region".** Structures 14:197–208, 2018. https:// doi. org/ 10. 1016/j. istruc. 2018. 03. 012.
18. Al-Nasrawi, J.T.A. **"Ultimate Strength Capacity of R.C Space Frames Strengthened by FRP"** Ph.D. Thesis, Civil Department, College of Engineering, University of Babylon, Iraq, 2008.
19. Alsaffar N. S., Al Sulaifanie B. J., and Mahmood M. N**., "Flexural Strength of Steel Fiber Ultra High Strength Concrete Beams under**

Static and Repeated Loads", Tikrit Journal of Engineering Sciences 2020; 27(3): 73- 81. DOI: http://doi.org/10.25130/tjes.27.3.08.

20. Anson M & Newman K., **"The Effect of Mix Proportions and Method of Testing on Poisson's Ratio for Mortars and Concretes,"** Magazine of Concrete Research, Vol. 18, No. 56, September 1966, pp. 115-130.
21. Archundia-Arandaa H. I., Tena-Colungaa A., Alejandro G. **"Behavior of reinforced concrete haunched beams subjected to cyclic shear loading''** Engineering Structures 49 (2013) 27–42.
22. ASTM A615/615M, **"Standard Specifications for Deformed and Plain Carbon Structural Steel Bars for Concrete Reinforcement",** Annual Book of ASTM Standard. Grade, 2016.
23. ASTM C1856, "**Standard practice for fabricating and testing specimens of ultra-high performance concrete".** ASTM Int, 1: 4, 2017, doi: https:// doi. org/ 10. 1520/ C1856.
24. ASTM C39/C39M-15a, **" Standard Test Method for Compressive Strength of Cylindrical Concrete Specimens "**, 2015, pp.1-7.
25. ASTM C469/C469M, **"Standard Test Method for Static Modulus of Elasticity and Poisson's Ratio of Concrete in Compression",** USA:ASTM International ,2014 pp.1-5.
26. ASTM C78/C78M, **"Standard Test Method for Flexural Strength of concrete (Using Simple Beam with Third-Point Loading)** ", USA: ASTM International, 2015, pp.1-4
27. Aziz O. Q. and Ahmed G. H., **"Mechanical properties of ultra-high-performance concrete (UHPC)".** Am Concr Institute ACI Spec Publ, 289 SP, pp. 331–346, 2012, doi: https:// doi. org/ 10. 14359/ 51684 273.

28. Balduzzi G., and et al, **"Non-prismatic beams: A simple and effective Timoshenko-like model"** International Journal of Solids and Structures, 90 (2016), 236-250.
29. Basim S., Hejazi F. and Rashid R. S. B. M**., "Embedded carbon fiber-reinforced polymer rod in reinforced concrete frame and ultra-high-performance concrete frame joints"**, International Journal of Advanced Structural Engineering, (Suppl 1):S35–S51, 2019.
30. BS-4-2000, EN 12390," Testing hardened concrete. Compressive strength. Specification for testing machines", British Standards Institution, 2000.
31. Christophe D., **"Special concrete may give steel stiff competition"**. Article in daily journal of commerce, U.S.A., May 1997. Web site: https://www.djc.com/special/concrete97/10024304.htm
32. Dakhil R. Y., **"Structural Behavior of Continuous Steel-Reactive Powder Concrete Composite Member under Repeated Loads",** M.Sc. Thesis, Civil Department, College of Engineering, University of Babylon, Iraq, 2018.
33. Dawood M. B. and Abdulkhaleq M. H., **"Structural Behavior of Non-Prismatic Reactive Powder Concrete (RPC) Continuous Members Under Effect of Static and Repeated Loads",** International Journal of Scientific & Engineering Research, Volume 8, Issue 1, January-2017, ISSN 2229-5518.
34. Forster S. W., **"High-Performance Concrete Stretching the Paradigm".** Concrete International, Vol. 16, No. (10), PP. 33-34, U.S.A., Oct, 1994.

35. Genikomsou A. S. and Polak M. A., **"Finite Element Analysis of Punching Shear of Concrete Slabs Using Damaged Plasticity Model in ABAQUS,"** Engineering Structures, Vol. 98, pp. 38–48, 2015, doi: 10.1016/j.engstruct.2015.04.016.
36. Ghadhban H. N., **"Experimental Behavior of Hollow Non-Prismatic Reinforced Concrete Beams Retrofit With CFRP Sheets",** Journal of Engineering and Development, Vol. 17, No.5, November 2013 , ISSN 1813- 7822.
37. Goodchild C. H., and Glass, J. **"Best Practice Guidance for Hybrid Concrete Construction"**. Published by The Concrete Centre on behalf of industry sponsors, INC research, London, 2004.
38. Graybeal B., Davis M. **"Cylinder or cube: strength testing of 80 to 200 MPa (11.6 to 29 ksi) ultra-high-performance fiberreinforced concrete".** ACI Mater J 105(6):603–609, 2008. https:// doi. org/10. 14359/ 20202 .
39. Graybeal, B. A., **"Compressive behavior of ultra-high-performance fiber-reinforced concrete"**. ACI Material. https:// doi. org/ 10. 14359/ 18577, 2007.
40. Hassan S. A., and Faroun G. A., **"Behavior of Hybrid Reinforced Concrete Deep Beams under Repeated Loading"**, Civil and Environmental Research., vol. 8, pp. 14–37, 2016.
41. Hemmati1 A., Kheyroddin A. and Farzad M., **"Experimental Study of Reinforced Concrete Frame Rehabilitated by Concentric and Eccentric Bracing"**, Journal of Rehabilitation in Civil Engineering, 2017.
42. Hibbit H. D., Karlsson B. I., and Sorensen E. P., **"ABAQUS user manual, version 6.12,"** Simulia, Provid. RI, 2012.

43. Hibbitt K., Karlsson B. I., and Sorenson E. P., **"ABAQUS/Standard theory manual"**. Sorenson Inc, 2016.
44. Hibbitt K., Karlsson B. I., and Sorenson E. P**., "ABAQUS/Standard theory manual,"** Sorenson Inc, 2016.
45. Ihssan, M. A., ''**Reinforced Concrete Beams with Steel Fibers Subjected to Static Cyclic Loads**'', M.Sc., University of Technology, Baghdad, 1993.
46. IQS No. 45/1984, Iraqi Specification, "Aggregate from Natural Sources for Concrete and Construction".
47. IQS No. 5/1984, Iraqi Specification, "Portland Cement".
48. Jung W. T. and et.al., **"Experimental investigation on flexural behavior of RC beams strengthened by NSM CFRP reinforcements"** American Concrete Institute 2005, pp.795-806.
49. Kadhim, M. J., "**Nonlinear Analysis of Reinforced Concrete Space Frames under Cyclic Loading Including Time Dependent Effects",** Ph.D. Thesis, Civil Department, College of Engineering, University of Babylon, Iraq, 2007.
50. Kaveh A., Mottaghi L., and Izadifard R. A. (2020) **"Sustainable design of reinforced concrete frames with non‐prismatic beams"** Engineering with Computers, https://doi.org/10.1007/s00366-020-01045-4
51. Kmiecik P. and Kamiński M., **"Modelling of Reinforced Concrete Structures and Composite Structures with Concrete Strength Degradation Taken Into Consideration,"** Archives of Civil and Mechanical Engineering, Vol. XI, No. 3, pp. 623–636, 2011, doi: 10.1016/s1644-9665(12)60105-8.

52. Kushartomo W., and Ivan R., **"Effect of Glass Fiber on Compressive, Flexural and Spliting Strength of Reactive Powder Concrete"**, MATEC Web of Conferences 138, 03010 (2017). DOI: 10.1051/matecconf/201713803010.
53. Lubbers A. R., **"Bond performance between ultra-high performance concrete and prestressing strands"**. M.Sc. thesis, Ohio University, U.S.A., 2003.
54. MacLeod IA H A, "**Shear strength of haunched beams without shear reinforcement".** ACI Struct. 1994, J. 91 79–89.
55. Malm R., "**Shear cracks in concrete structures subjected to in-plane stresses. Lic."** Thesis, Royal Institute of Technology (KTH), Stockholm, 2006.
56. Maroliya M. K. and Modhera Ch. D. ***"A Comparative Study of Reactive Powder Concrete Containing Steel Fibers and Recrons Fibers".*** Journal of Engineering Research and Studies, JERS/Vol. I/Issue I/83-89, National Institute of Technology India, July September 2010.
57. MasterGlenium® 54, Supplied by the manufacturer.
58. Mínguez J. and et al **"Plain and Fiber-Reinforced Concrete Subjected to Cyclic Compressive Loading: Study of the Mechanical Response and Correlations with Microstructure Using CT Scanning".** Applied sciences, 2019, 9, 303**.** doi:10.3390/app9153030.
59. Mohammed H. M**., "Flexural behavior of hybrid beams containing reactive powder concrete and conventional concrete"**. Ph.D. thesis, University of Al-Mustansiriya, Iraq ,2013.
60. Moosa M. K. and Ali A. Y., **"Structural behavior of continuous hybrid reinforced concrete spliced girder under monotonic and cyclic**

load: experimental investigation", Innovative Infrastructure Solutions (2023) 8:9. https://doi.org/10.1007/s41062-022-00984-9

61. Nabbat R. A.," **Flexural and Shear Behavior of Non-Prismatic Reinforced High Strength Concrete Beams with Openings and Strengthened with CFPR Products",** Master thesis, University of Babylon, Iraq, 2015.
62. O'Neil E.F. and Dowd W.H., **"Reactive Powder Concrete: A New Material for the Construction Industry"**, Third National Concrete and Masonary Engineering Conference, June 15 – 17, 1995, San Fracisco, CA, pp. 43 – 50.
63. Qissab M.A. and Dhaiban Z.M., **"Shear Resistance of Nonprismatic High Strength Reinforced Concrete Beams"**, European Journal of Scientific Research, ISSN 1450-216X / 1450-202X Vol. 135 No 1 October, 2015, pp.15-29.
64. Rahmani T., Kiani B., Sami F., Fard B. N., Farnam Y., and Shekarchizadeh M., **"Durability of Glass, Polypropylene and Steel Fiber Reinforced Concrete"**, KII DBMC International Conference on Durability of Building Materials and Components, XII DBMC, PORTO - PORTUGAL, April 12th-15th, 2011.
65. Raza S.S., and et al. **"Effect of different fibers (steel fibers, glass fibers, and carbon fibers) on mechanical properties of reactive powder concrete"**. Structural Concrete. 2020;1–13. DOI: 10.1002/suco.201900439.
66. Resif L. G. S., **" Compatibility between the Reactive Powder Concrete as Repair Materials and Different Types of Concrete in Damaged Reinforced Concrete Beams"**, M.Sc. Thesis, Civil Department, College of Engineering, University of Babylon, Iraq, 2020.

67. Tena-Colunga A., Archundia-Aranda H.I., González-Cuevas O.M., **"Behavior of reinforced concrete haunched beams subjected to static shear loading"**. Eng. Struct ;30(2008):478–492. http://dx.doi.org/10.1016/j.engstruct.2007.04.017.

68. Wang T. and Hsu T.T.C., **"Nonlinear Finite Element Analysis of Concrete Structures Using New Constitutive Models,"** Computers and Structures, Vol. 79, No. 32, pp. 2781–2791, 2001, doi: 10.1016/S0045-7949(01)00157-2.

69. Yanga I. H., Joh C., Kimb B., **"Structural behavior of ultra high performance concrete beams subjected to bending"**, Engineering Structures 32 (2010) 3478–3487.

70. Yen Lei Voo, Stephen J., and Foster, **"Characteristics of ultra-high performance 'ductile' concrete and its impact on sustainable construction**, The IES Journal Part A: Civil & Structural Engineering, Vol. 3, No. 3, August 2010, 168–187.

71. Yu T., Teng J. G., Wong Y. L., and Dong S. L., **"Finite element modeling of confined concrete-II: Plastic-damage model,**" Eng. Struct., vol. 32, no. 3, pp. 680–691, 2010.

72. Zebalah A. S., **"Flexural Behavior of Reinforced Concrete Composite Continuous T-Beam with Hybrid Reinforcement under Repeated Load"**, Ph. D. thesis, University of Babylon, Iraq, 2020.

APPENDIXES

Appendix A

Material Tests

A-1: Physical and Chemical Properties of the Cement Used:

Chemical Requirements		IQS No. 5 / 2019 Standard for Ordinary Portland Cement	
		Limitation	Test Result
Lime saturation coefficient	%	0.66-1.02	1.0
Magnesium Oxide (as MgO)	%	≤ 5.0	3.3
Sulfate Content (as SO_3)	%	2.5 if $C_3A \leq 5$	2.20193
		2.8 if $C_3A \geq 5$	
Loss on ignition (as LOI)	%	≤ 4.0	3.3
Non soluble substances	%	≤ 1.5	0.7
Physical Requirements		**IQS No. 5 / 2019 Standard for Ordinary Portland Cement**	
		Limitation	**Test Result**
Finesse (Blaine)	kg/m^2	≥ 230	332
- Initial setting time	minute	≥ 45	145
- Final setting time	hours	≤ 10	3:10
Soundness (expansion)	%	≤ 0.8	0.2

Appendix B

Trial Mixes of Reactive Powder Concrete

B-1: Introduction:

A number of trail mixes have been done to select the best proportion mix for RPC with two fiber types (SF and GF) in order to get approach compressive strength. Different dosages for two types of chemical admixture (MasterGlenium 54 (MG) and EPSILONE HP 580 (HP)) (SP) are used to improve the workability of the fresh concrete with a very low water-cement ratio (W). Moreover, different volume of silica fume–cement ratio (S) was used to work as the filler and two types of concrete (ALJISER and al Kufa) were used. A number of mixing proportions from the previous studies were considered and modified with these mix proportions, numerous mix proportions were done. where three cubes were examined for each mixture at the age of 7 days and the age of 28 days. Table (B-1) and Table (B-2) show the trial mix for steel fiber and glass fiber RPC, respectively.

Table (B.1) Results of trail mixes for steel fiber RPC

Mix no.	Cement type	Type of SPA	Cement content (kg/m^3)	Sand (%)	Slica fume (%)	SP (%)	W (%)	SF% (Volume ratio)	Compressive strength (MPa)		Notes
									7 days	28 days	
1	Kufa	MG	950	105	20	2.25	25	2.0%	98.5	120.1	Bad workability
2	Kufa	MG	950	105	20	3.00	20	2.0%	108.8	125.9	Bad workability

3	Kufa	MG	950	105	20	3.50	20	2.0%	109.9	127.9	Bad workability
4	Kufa	MG	950	105	25	3.50	25	1.5%	67.3	84.5	
5	Kufa	MG	950	105	25	3.00	25	1.50%	59.2	81.6	
6	Kufa	MG	950	105	25	3.00	25	2.0%	59.1	81.4	
7	Kufa	MG	950	105	25	2.50	25	2.00%	63.8	82.9	
8	Aljiser	MG	950	105	25	2.25	25	2.00%	72.4	97.4	
9	Aljiser	MG	950	105	25	2.25	20	2.00%	80.4	120.4	
10	Aljiser	MG	950	105	25	3.00	22	2.00%	75.3	106.7	
11	Aljiser	MG	950	105	25	3.50	22	2.00%	74.7	98.6	
12	Aljiser	MG	950	105	25	3.50	20	2.00%	82.8	119.3	
13	**Aljiser**	**MG**	**950**	**105**	**25**	**3.00**	**22**	**1.50%**	**67.9**	**86.8**	Selected
14	Aljiser	MG	950	105	25	3.50	20	1.50%	79.3	107.6	
15	Aljiser	MG	950	105	25	2.50	22	1.50%	71.7	95.0	

Table (B.2) Results of trail mixes for glass fiber RPC

Mix no.	Cement type	Type of SPA	Cement content (kg/m^3)	Sand (%)	Slica fume (%)	SP (%)	W (%)	GF% (Volume ratio)	Compressive strength (MPa)		Notes
									7 days	28 days	
1	Aljiser	MG	950	105	25	2.50	22	2.00%	38.8	57.6	
2	Aljiser	MG	950	105	25	3.50	22	2.00%	52.3	67.6	
3	Aljiser	MG	950	105	25	3.00	25	2.00%	41.8	61.4	
4	Aljiser	MG	950	105	25	3.50	22	1.50%	51.9	66.1	
5	**Aljiser**	**MG**	**950**	**105**	**25**	**3.00**	**22**	**1.50%**	**54.4**	**76.0**	Selected
6	Aljiser	HP 580	950	105	25	5.00	20	2.00%	35.7	39.3	
7	Aljiser	HP 580	950	105	25	4.00	20	2.00%	60.8	30.4	
8	Aljiser	HP 580	950	105	25	4.00	22	2.00%	54.4	51.2	

Appendix C

Design of Experimental Frames

C-1: Introduction:

The frame is limited in dimensions according to the dimensions of the test device (1.0 m height and 1.0 m length). The members cross section is 0.15 m x 0.15 m, the material properties are:

- f_y = 422 MPa (for steel Ø6)
  = 512 MPa (for steel Ø10)
- f'_c =30.13 MPa.

C-2: Design of Beam:

A beam 0.15*0.15 m is specified for plane prismatic frame:

- **Design of shear reinforcement:**

b = 150 mm, h = 150 mm

d = h – cover - dia.stirrups- dia. bar/2

cover = 20mm, dia.stirrups= 6mm, dia.bar = 10mm.

d = 150 - 20 - 6 - 10/2 = 119mm

$$V_c = 0.17 * \sqrt[2]{f_c'} bd = 0.17 * \sqrt[2]{30} * 150 * 119 * 10^{-3} = 16.66\ kN$$

The distance between the stirrups is:

$$S_{max} \leq \left\{ \begin{matrix} \frac{d}{2} = \frac{119}{2} = 60\ mm \quad (control) \\ or \quad 600\ mm \end{matrix} \right\}, \text{so, use Ø 6mm @ 60 mm}$$

$$V_s = \frac{A_v f_y d}{S_{max}} = \frac{56.57 * 422 * 119}{60} = 47.35\ kN$$

$V_u = \emptyset(V_s + V_c) = 0.75 * (47.35 + 16.66) = 48$ kN

$V_u \leq \frac{5}{8} \cdot \sqrt{f_c'} \cdot b_w \cdot d \cdot 10^{-3} = 61.1\ kN$, ∴ the section dimension is o.k.

For use actual shear strength, let $\emptyset = 1$

$So, \quad P = 64 * 2 = 128\ kN$

- **Design of Bending moment reinforcement:**

From STAAD pro program $M_{at\ edges}$ = 0.137 P/2

M=0.137*64=8.77 kN.m

$$R = \frac{M * 10^6}{f_c' \cdot b \cdot d^2} = \frac{8.77 \cdot 10^6}{30.13 \cdot 150 \cdot 119^2} = 0.137$$

$$\omega = \frac{1 - \sqrt{1 - 4 * 0.59 * R}}{2 * 0.59} = 0.15$$

$$\rho = \omega \cdot \frac{f_c'}{f_y} = 0.15 * \frac{30.15}{512} = 0.00883$$

Compare with ρ_{min} and ρ_{max}

$$\rho_{min} = \frac{0.25 \cdot \sqrt{f_c'}}{f_y} = 0.00258 > \frac{1.4}{f_y} = \frac{1.4}{532} = 0.00263$$

$$\rho_{max} = 0.85 * \beta_1 \frac{f_c'}{f_y} \frac{\varepsilon_u}{\varepsilon_u + 0.004}$$

where

$\boldsymbol{\rho_{max}}$= maximum reinforcement ratio,

$\boldsymbol{\rho_{min}}$= minimum reinforcement ratio

$\boldsymbol{\beta_1}$= ratio between compressive result to neutral axis, and

ε_u= maximum strain in concrete.

$$\rho_{max} = 0.85 * 0.85 * \frac{30.13}{532} * \frac{0.003}{0.003 + 0.004} = 0.0175$$

$$\therefore \rho_{min} < \rho < \rho_{max} \quad \text{O.K.}$$

$$A_{s\,req} = \rho \cdot b \cdot d = 151.64\, mm^2$$

When use 2Ø10 with area 2*78.5

$$\therefore A_{s\,pro} = 157\, mm^2 \quad \text{O.K.}$$

C-3 design of column:

A column 0.15x 0.15 m is specified, and reinforcement distributed around the column perimeter will be used. Bar cover is estimated to be 0.02m. The column parameters (assuming bending about the strong axis) are:

$$e = \frac{P}{M} = 7.32$$

$$\gamma = \frac{h - 2d'}{h} = \frac{150 - 231}{150} = .56$$

$$K_n = \frac{P_u}{f_c' A_g}$$

$$R_n = \frac{M_u}{f_c' A_g h}$$

where

$\boldsymbol{P_u}$= factored load, according to the ACI safety provisions, the column must be designed for factored load $\boldsymbol{P}$= 64 kN,
$\boldsymbol{M_u}$= factored moment (M = 8.77 kN.m),
$\boldsymbol{A_g}$= gross area of the cross section, and
$\boldsymbol{h}$ = depth of column.

For this column geometry and material strength, Graph A.7 (***Nilson, and et.al*** 2003) for that figure, with the calculated value of $\boldsymbol{k_n}$ and $\boldsymbol{R_n}$ as follow:

$$K_n = \frac{P}{f_c' A_g} = \frac{64 * 10^3}{30.13 * 150 * 150} = 0.09$$

$$R_n = \frac{M}{f_c' A_g h} = \frac{8.77 * 10^6}{30 * 150 * 150 * 150} = 0.09$$

The reinforcement ratio $\rho_g = 0.01$

Thus, the requirement reinforcement is $A_s = 0.01 * 150 * 150 = 225$ mm^2

Use 4Φ 10 mm → A_s=314.16 mm^2,

then if use ∅ 6 mm for ties, the distance between ties is:

$$S \leq \begin{Bmatrix} 48 * d_{stirrups} = 48 * 6 = 288\, mm \\ 16 * d_{bar} = 16 * 10 = 160\, mm \\ h = 150\, mm \quad (conrol) \\ b = 150\, mm \quad (conrol) \end{Bmatrix}$$

Use ties ∅ 6 mm @ 120 mm to ensure the failure in not happen in the columns.

Appendix D

Concrete Damage Plasticity (CDP)

D-1: Concrete Damage Plasticity (CDP):

At this stage, the concrete is represented by three steps: plasticity parameter, compression behavior, and tensile behavior. They are as follows:

D-1-1: plasticity parameter:

The required plasticity parameters for the CDP model in ABAQUS are:

- **Dilation angle (ψ)**, is a material parameter determined at a high confining pressure in confining pressure (p) and von Mises stress (q) plane and indicates the inclination of an incremental plastic strain. ψ has a maximum value of 56.3^0 and a minimum value is approximately 0^0. Upper values are more ductile behavior, whereas lower values are more brittle. According to **(Malm, 2006),** better agreement was reached with the experimental findings for dilation angles between 30^0 to 40^0 and for normal concrete ψ equal 30^0 considers suitable.
- **Eccentricity (Є)**: defines the change rate of plastic flow potential function. In ABAQUS 0.1 can be considered as the eccentricity default value, where the dilation angle has no change for a wide range of confining pressure. For low confining pressure a higher eccentricity value than 0.1 induces a rapid increase in the dilation angle. Although a lower value than 0.1 will cause a problem of convergence when the material is submitting to the low values of

confining pressure.

- σ_{bo}/σ_{co} : refers to the ratio of initial equiaxial compressive yield stress to initial uniaxial compressive yield stress. In the present study the value 1.16 was used which is ABAQUS default amount.
- K_c : is the rate of the second stress invariant in the tensile meridian to compressive meridian for any known value of the pressure invariant at initial yield. The value of Kc is in range (0.5-1) and its default value that used in ABAQUS is 0.667.
- μ : represents the viscosity parameter which is used in ABAQUS to improve the convergence. Its default value is zero.

The parameters inputted to define conventional concrete and RPC models are tableted in **Figure (D-1).**

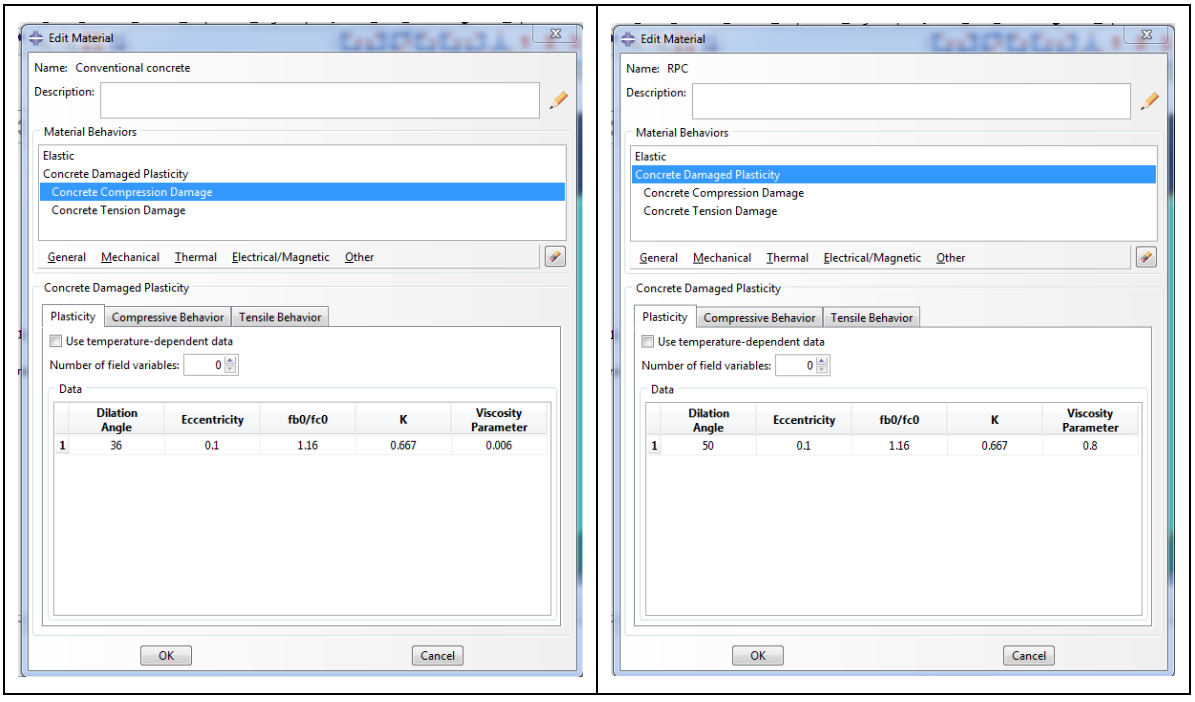

Figure (D-1): The Plasticity parameters inputted to define conventional concrete and RPC

D.1.2: Compression Behavior:

The compressive behavior for concrete under uniaxial compressive

load can be noticed in **Figure (D-2)**, the stress-strain relationship in this figure canbe divided into three stages : the first is linear-elastic relation up to yield stress (σ_{co}), in the second stage, stress hardening occurs until reaching the ultimate compressive stress value (σ_{cu}) followed by the last stage which is strain hardening. CDP model takes in account the degradation in the concrete stiffness at elastic through using the damage parameters d_t (at tension) and d_c (at compression) which are functions of strains in plastic stage and temperature. These variables change in limits (0 to 1) where zero mean un damaged material and 1 refers to completely lost for material strength.

The flowing equations were used to calculate the damage parameters **(Yu et al, 2010):**

$$d_t = 1 - \frac{\sigma_t}{\sigma_{tu}} \quad \ldots\ldots\ldots\ldots\ldots\ldots\ldots\ldots\ldots\ldots\ldots\ldots \text{(D-1)}$$

$$d_c = 1 - \frac{\sigma_c}{\sigma_{cu}} \quad \ldots\ldots\ldots\ldots\ldots\ldots\ldots\ldots\ldots\ldots\ldots\ldots \text{(D-2)}$$

Figure (D-2) demonstrates a standard stress-strain relation of uniaxial concrete compressive in the finite element model.

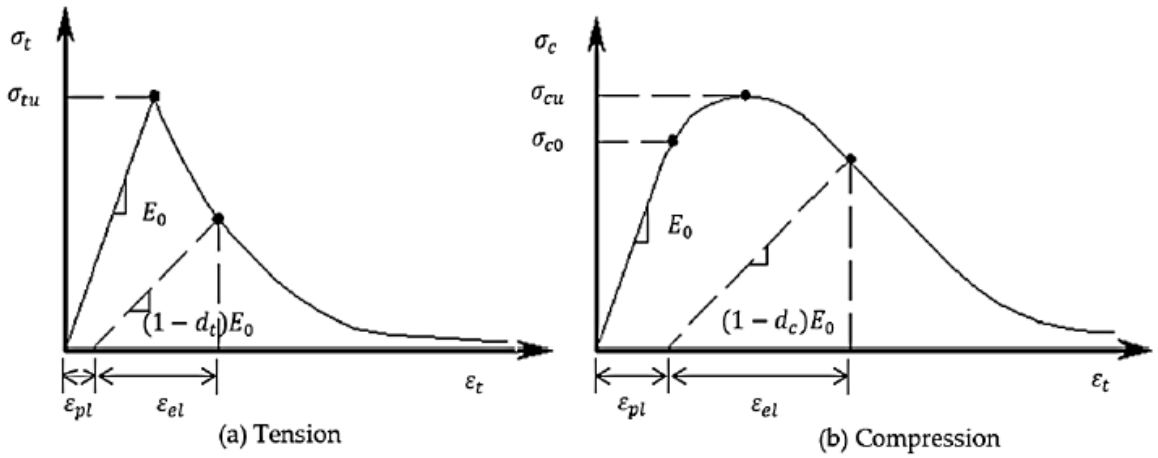

Figure (D-2) Concrete response to uniaxial loading based on manual of the ABAQUS theory (Abaqus, 2013)

In the current study, the concrete in compression was modeled with Hognestad parabola **(Genikomsou and Polak, 2015)**. Under uniaxial compressive loading, the expected stress-strain relationship behavior of

the concrete can be split into three domains. The linear-elastic branch is represented by the first one. The stress level is σco when the linear branch comes to an end that was taken here as $\sigma_{co} = 0.4f'_c$ for HSC and $\sigma_{co} = 0.3f'_c$ for conventional concrete. The second part discusses the rising branch of the uniaxial stress-strain relationship when compression loading is applied to the peak load at the corresponding strain level $\varepsilon_o = \frac{2f'_c}{E_c}$. The final segment of this stress-strain curve, beginning with the peak stress and ending with the strain $\varepsilon c < 0.01$ that is referred to as the post-peak part. The assumed compressive stress-strain curve's equation is given in **Equation (D-3)**. **Figure (D-3)** represents the compressive stress-strain curves for all concrete.

$$\sigma_c = f'_c[2\left(\frac{\varepsilon_c}{\varepsilon_o}\right) - \left(\frac{\varepsilon_c}{\varepsilon_o}\right)^2] \quad \ldots\ldots\ldots\ldots\ldots\ldots\ldots\ldots\ldots\ldots \text{(D-3)}$$

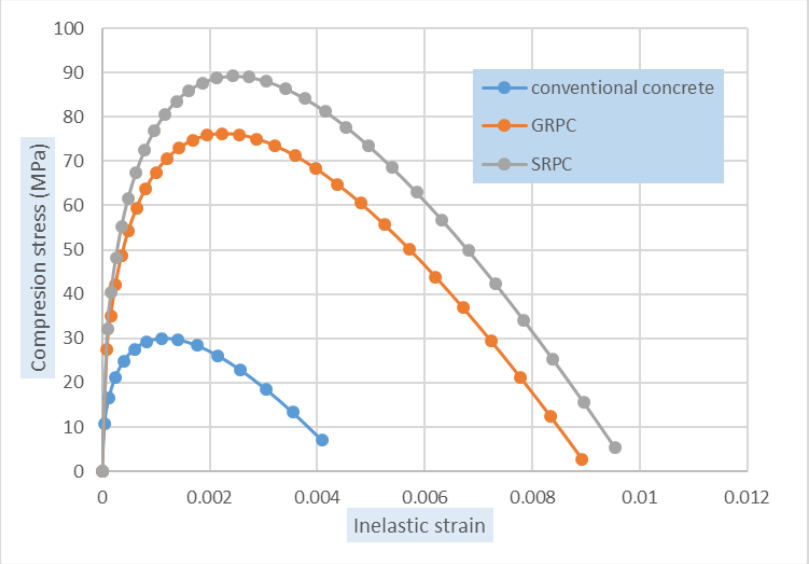

Figure (D-3) Compressive stress-inelastic strain curves

Damage parameter in terms of the compression (dc) of concrete damaged plasticity model was introduced for all concrete types according to **Figure (D-3)**, the values of dc were calculated according to **Equation**

(D-2).

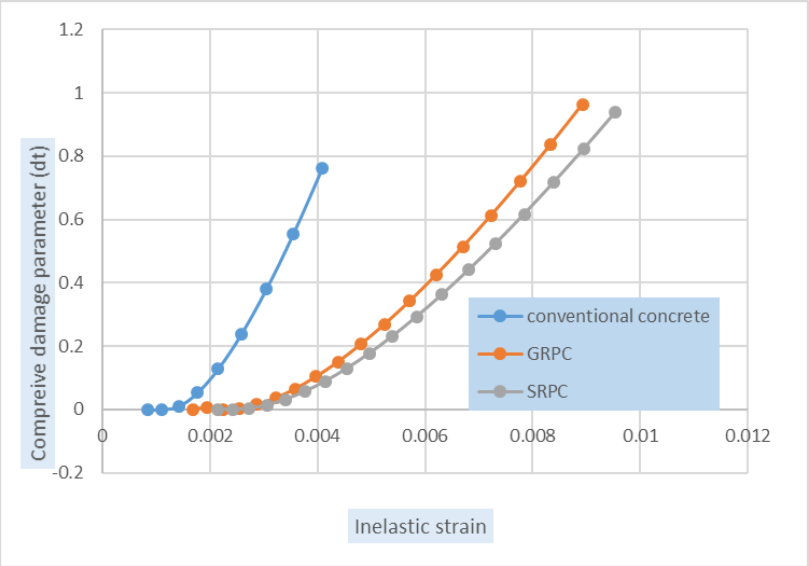

Figure (D-3) Compressive damage parameter-strain relationship for all concrete types

D.1.3: Tensile Behavior:

The stress-strain relation, the stress-displacement relation, and the fracture energy (Gf) **(Hibbitt et al, 2016)** approaches are all included in ABAQUS for defining tension softening behavior.

In the present study, the stress-strain relationship of concrete in tension was modeled by using a relation that suggested by **(Wang and Hsu, 2001)** and modified by **(Kmiecik and Kaminski, 2011),** consisting of two parts. The first one, the curve linearly increases up to the point of cracking failure (fcr), is taken from **Table (4-3).** Afterward, the second part is the curve gradually descends and follows a parabola shape. This behavior is expressed as follows:

$$\varepsilon_{cr} = \frac{f_{cr}}{E_c} \quad \ldots\ldots\ldots\ldots\ldots\ldots\ldots\ldots\ldots\ldots\ldots\ldots\ldots\ldots\ldots\ldots\ldots\ldots\ldots\ldots\ldots\ldots \text{(D-4)}$$

$$f_t = E_c \,.\, \varepsilon_t \qquad \text{for} \quad \varepsilon_t < \varepsilon_{cr} \quad \ldots\ldots\ldots\ldots\ldots\ldots\ldots\ldots\ldots\ldots\ldots\ldots\ldots\ldots\ldots\ldots\ldots\ldots\ldots\ldots\ldots\ldots \text{(D-5)}$$

$$f_t = f_{cr} \cdot \left(\frac{\varepsilon_{cr}}{\varepsilon_t}\right)^n \quad \text{for} \quad \varepsilon_t > \varepsilon_{cr} \quad \ldots\ldots\ldots\ldots\ldots\ldots\ldots\ldots \text{(D-6)}$$

Where:

n: Rate of weakening, this study calibrated the n values at (0.6 for conventional concrete and 0.4 for RPC). **Figure (D-4)** shows the theoretical stress-strain behavior for concrete in tension.

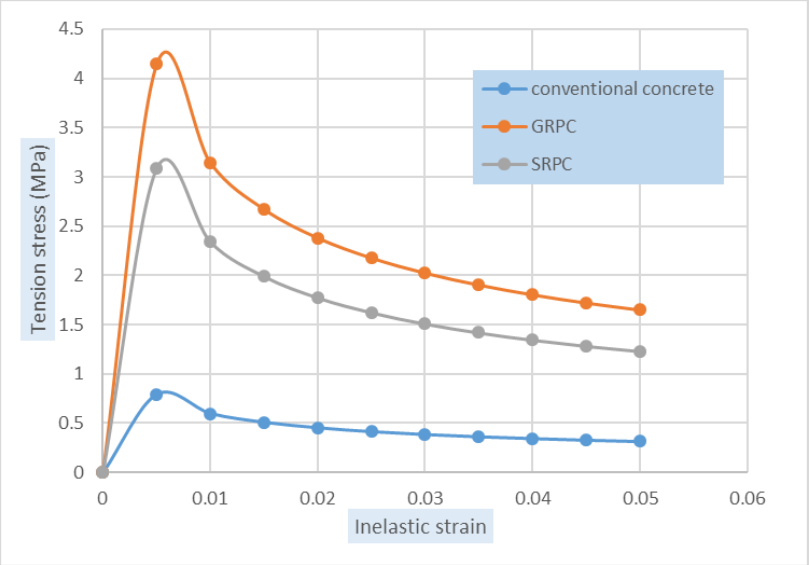

Figure (D-4) Tension stress-inelastic strain curves for all concrete type

Damage parameter in terms of tension (dt) of concrete damage plasticity model was introduced for all concrete types according to **Figure (D-4)**, the values of dt were calculated according to Equation (D-1).

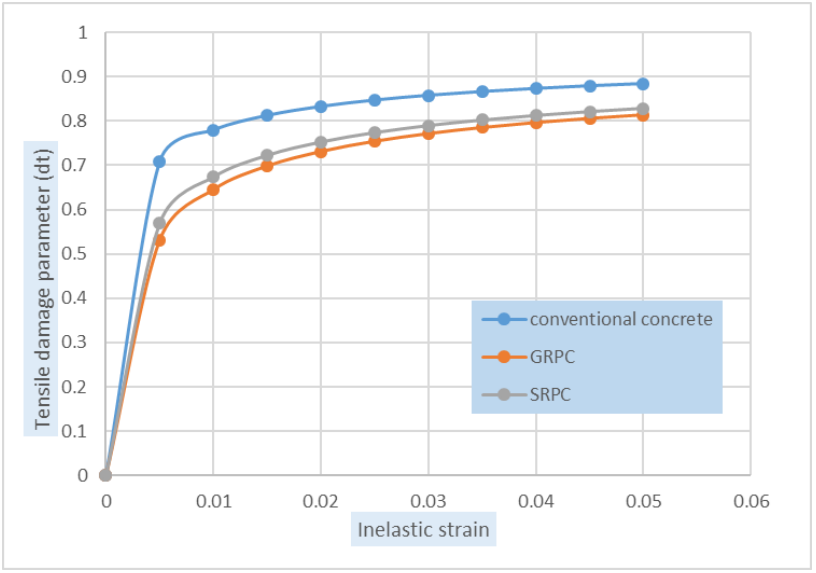

Figure (D-5) Tension damage parameter-strain relationship for all concrete types

الخلاصة

هذه الدراسة تتضمن تحريات عملية ونظرية لهياكل خرسانية مستوية ذات مقاطع موشورية وغير موشورية من خلال صب ثمانية عشر نموذج بأنواع مختلفة من الخرسانة ذو نوع واحد والخرسانة المهجنة. تم فحص النماذج تحت احمال باتجاه واحد واحمال تكرارية.

الهدف من هذا البحث هو الاستخدام الامثل للخرسانة في الهيكل الخرساني عن طريق اعادة توزيع الخرسانة على طول الاعضاء الانشائية باستخدام مقاطع غير موشورية بالأعمدة والعتبة. كما يهدف البحث الى معرفة سلوك الهيكل الخرساني عند استخدام خرسانة مساحيق فعالة ذات الياف زجاجية (GRPC) وكذلك عند تهجين الخرسانة الاعتيادية بGRPC تحت احمال باتجاه واحد وتكرارية.

المتغيرات الرئيسية في البرنامج العملي يتضمن استخدام مقاطع غير موشورية بالأعمدة والعتبة حيث نسبة البعد الكبير الى البعد الصغير 1.3. كما تم استخدام هيكل خرساني ذات خرسانة مساحيق فعالة بألياف حديدية (SRPC) وGRPC اضافة الى الخرسانة الاعتيادية. فضلا عن استخدام هياكل خرسانية ذات خرسانة اعتيادية مهجنة بGRPC بنسب مختلفة تتراوح بين 25%-100% في مواقع مختلفة. اضافة الى دراسة جميع الحالات اعلاه تحت تأثير حمل تكراري بواقع عشرة دورات لكل دورة حمل اقصى مقداره 65% من الحمل الاقصى للنموذج ذات التحميل باتجاه واحد.

النتائج بينت زيادة في الحمل الاقصى مقداره (16%-25%) عند استخدام هيكل خرساني ذو مقاطع غير موشورية مقارنة مع الهيكل ذو المقاطع الموشورية. كما يزداد الحمل الاقصى بمقدار 41% و46% عند استخدام هيكل خرساني ذو GRPC وSRPC على التوالي مقارنة مع الهيكل ذو الخرسانة الاعتيادية. عند تهجين الخرسانة الاعتيادية ب GRPC يلاحظ توافق جيد بين نوعي الخرسانة وعدم حدوث اي انعزال بينهما عند الفحص وكذلك تحسن واضح في سلوك الهيكل الخرساني حيث يزداد الحمل الاقصى بمقدار (4-22) % حسب نسبة وموقع التهجين.

بالإضافة الى ذلك، عند فحص الهيكل الخرساني بحمل تكراري فان الحمل الاقصى يقل بشكل كبير عندما يكون الهيكل ذو خرسانة اعتيادية حيث يقل الى 27% مقارنة مع الحمل ذو الاتجاه الواحد. وعندما يستخدم خرسانة مساحيق فعالة ذات الياف حديدية او زجاجية او حتى خرسانة مهجنة فان نسبة النقصان تقل. حيث يقل الحمل الاقصى بمقدار 2% فقط عند استخدام خرسانة مساحيق فعالة بألياف

حديدية وزجاجية اما عند استخدام خرسانة مهجنة فان النقصان يكون (16-4) % حسب نسبة التهجين وموقعه.

تحسين سلوك الهيكل الخرساني باستخدام GRPC وSRPC لا ينحصر فقط في الزيادة بالحمل الأقصى بل يحسن قوة القص للهيكل الخرساني ويغير نوع الفشل من فشل قص كما في الهيكل الخرساني ذو الخرسانة الاعتيادية الى فشل انحناء كما تزيد صلادة الهيكل الخرساني. كما ان استخدام الخرسانة المهجنة في بعض المناطق أيضا تحسن قوة القص وتغير نوع الفشل إضافة الى زيادة في صلادة الهيكل الخرساني.

على الجانب الاخر، تم استخدام تحليل العناصر المحددة (اباكوس/2017) لمحاكاة الهياكل الخرسانية الموشورية وغير الموشورية. النتائج بينت توافق جيد بين نتائج التحليل النظري والفحوصات التجريبية حيث يكون الفرق لا يزيد عن 7% للحمل الاقصى ولا يزيد عن 23% للهطول في منتصف العتبة. لذلك استخدم البرنامج لإيجاد حالات دراسة جديدة.

باستخدام برنامج الاباكوس، وجد ان استخدام مقاطع غير موشورية بالهيكل على طول العتبة وبنسبة العمق الكبير الى العمق الصغير (1.1-2.0) يزداد الحمل الاقصى بمقدار (13-20)% وأفضل نسبة هي (1.5-2.0). بينما إذا المقطع غير الموشوري في الثلثين الطرفين للعتبة فان الزيادة في الحمل الاقصى تكون (16%-42%) عندما تكون نسبة العمق الكبير الى العمق الصغير (1.1%-2.0%).

كذلك عند تهجين الهيكل الخرساني بخرسان مساحيق فعالة ذات الياف زجاجية في الثلثين الطرفيين للعتبة (منطقة اجهادات القص) بنسبة تهجين (18%-70%) فان الزيادة في الحمل الأقصى تكون ثابتة بحدود 6%. بينما عند تهجين الفضاء الصافي للعتبة فقط بنسبة تهجين (13%-62%) فان الحمل الأقصى يزداد بمقدار (0%-17%).

جمهورية العراق
وزارة التعليم العالي والبحث العلمي
جامعة بابل- كلية الهندسة
قسم الهندسة المدنية

السلوك الانشائي للهياكل الخرسانية المسلحة غير الموشورية باستخدام خرسانة هجينة تحت تأثير احمال باتجاه واحد وتكرارية

اطروحة

مقدمة إلى كلية الهندسة / جامعة بابل

كجزء من متطلبات نيل درجة الدكتوراه فلسفة في الهندسة / الهندسة المدنية/ انشاءات

من قبل

ضرغام حسين علي حسين

إشراف

الاستاذ الدكتور مصطفى بلاسم داوود **الاستاذ الدكتور غالب محسن حبيب**

1445هـ **2023 م**